UNIVERSITÀ
DEGLI STUDI
DI PADOVA

Head Office: Università degli Studi di Padova

Department of Biology

Ph.D. COURSE IN: Biosciences
CURRICULUM: Cell Biology and Physiology
SERIES XXXII

Contribution of microglia to the pathogenic mechanisms behind LRRK2-associated Parkinson's disease

Coordinator: Prof. Ildikò Szabò
Supervisor: Prof. Elisa Greggio
Co-Supervisor: Dr. Mark Cookson

Ph.D. student: Alice Kaganovich

About 200 years ago James Parkinson described the "Shaking Palsy" and almost 60 years ago levodopa drug was introduced in the market. With all the advances in technology and science, we learned how to reach Mars and how to see each other through Skype from pretty much every spot on this planet. Still, we are puzzled about the incredible complexity of our own brain and levodopa remains the most effective, but only symptomatic therapy for Parkinson's disease due to our limited understanding of the circuitries and molecular pathways that govern brain function.

Table of contents

Acknowledgements

This work is a result of an intensive collaborations between NIH, Padova University and Core facilities that participated in the research. Behind those official names, there are enthusiastic and knowledgeable people, who are ready to share their knowledge, support and constructively criticize in order to move our research a step forward to understanding of the human brain.

First, I'd like to thank my PhD supervisors, **Dr.Mark Cookson** and **Prof.ssa Elisa Greggio.**

Mark, when I popped-up in your office with the idea of Italian PhD, thank you for your support and encouragement! I really appreciate the stimulating research environment in our group, and the fact that you always encourage us to try the new scientific approaches.

Elisa, your positive attitude and support are incredible! Thank you so much for the constructive feedback and discussions! Thank you for accommodating me and let me be the part of your family, those are the happy times!

I'd like to thank my PhD scientific advisors, **Prof.Ildiko Szabo** and **Prof.Georgio Valle,** for your time, effort and scientific support.

Michael Lehmann, thank you for sharing your broad knowledge, I'm really amazed at your passion for the science! Starting from the "mysterious microglia ring" in a 15ml tube and up to the short and productive discussions, I learn from you every time we meet and hope for more collaborations.

Isabella Russo, my dear friend and collaborator – always inspired by your hardworking personality and determined spirit! Thank you for being such an engine for the first part of this work!

Natalie Landeck, I appreciate all your help, professionalism and the sense of humor while teaching me the brain anatomy! (10pm in the lab? Ice-cream? Good idea!)

Noemi Kedei, thank you so much for your enthusiasm, expertise and support on the new field of the single cell westerns! It is bringing us for the new level of research!

Ruth Chia, thank you for your emotional support and positivity! Also, for encouraging me to start moving on with R-coding and giving the great and simple explanations.

LNG lab, dear all, you are great scientists and a cool people, it's a great pleasure and fun to work together!

Padova lab, my big appreciation to the great Padova group – thanks to all of you for welcoming me into your lab so warmly and for the constant scientific and personal support. My Italian soul is always with all of you, let's keep in touch!

Andy Singleton, it is my pleasure and honor to be a part of an amazing LNG-lab! Thank you for keeping this incredible collaborative and friendly spirit of the lab!

In addition, my deep appreciation for the members of the Core facilities, **Heather Kalish** (ELISA multiplex), **Mike Kelly** and **Zach Rae** (single cell RNA-seq), **Noemi Kedei** (single cell WB), **Jinhui Ding** (Bioinformatics), **Francesco Boldrin** and **Federico Caicci** (Electron microscopy) - this work would not be possible without your time and effort!

My family, thank you for all your love and support.

Abstract.

Microglia are immune cells of the brain playing critical roles during the inflammatory response. Among the genes mutated in familial Parkinson's disease, those encoding LRRK2 and α-synuclein have been associated with neuroinflammatory processes. Previous work showed that LRRK2 is a positive regulator of inflammation, while aggregated α-synuclein released by dying neurons can activate microglia triggering the neuroinflammatory process.

The main goal of this project was to gain novel insights into the contribution of microglial cells to the pathogenic mechanisms of LRRK2-associated Parkinson's disease.

To this aim, we initially performed RNA-sequencing (RNA-seq) of Lrrk2 wild-type (WT) and knockout (KO) primary microglia treated with α-synuclein pre-formed fibrils (PFFs) or lipopolysaccharide (LPS). We found that LPS and α-synuclein triggered in part overlapping but also different responses, while loss of Lrrk2 had a subtle effect in attenuating the pro-inflammatory response. Moreover, treatment with α-synuclein PFFs caused a significant induction of the antioxidant superoxide dismutase-2 (SOD2) enzyme in WT cells, with the effect attenuated in Lrrk2 KO microglia cells.

Since loss of Lrrk2 in primary microglia revealed only small differences in gene expression both under resting or pro-inflammatory conditions, we next moved to an experimental condition that more closely resembles the physiological situation, e.g. acutely isolated microglia cells from LPS-injected adult mouse brains. Using single cell RNA sequencing (scRNA-seq), we confirmed a subset of the genes nominated in primary culture experiments, including IL-1β, SOD2 and TXNIP as differentially expressed upon inflammatory stimulation with LPS. However, the overall effect on gene transcription due to loss of Lrrk2 remained subtle. To further explore the impact of LRRK2 on microglia function, we performed *ex vivo* phagocytic assays. Lrrk2 KO microglia displayed the highest phagocytic activity compared to microglia isolated from WT and pathogenic mutants G2019S and R1441C mice upon treatment with α-synuclein PFFs, suggesting that LRRK2 negatively regulates phagocytosis or delays lysosomal degradation.

Additionally, we performed intrastriatal brain injections with lipopolysaccharide (LPS)-inflammatory agent or with PBS as a control, that demonstrated a significant morphological changes in microglial shape (increase in circularity and soma area) in LPS-stimulated animals compare to PBS-treated and a modest differences between LRRK2 genotypes. Additionally, the branch complexity was reduced in LPS-injected animals with stronger effect in Lrrk2-KO and R1441C genotypes and a less response in G2019S animals. Next, we evaluated LRRK2 mRNA and protein expression at the single cell level. We found that LRRK2 has a low and sparse pattern of expression in unstimulated resident microglia. However, upon stimulation with LPS, the proportion of microglia cells expressing LRRK2 increased, while LRRK2 levels remained unchanged per cell. This is, to date, the first attempt to analyze LRRK2 protein expression at the single cell level in brain cells.

In summary, the present work provides new insights into the biology of LRRK2 in the brain resident microglia and shows that inflammatory stimulations with α-synuclein PFFs cause a significant induction of pro-inflammatory and anti-oxidant responses, which are attenuated in LRRK2-KO microglia.

Abbreviations

cDNA……complementary DNA

Crx……..cortex

CTR……...control

DA……Dopaminergic neurons

ddPCR……...digital droplet polymerase chain reaction

ELISA……..enzyme-linked immunosorbent assay

GO……gene ontology

IHC…….immunohistochemistry

IL-1ß……...Interleukin 1 beta

KO……knock-out

LB……...Lewy body

L-DOPA (levodopa)……L-3,4-dihydroxyphenylalanine

LPS……...lipopolysaccharide

LRRK2……Leucine-rich repeat kinase-2

MACS……..magnetic-activated cell sorting

MIPs…….maximum intensity projections

MPTP…… mitochondrial parkinsonian neurotoxin

P0 (P1)……postnatal day 0 (postnatal day 1)

PBS…….phosphate-buffered saline

PCR……polymerase chain reaction

PD……..Parkinson's disease

PFA…….paraformaldehyde

PFC……..prefrontal cortex

PFFs, α-syn PFFs ……..α-synuclein pre-formed fibrils

PKCd……protein kinase C delta type

qRT-PCR……quantitative reverse transcription polymerase chain reaction

RIN……..RNA integrity number

ROS……reactive oxygen species

RT……..room temperature

scRNA-seq……..single cell RNA sequencing

SN (SNc)……..substantia nigra (substantia nigra pars compacta)

SNCA, Syn, α-syn……..alpha-Synuclein

SOD2……..superoxide dismutase 2

Str (dStr, vStr)……striatum (dorsal striatum, ventral striatum)

TEM……transmission electron microscopy

TH……tyrosine hydroxylase

TLR4……Toll-like receptor 4

TMEM119……transmembrane protein 119

t-SNE……T-Distributed Stochastic Neighbor Embedding

TXNIP……Thioredoxin-interacting *protein*

WB (scWB)……Western blot (singe cell Western blot)

WT……wild-type

List of figures and tables

Chapter 1

Introduction

1.1 Parkinson's disease

1.1.1 Brief History

In 1817, English doctor James Parkinson made the first clear medical description of the disease, reporting six cases of what he called *paralysis agitans* in his "Essay on the Shaking Palsy" (Goetz, 2011; Parkinson, 2002) The term "Parkinson's disease" was first proposed in 1865 by William Sanders and later popularized by French neurologist Jean-Martin Charcot, who provided detailed clinical description of the disease and made the distinction between rigidity, weakness and bradykinesia (Charcot, 1886; Goetz, 2011).

In 1912 Fredrich Lewy reported a pathologic finding in some brain regions outside of the substantia nigra (SN) and described proteinaceous intracellular inclusions within both nerve cell bodies and processes, later named "Lewy body" (LB) (Lewy,1912). A few years later, in 1919 Konstantin Tretiakoff found similar aggregates in the SN and named them after Lewy. In addition, he reported that the SN was the main cerebral structure affected in disease. His finding was not widely accepted until it was confirmed by further studies published by Rolf Hassler in 1938, stating that degeneration of the SN was the cause of parkinsonism (M. Goedert, Spillantini, Del Tredici, & Braak, 2013). Loss of neurons in the SN and the presence of LB were subsequently considered the definitive criteria for *post mortem* diagnosis of Parkinson's disease (Greenfield & Bosanquet, 1953).

The underlying biochemical changes in the brain neuropathology were identified in the late 1950s, by the discovery of the neurotransmitter dopamine (DA) by Arvid Carlsson,

Eric Kandel and Paul Greengard whose work was awarded with a Nobel Prize (Carlsson, Lindqvist, Magnusson, & Waldeck, 1958). DA was found to be highly concentrated in the nigral projections to the striatum and its decreasing levels positively correlated with nigral cell loss in patients (Bertler & Rosengren, 1959; Ehringer & Hornykiewicz, 1960).

For many years PD was considered a non-genetic disease and the causes were ascribed to head injury and exposure to environmental factors such herbicides and pesticides (Goetz, 2011).

Only in 1997, the discovery of missense mutation in *SNCA* gene (encoding α-synuclein) as the cause of a dominantly inherited form of PD with Lewy pathology, revolutionized the field of PD, challenging the dogma of PD as disease with no genetic component (Polymeropoulos et al., 1996). Shortly after this discovery, α-synuclein was recognized as a major protein present in LBs (Spillantini et al., 1997), representing a great revolution in the PD timeline and beginning the new genomic era in research on Parkinson's disease.

1.1.2 Neuropathology

Classically, Parkinson's disease (PD) is defined as common, slow progressing neurodegenerative disease that affects more than 10 million people, accounting for 1-2 % of the population worldwide (https://www.parkinson.org/Understanding-Parkinsons/Statistics). PD is characterized by the loss of dopaminergic neurons in the substantia nigra associated with the formation of fibrillar aggregates that are composed of α-synuclein and other proteins (Lees, Hardy, & Revesz, 2009), (Figure 1-1). However, it is increasingly clear that PD is not a simple disorder exclusively affecting DA neurons of the SNpc. It is likely a complex, multisystemic syndrome, affecting different organs, not just the brain. Early signs of disease include hyposmia, sleep disorder, constipation and depression, suggesting different neurons are likely affected. Supporting a more complex view of PD, Braak proposed a classification based on different stages of the α-synuclein

pathology, which starts from the enteric and/or olfactory system and travels along neuroanatomically connected areas finally reaching the SNpc and the cortex (Braak & Braak, 1991).

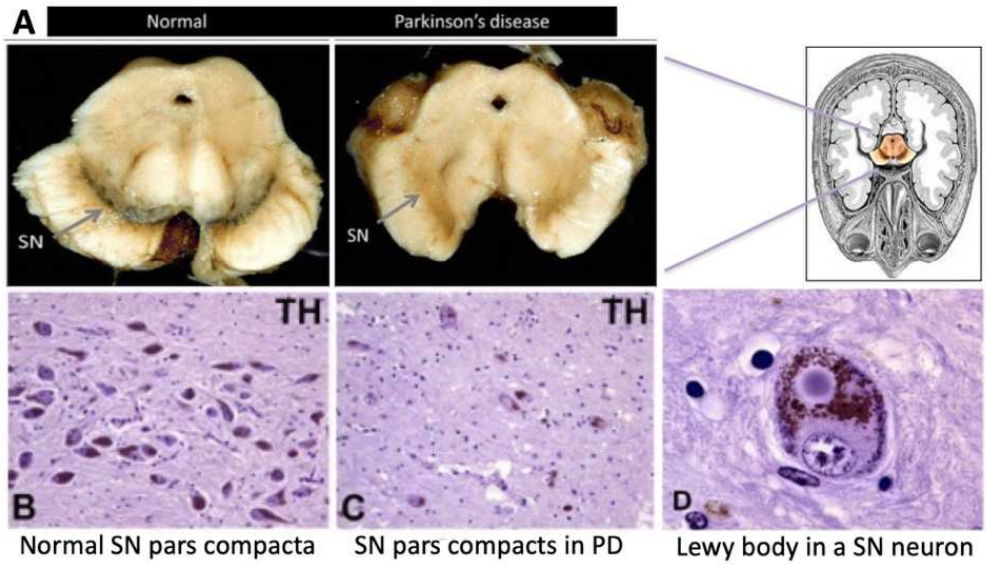

Figure 1-1. The substantia nigra (SN) in the midbrain is the most susceptible region in Parkinson's disease. A) Dopaminergic neurons are lost in PD substantia nigra (pigmented area, with grey arrows). B) Normal substantia nigra showing TH-staining of dopaminergic neurons, which are lost in PD cases (C). D) PD is associated with the buildup of aggregated α-synuclein into cytoplasmic neuronal inclusions termed Lewy bodies (LB). Adapted from D.P.Agamanolis, 2011 (http://neuropathology-web.org/chapter9/chapter9dPD.html).

By the time a patient first presents with the motor symptoms of PD, a significant proportion (50-70%) of the cells in the SNpc have already degenerated and the striatal neurotransmitter DA has been depleted up to 80% (Fearnley & Lees, 1991). This degeneration progresses until, within a few years, most of the cells have died. PD is mainly treated with symptomatic therapies, replacing the low levels of endogenous DA with its precursor levodopa or with DA receptor agonists. After a few years however, these treatments typically lose their effectiveness and important motor complication like dyskinesia can arise (George et al., 2009).

A definite diagnosis of PD can only be made by post mortem findings of DA cell loss in the SNpc and the presence of Lewy pathology in surviving neurons (Lees et al., 2009).

Some DA neurons contain neuromelanin, that is responsible for the normal dark pigmentation of the SN. In advanced PD, loss of pigmented neurons results in gross depigmentation of the SN. The neurotransmitter DA belongs to the family of catecholamines. It is synthesized from tyrosine within the SNpc neurons, but also by other neurons in the brain, within their nerve terminals, where it neuromodulates the glutamatergic neurotransmission of the cortico-striatal pathway, important for coordinating voluntary motor functions (Agamanolis, 2011). The depletion of DA in the striatum results in a net stimulatory effect on the output nuclei of the basal ganglia and the resulting hyperactivity of the motor thalamus confers the typical motor deficiencies of PD (Obeso et al., 2008).

The presence of LBs in the surviving neurons is the second major neuropathological feature of PD after the DA neuronal loss in the SNpc. LBs are cytoplasmic spherical inclusions with a diameter between 8 and 30 μm. Although most neurons contain single LBs, some neurons contain multiple or polymorphic inclusions. Until recent years, it was proposed that LBs primarily contain misfolded, aggregated α-synuclein, but also many other proteins, as well as lipids and other insoluble aggregated proteins including tau, tubulin and ubiquitin (Jellinger, 2012).

Recently, using cutting-edge electron and light microscopy techniques, the majority of LBs contains lipid structures, rather than proteinaceous filaments. α-Synuclein is mixed in with membranes and organelles and does not appear to be in large aggregates. These data support a new model of LB formation, suggesting that excess α-synuclein disrupts membranes and impairs organelle trafficking, leading these types of debris to accumulate and eventually compact into a LB or Lewy neurite (Shahmoradian et al., 2019).

It is important to note that although LBs are characteristic of PD, they also may be found in normal aging and in other neurodegenerative conditions, including dementia with Lewy bodies and multiple system atrophy, collectively called synucleinopathies (Michel Goedert, 2001; Kotzbauer, Trojanowsk, & Lee, 2001).

1.1.3 Clinical Features

PD is characterized by neurological symptoms, including both motor and non-motor features. The onset of disease is gradual and the earliest symptoms might be unnoticed or misinterpreted for a long time (Lees et al., 2009). Non-motor symptoms include impairment of olfaction (hyposmia), constipation, rapid eye movement (REM) and sleep disorder (Schapira & Jenner, 2011). These non-motor symptoms typically characterize the prodromal phase of the disease.

The onset of motor symptoms is typically asymmetric and progressive, with a mean age at onset of 55 years old, although the range is wide (Hoehn & Yahr, 1967). Parkinsonism is the main clinical feature of PD and is characterized by four cardinal motor symptoms, that clinicians usually group under the acronym TRAP: Tremor at rest, muscle Rigidity, Akinesia (or bradykinesia, means slowness of movement) and Postural imbalance. Additional motor impairments can include gait and motor freezing (Lees et al., 2009). PD is clinically diagnosed by the presence of at least two cardinal motor symptoms including bradykinesia and secondary motor or non-motor symptoms as well as the absence of indications for other parkinsonisms than PD. Responsiveness to L-DOPA (L-3,4-dihydroxyphenylalanine), a DA precursor, is often included in the examination to support a correct diagnosis (Lees et al., 2009; Postuma et al., 2015).

Making a diagnosis of PD can be challenging as many conditions including tremor, gait and atypical parkinsonian disorders can mimic PD. Additionally, non-motor symptoms can occur up to 20 years before PD motor onset and could indirectly support the PD diagnosis (Ali & Morris, 2015).

1.1.4 Treatments

Currently, there are no disease-modifying therapies for PD. Symptomatic treatments include administration of DA precursors (levodopa, L-3,4-dihydroxyphenylalanine) or DA receptor agonists. Levodopa therapy remains the most common treatment in the management of motor features of PD. Since prolonged treatment with levodopa often results in side effects that can be more severe that those due to PD, e.g. dyskinesia and

wearing-off, new formulations of levodopa and novel delivery systems are gradually being introduced in clinical practice (Tarakad & Jankovic, 2017).

As the disease progresses, an additional therapy for PD patients whose motor symptoms are not effectively controlled by medication and who do not have dementia is deep brain stimulation (DBS). In DBS, electrodes implanted into the subthalamic nucleus or inner part of the globus pallidus provide electrical stimulation to these structures. This stimulation induces physiological and chemical changes that ameliorate some of the motor symptoms of PD (Agamanolis, 2011).

Since the discovery of familiar mutations in the gene encoding the kinase LRRK2 (as will be discussed later) (Paisan-Ruiz et al., 2004; Zimprich et al., 2004), the identification of specific LRRK2 inhibitors able to halt or slow PD has stimulated much academic and pharmaceutical research, with more than 100 inhibitors developed to date (Zhao & Dzamko, 2019). Denali Therapeutics is currently developing and testing small molecules inhibiting the kinase activity of LRRK2, with no evident side effects reported in phase I clinical trials (https://denalitherapeutics.com/), making LRRK2 inhibitors among the most promising cure for PD.

Several new or repurposing drugs underwent clinical trials or are currently fueling the PD therapeutic pipeline but, at present, none of them has proven to convincingly halt PD progression.

Additional potential therapeutic target in PD includes α-synuclein. Accumulation of misfolded α-synuclein into aggregates has a central place in the pathogenesis of Parkinson's disease (PD) and other related synucleinopathies, such as Dementia with Lewy Bodies (DLB) and multiple system atrophy (MSA).

Several treatment approaches that trying to reduce the level of alpha-synuclein production and/or its aggregation in the cells are currently under clinical trials aiming to reduce neurodegeneration due to misfolded protein (Brundin, Dave, & Kordower, 2017).

1.1.5 Genetics of Parkinson's disease

Over the past two decades, substantial progress has been made in understanding the genetics of PD. Inherited mutations producing rare, monogenic forms of the disease have been discovered in single genes such as *SNCA*, *Parkin*, *DJ-1*, *PINK1*, *LRRK2*, and *VPS35*. Unique variants with incomplete penetrance, such as *LRRK2* and *GBA* have been shown to be strong risk factors for PD (Hernandez, Reed, & Singleton, 2016). More recent genome-wide association studies (GWAS) have highlighted a number of risk factor genes for PD, including *LRRK2* and *SNCA*, suggesting the complex genetic architecture of PD..

1.1.5.1 Monogenic forms of Parkinson's disease

A total of 23 chromosomal loci have been linked to rare monogenic familial forms of PD with Mendelian inheritance (Karimi-Moghadam, Charsouei, Bell, & Jabalameli, 2018). There appears to be an overlap in the genes that contain disease-causing mutations and those that contain risk variants (Table 1-1). Mutations in some genes, for example *SNCA* (*PARK1*; encoding α-synuclein), *LRRK2* (*PARK8*; encoding Leucine-rich repeat kinase 2 or LRRK2), and *VPS35* (*PARK17*; encoding vacuolar protein sorting 35) have been shown to cause autosomal dominant forms of PD. Mutations in other genes, *PINK1* (*PARK6*; encoding PTEN-induced kinase 1), *DJ-1* (*PARK7;* encoding DJ-1), *Parkin* (*PARK2*; encoding parkin), *ATP13A2* (*PARK9*; encoding lysosomal type 5 ATPase), *FBXO7* (*PARK15*; encoding F-box only protein 7), and PLA2G6 (PARK14; encoding phospholipase A2) have been shown to cause autosomal recessive PD and/or parkinsonism (Hernandez et al., 2016). The mutations in these genes, with the exception of LRRK2, cause PD in a small subset of patients. All known monogenic forms of PD combined explain only about 30% of familial and 3–5% of sporadic cases (Kumar, Djarmati-Westenberger, & Grunewald, 2011).

Locus	Gene	Protein	Inheritance
Park1	*SNCA*	α-synuclein	AD
Park2	*PARK2*	Parkin	AR
Park4	*SNCA*	α-synuclein	AD
Park5	*UCHL1*	Ubiquitin C-terminal hydrolase L1	AD
Park6	*PINK1*	Pten-induced putative kinase 1	AR
Park7	*PARK7*	DJ-1	AR
Park8	*LRRK2*	Leucine rich repeat kinase 2	AD
Park9	*ATP13A2*	lysosomal type 5 ATPase	AR
Park11	*GIGYF2*	GRB10 interacting GYF protein 2	AD
Park13	*Omi/HTRA2*	Serine peptidase 2	AD
Park14	*PLA2G6*	Phospholipase A2	AR
Park15	*FBXO7*	F-box only protein 7	AR
Park17	*VPS35*	Vacuolar protein sorting 35	AD
Park18	*EIF4G1*	Eukaryotic translation initiation factor 4 gamma, 1	AD
Park19	*DNAJC6*	DNAJ/HSP40 homolog subfamily C member 6	AR
Park20	*SYNJ1*	Synaptojanin-1	AR
Park21	*DNAJC13*	DNAJ subfamily C member 13	AD
Park22	*CHCHD2*	Coiled-coil-helix-coiled-coil-helix domain 2	AD
Park23	*VPS13C*	Vacuolar protein sorting 13C	AR
-	*SNCA*	α-synuclein	Risk locus
-	*LRRK2*	Leucine rich repeat kinase 2	Risk locus
-	*GBA*	Glucocerebrocidase	Risk locus

Table 1-1. Genes involved in monogenic forms of Parkinson's disease (PD) and identified risk loci. AD, autosomal dominant; AR, autosomal recessive. (Hernandez et al., 2016; Karimi-Moghadam et al., 2018).

1.1.5.2 Risk loci for Parkinson's disease

In addition to the Mendelian forms of PD, genetic risk factors for the disease have been investigated in several candidate genes and in GWAS. Recent GWAS work identified 28 independent disease associated risk loci, following with the largest PD GWA study to date, discovering 39 novel risk loci (Mike A. Nalls et al., 2019; M. A. Nalls et al., 2014; Simon-Sanchez et al., 2009).

The schematic shown in Figure 1-2 provides an overview of the complex genetic architecture of PD with frequency and conferred risk of gene and genetic loci associated with monogenic familial and idiopathic PD.

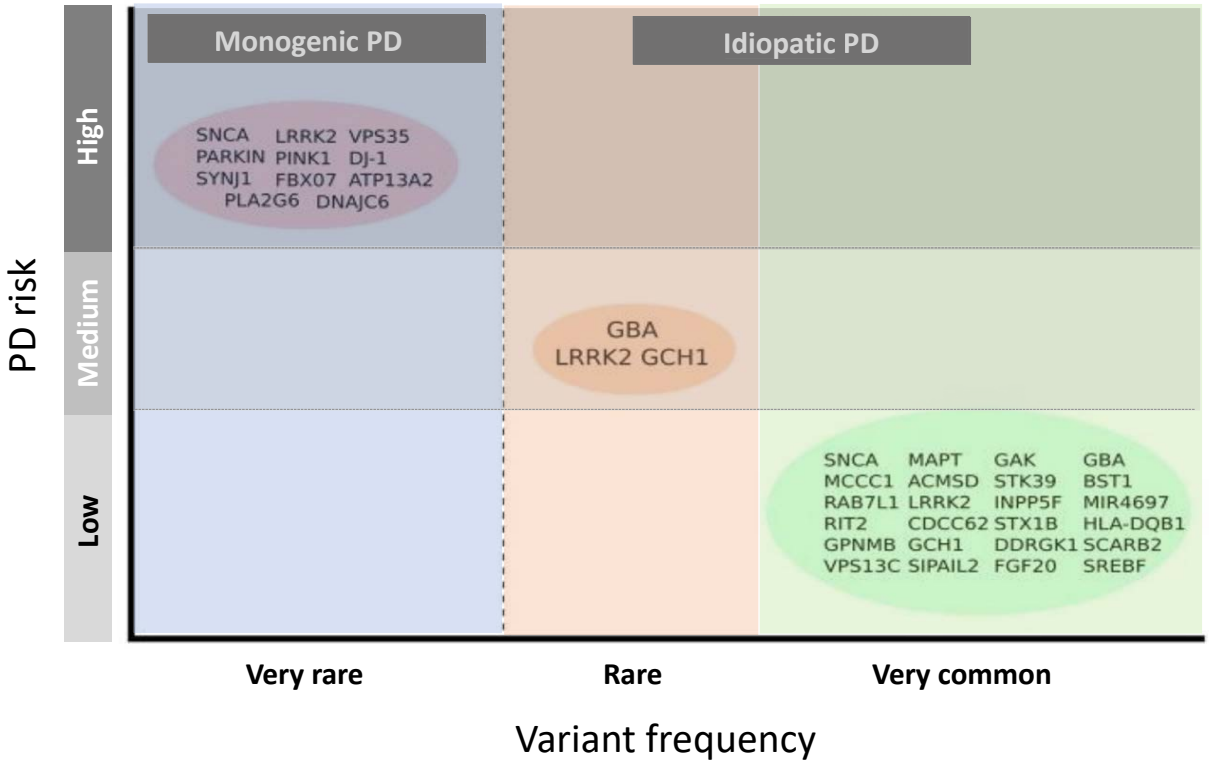

Figure 1-2. Schematic overview of frequency and conferred risk of genes and genetic loci associated with the development of familial and idiopathic PD/parkinsonism. Genes listed in the red circle represent those identified through analysis of familial cases and give rise to monogenic forms of PD. The green circle contains genes in loci nominated as risk factors for idiopathic PD following meta-analysis of all European GWAS data sets. Lastly, the orange circle highlights a number of high-risk variants with reported odds ratios of >5. Image drawn based on (Kumaran & Cookson, 2015).

Both GWAS and candidate gene association studies show that the most statistically significant signals associated with PD are common variants located close to *SNCA* (α-synuclein), *LRRK2*, and *MAPT* (microtubule-associated protein tau) as well as low-frequency coding variants in *GBA* (Billingsley, Bandres-Ciga, Saez-Atienzar, & Singleton, 2018).

Notably, risk loci include *GCH1* (encoding the enzyme GTP cyclohydrolase-1) that catalyzes a cofactor for dopamine synthesis and *HLA* (encoding the major histocompatibility complex), supporting a role for the complement system in PD (Kumaran & Cookson, 2015).

Homozygous mutations in *GBA* gene (encoding the beta-glucocerebrosidase enzyme), cause a lysosomal storage disorder known as Gaucher's disease, while heterozygous mutations confer 5 to 7-fold increase risk for PD (Huang, Deng, Zhong, & Yi, 2018). Screening of PD patients for GBA mutations showed a higher number of heterozygous mutations carriers compared to healthy controls. GBA mutations have been found in 2-4% of PD patients (Aharon-Peretz, Rosenbaum, & Gershoni-Baruch, 2004).

From the combined genetic studies on PD architecture, it is evident that the same loci can show up under different risk categories. This phenomenon has been referred to as pleomorphic risk loci (Singleton & Hardy, 2016).

In addition to identifying specific genes or variants involved in PD, GWAS can enhance our understanding of the mechanism underlying PD pathogenesis. Reports in the literature start to support the functional validation of these risk associations from GWA studies. For example, an unbiased survey of protein–protein interaction arrays showed that GAK and RAB7L1, encoded by genes within PD risk loci, physically interact with LRRK2 implicating these genes as being likely functional candidates at their respective loci (Beilina et al., 2014). Additionally, MAPT aggregates have been reported to be present in both neurons and glia of patients with various forms of parkinsonism (Ludolph et al., 2009).

1.2 LRRK2 and Parkinson's disease

1.2.1 LRRK2 genetics

LRRK2 is located within the *PARK8* locus on chromosome 12, that was identified from linkage analysis of a large Japanese family with familial PD affected in 2002 (Funayama et al., 2002). In 2004 two independent groups identified autosomal dominant mutations in one gene within the locus leucine-rich repeat kinase 2 (LRRK2) (Paisan-Ruiz et al., 2004; Zimprich et al., 2004).

Although more than 100 missense and nonsense coding variants have been reported in LRRK2 (Rubio et al., 2012), only eight have been shown to segregate with familial PD; R1441C/G/H/S, N1437H, Y1699C, G2019S and I2020T (Cookson, 2010; Mata et al., 2016; Paisan-Ruiz, Lewis, & Singleton, 2013), representing relatively penetrant causative variants. In addition, three coding variants in LRRK2, M1646T, A419V and G2385R have been nominated as risk factors (Ross et al., 2011).

All these LRRK2 mutations show age-dependent incomplete penetrance, meaning that some LRRK2 mutation carriers do not show clinical phenotypes during their lifetime (Cookson, 2015). For example, in the case of the relatively common G2019S mutation, penetrance estimates vary between 25% and 42.5% at age 80, meaning that the probability of manifesting the disease for these subjects is relatively low (Hernandez et al., 2016).

Additionally, the G2019S variant accounts for an appreciable percentage of all PD cases, depending on the population (Benamer & de Silva, 2010; Inzelberg, Hassin-Baer, & Jankovic, 2014). G2019S has been found in 5% of familial cases and 2% of apparently idiopathic PD in Caucasian populations. However, up to 40% of familial cases and 13%-40% of sporadic cases have this single mutation in some human populations, including Ashkenazi Jewish and North African Berber Arab populations (Hernandez et al., 2016). Overall, mutations in LRRK2 are the most common known genetic cause of late-onset PD and are found in both autosomal dominant and sporadic cases.

Clinically, patients with LRRK2 mutations are essentially indistinguishable from sporadic PD demonstrating mid to late onset of disease around 60 years of age, with a slow

progression and a good response to levodopa therapy. Neuropathological features are consistent with typical PD, showing α-synuclein-positive LB in the brainstem and loss of pigmented DA neurons that arise in the SNpc and project to the striatum (Cookson, 2017; Haugarvoll & Wszolek, 2009).

Since mutations in LRRK2 cause inherited PD and, additionally, GWA approaches have nominated LRRK2 as a risk factor for sporadic PD (M. A. Nalls et al., 2014), the chromosomal region containing LRRK2 is an example of a pleomorphic risk locus, carrying several different types of genetic risk factors (Singleton & Hardy, 2011).

1.2.2 LRRK2 structure

LRRK2 (Leucine-rich repeat kinase 2) encodes a large 286kDa (2527 amino acids) protein, harboring multiple functional domains with several protein–protein interaction regions surrounding a central catalytic core. This core region contains two enzymatic activities (namely, GTPase and kinase activities) and consist of a GTP-binding Ras-of-complex (Roc) domain, a C-terminus Of Roc (COR) domain and a serine/threonine kinase domain. In addition, several protein interaction domains are located within N-terminal (armadillo, ankyrin and leucin-rich repeat) and C-terminal (WD40 repeats) regions of LRRK2 (Figure 1-3).

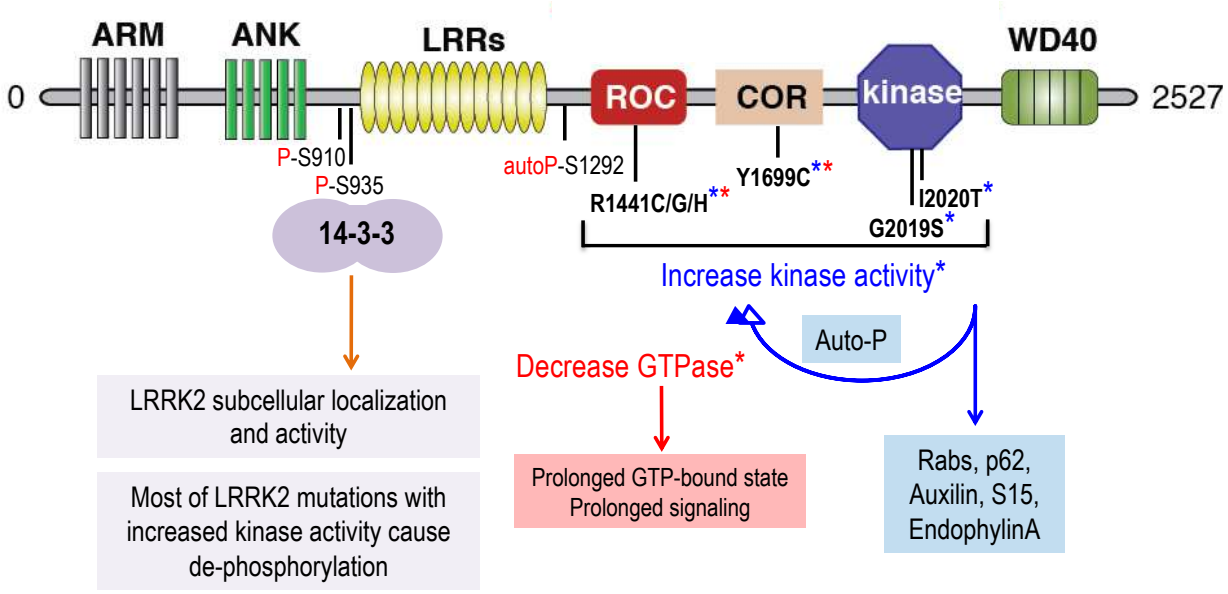

Figure 1-3. Overview of LRRK2 domain architecture. Linear model of the LRRK2 domains and PD-pathogenic mutations.

Interestingly, pathogenic mutations that have been proven to cause PD tend to cluster within the central catalytic core region of LRRK2 (Rudenko & Cookson, 2014). Several studies showed that LRRK2 can form a membrane-associated homodimer with potential intramolecular regulation between its kinase and GTPase activities (Berger, Smith, & Lavoie, 2010; Greggio et al., 2008). These two enzymatic activities of LRRK2 are affected by pathogenic mutations, resulting in correlated effects of persistent signaling.

First, R1441C/G and Y1699C mutations (in the ROC-COR tandem bidomain), diminish the normally modest GTPase activity of LRRK2, potentially keeping LRRK2 in a prolonged active configuration (Daniëls et al., 2010; Lewis et al., 2007; Liao et al., 2014). Second, the G2019S overactive mutation clearly increases kinase activity (Greggio & Cookson, 2009). Both effects are related to the increase signaling from LRRK2 either directly from kinase activity (G2019S) or indirectly through mutation-dependent prolonged GTP-bound state that makes LRRK2 to be associated with persistence of signaling (R1441C/G andY1699C). Making an assumption that these activities are not antagonistic to each other, the “loss” and “gain” of function can be confounding terms in a complex molecule such as LRRK2 (Cookson, 2017). Additional studies suggested that these

activities might be coupled such that the GTPase activity of Roc might modulate the kinase activity through intramolecular regulation (Nguyen & Moore, 2017). This notion is supported by the fact that artificial point mutations disrupting GTP binding (K1347A and T1348N) destabilize the protein and render the kinase catalytically dead (Biosa et al., 2013).

In addition to the catalytic core and its double enzymatic function, other LRRK2 domains harbor multiple phosphorylation sites, including Ser910/Ser935 at the N-terminal part of LRRK2 mediating the binding with 14-3-3 proteins, which is important to control LRRK2 cellular localization and activity (Lavalley, Slone, Ding, West, & Yacoubian, 2016; R. J. Nichols et al., 2010). This interaction is impaired by common LRRK2 mutations, which results in LRRK2 dephosphorylation and relocalization of mutant proteins (N. Dzamko et al., 2010; R. J. Nichols et al., 2010)

1.2.3 LRRK2 substrates

The characterization of LRRK2 kinase activity and its physiological substrates has received a lot of attention for the last 15 years.

LRRK2 has been known to undergo autophosphorylation *in vitro*, with the G2019S mutation, but not other mutations, increasing Vmax by ~2fold (Greggio et al., 2006; West et al., 2005). Autophosphorylation was subsequently shown to occur in cellular systems, specifically occurring at Ser1292 (Sheng et al., 2012).

A long list of heterologous LRRK2 substrates have been proposed (Lobbestael, Baekelandt, & Taymans, 2012; Seol, Nam, & Son, 2019), however only a handful of them have been validated in a cellular context. Among these, a subset of Rab GTPases have been robustly validated as physiological LRRK2 substrates across independent laboratories, representing, together with autophosphorylation, the only independently confirmed substrates known to date (Seol et al., 2019; Steger et al., 2016).

Other candidate substrates such as S15, EndophilinA, p62, Auxilin and few others, for which phospho-specific antibodies were generated, still require independent validation (Kalogeropulou et al., 2018; Martin et al., 2014; Matta et al., 2012).

Of interest, in kinase assays performed in a test tube with isolated proteins only, the G2019S mutation within the kinase domain results in increased kinase activity (West et al., 2005; Greggio et al., 2006). In contrast, all pathogenic mutations, including those outside of the kinase domain are hyperactivating in the cellular environment, suggesting that different but converging mechanisms confer a gain of function to mutant LRRK2, e.g. direct effect on catalytic activity (G2019S) or indirect via abnormal compartmentalization of the signaling via a prolonged GTP-bound state (R1441C/G and Y1699C).

LRRK2 phosphorylation is suggested to be involved in the PD pathological process. Furthermore, treatment of cells with inhibitors of LRRK2 kinase activity are considered as potential disease-modifying therapeutics for PD and leads to a rapid decrease in the phosphorylation levels of LRRK2 (Lobbestael et al., 2012). Understanding the cellular role and regulation of LRRK2 kinase activity and finding its additional substrates has become the focus of intense investigation.

1.2.4 LRRK2 and α-synuclein – genetics and functional interplay

Among all the causative genes, mutations in *LRRK2* and *SNCA* (encoding α-synuclein) have been proven to be associated with autosomal dominant PD. *SNCA* and *LRRK2* loci contain multiple types of risk allele. Both genes contain missense mutations that cause disease and both genes also contain non-coding variability that imparts moderate risk for disease, presumably through modulating expression levels (Hernandez et al., 2016). In addition, LRRK2 contains common protein coding changes that increase risk for disease and SNCA gene multiplications can be causal for PD.

α-Synuclein, a presynaptic neuronal protein, was identified as the major component of LB, the pathological hallmark of PD.

α-Synuclein may contribute to PD pathogenesis in a number of ways. It is generally thought that its aberrant soluble oligomeric conformations (protofibrils) representing toxic species can mediate disruption of cellular homeostasis and cause neuronal death (Stefanis, 2012). However, the molecular mechanisms through which α-synuclein

abnormally accumulates and contributes to neurodegeneration remains debated. Many studies support the hypothesis that the processes of α-synuclein oligomerization and fibrillization play central roles in the pathogenesis of PD and other synucleinopathies (Daher, 2017), although the mechanism by which α-synuclein converts from its physiologic to pathologic form remains to be fully understood.

Additionally, it was proposed that stressors and/or PD-linked mutations may promote a shift in α-synuclein protein from an oligomeric membrane-associated form to a soluble monomeric form prone to misfolding and aggregation (Burre, Sharma, & Sudhof, 2015).

As about 50% of brains of PD cases with LRRK2 mutations exhibit α-synuclein positive LB pathology, one hypothesis is that LRRK2 might function upstream of α-synuclein, modulating its aggregation and toxicity (Zimprich et al., 2004).

Several studies have examined the existence of a link between LRRK2 and α-synuclein aggregation. Experiments showed that LRRK2 WT can modulate aggregation, whereas the PD-linked G2019S LRRK2 mutation enhances aggregation of α-synuclein in primary cultured neurons and in dopaminergic neurons of the SNpc, which is reverted by kinase inhibition (Lewis, 2018; Volpicelli-Daley et al., 2016). However, other studies found opposite results, showing that LRRK2 inhibition does not protect from α-synuclein pathology in non-transgenic mice (Bae et al., 2018) and that LRRK2 kinase activity does not substantially modify α-synuclein aggregation in primary neurons (Henderson, Peng, Trojanowski, & Lee, 2018). Clearly, more investigations are needed to definitively conclude whether LRRK2 modifies α-synuclein pathology.

1.2.5 Cellular functions of LRRK2

Within the brain, both neurons and glial cells express LRRK2, particularly in the striatum, which receives DA projections from the *substantia nigra pars compacta* (SNpc) (West et al., 2014). In addition, several peripheral organs and cell types express LRRK2 including kidney, lung and B cells suggesting that LRRK2 mutations may impact physiological processes and exert disease-relevant roles outside the nervous system (Herzig et al., 2011).

Previous studies have implicated a role for LRRK2 in a wide variety of cellular events, including neurite outgrowth, vesicular trafficking, cytoskeletal function, protein translation, autophagy, regulation of the endo-lysosomal system and the immune system (Rideout & Stefanis, 2014).

Several cellular functions of LRRK2 are regulated by its phosphorylation status, as well as by its GTPase activity, including its dimerization, interactions with other proteins such as 14-3-3 chaperones, and its turnover, as reviewed by (R. Nichols, 2017). There is accumulating evidence, however, that the kinase and the GTPase activities present in LRRK2 are able to regulate one another, therefore understanding how these two activities crosstalk may be required to fully understand LRRK2's role in other cellular pathways (Liu, Mobley, DeLucas, Kahn, & West, 2016).

LRRK2 kinase activity is important for a number of neuronal and non-neuronal processes related to membrane remodeling, including autophagy, vesicular trafficking, and cytoskeletal dynamics although the precise relationship of kinase activity to the etiology of PD is unclear.

There is accumulating evidence that the Roc/GTPase domain, likely in its guanine-nucleotide bound state, is an important intramolecular regulator of LRRK2 kinase activity as well as a platform for interaction with heterologous partners, including PKA, Sec16A, PAK6, clathrin and tubulins (Cogo, Greggio, & Lewis, 2017).

LRRK2 has been demonstrated to play an important role in maintaining neurite length and branching (MacLeod et al., 2006). Such morphological changes may be consequences of LRRK2-modulation of cytoskeletal dynamics through an association of LRRK2 with actin and microtubule structure.

LRRK2 was shown to phosphorylate ERM (ezrin/radixin/moesin) proteins involved in regulation of actin and microtubule structure (Jaleel et al., 2007).

Additionally, in cultured neurons derived from LRRK2 G2019S transgenic mice, the number of pERM-positive and F-actin-enriched filopodia was significantly increased, and this correlated with the retardation of neurite outgrowth (Parisiadou et al., 2009).

It is still an open question whether the regulation of cytoskeleton dynamics is a part of normal LRRK2 physiological function and whether it is altered during disease or if it is a

feature that gains relevance during disease only. Moreover, it is still not clear whether mutations in the GTPase or kinase domain of LRRK2 affect the regulation of cytoskeleton dynamics to the same extent, as discussed by (Wallings, Manzoni, & Bandopadhyay, 2015).

In addition to its role in cytoskeleton dynamics, several recent studies strongly support a role of LRRK2 in vesicular dynamics as was shown through LRRK2 interaction/phosphorylation of multiple vesicle-associated Rab GTPases proteins and of presynaptic proteins [reviewed in (Hur, Jang, Jeong, & Lee, 2019) and (Roosen & Cookson, 2016)].

Accumulating evidence links LRRK2-mediated PD to mitochondrial dysfunction and aberrant autophagy. It was shown that mitophagy is decreased in fibroblasts of LRRK2 G2019S patients compared to healthy controls and inhibition of LRRK2 activity normalized mitophagy rates (Korecka et al., 2019). Of interest, LRRK2 mutations impair mitophagy through excessive phosphorylation of RAB10 (Wauters et al., 2019), mechanistically linking mitochondrial and autophagy dysfunction with impaired kinase function.

1.2.6 LRRK2 and autophagy-lysosomal system

1.2.6.1 Lysosomal dysfunction in the pathogenesis of PD

Lysosomes are dynamic acidic organelles which could degrade intracellular components through several degradation pathways, including endocytosis, phagocytosis, and autophagy by hydrolytic enzymes (Luzio, Pryor, & Bright, 2007).

Emerging evidences indicate that impairment of lysosomal function may contribute to the pathogenesis of PD (J. Q. Li, Tan, & Yu, 2014). Reduced number of intraneuronal lysosomes and decreased levels of lysosomal-associated proteins (LAMP2A and Hsc70) was found in the SNpc and amygdala in postmortem brain samples from patients with idiopathic PD (Alvarez-Erviti et al., 2010). Additionally, lysosomal depletion was shown

to precede autophagosome accumulation and DA neurodegeneration in the neurotoxin treated MPTP-mouse model of PD (Dehay et al., 2010).

The involvement of lysosomal dysfunction in the pathogenesis of PD is also supported by genetic evidence. First, loss-of-function mutations in the *ATP13A2* gene, encoding lysosomal P-type ATPase, have been found in families with a rare hereditary form of juvenile-onset parkinsonism. *ATP13A2* mutations have been shown to contribute to lysosomal dysfunction and accumulation of α-synuclein through compromised Zn^{2+} homeostasis (Tsunemi & Krainc, 2014). However, additional studies are necessary to independently validate this finding.

Additional evident came from a large-scale genetic study confirming a strong association between *GBA* gene and sporadic PD (Sidransky et al., 2009). Mutations in the *GBA* gene cause Gaucher's disease (GD), an autosomal recessive lysosomal storage disorder with compromised lysosomal activity due to accumulation of enzyme glucocerebroside. A high prevalence of PD was previously reported in Gaucher's disease patients (Neudorfer et al., 1996), connecting lysosomal involvement with the pathogenesis of PD.

1.2.6.2 Role of LRRK2 in autophagy-lysosomal pathways

Recent observations suggest that LRRK2 may play a role in autophagy and lysosomal function (Araki, Ito, & Tomita, 2018; J. Q. Li et al., 2014; Roosen & Cookson, 2016).

In the kidneys of LRRK2 knockout animals, there is an accumulation of lipofuscin granules, aggregated α-synuclein and a bi-phasic changes of the autophagosomal markers LC3 (LC3-II accumulation) and the autophagy receptor p62 (degradation) were reported. An initial increase of p62 and LC3-II levels was observed at 7 months with a decrease at 20 months without signs of neurodegeneration (Youren Tong et al., 2010). Similar phenotypic changes, including lipofuscin accumulation and increase in lysosomal markers have been observed in LRRK2 KO rats (Ness et al., 2013). No changes in LC3-II were observed in an independent study of kidneys from 14 month-old LRRK2 KO mice (Herzig et al., 2011). Also, higher levels of the lysosomal protease cathepsin D are seen

in LRRK2 knockout mouse kidneys compared to their wild type counterparts irrespective of age (Y. Tong et al., 2012).

LRRK2 kinase inhibition has also been shown to increase levels of the lipidated autophagosome marker LC3-II and the adaptor protein p62 through Beclin-1 signaling and independently of mTOR/ULK1 signaling, pointing to non-canonical regulation of autophagy in H4 neuroglioma and primary astrocytes (Manzoni et al., 2016).

In contrast to results in H4 cells and LRRK2 knockout mice, in cultured BV2 microglial cells, knockdown of LRRK2 can decrease LC3-II formation after lysosomal inhibition (Schapansky, Nardozzi, Felizia, & LaVoie, 2014). It is possible that an effect of LRRK2 on autophagy can be modulated by a cell type specific signaling and that autophagy regulation may be a downstream consequence of LRRK2 deficiency rather than a primary event (Roosen & Cookson, 2016). Furthermore, in vivo studies have demonstrated, that LRRK2 transgenic mice carrying the G2019S or R1441C mutation show an accumulation of autophagic vacuoles in the cerebral cortex (Ramonet et al., 2011).

The collective data from mutant forms of LRRK2 suggest that their activity decrease LC3 lipidation and result in the accumulation of autophagic vacuoles, which point to the additional effects of mutations in LRRK2 on the overall function of the autophagy-lysosomal pathway, as reviewed by (Roosen & Cookson, 2016).

Overall mutations in the LRRK2 gene may contribute to lysosomal dysfunction, possibly leading to the formation of Lewy body protein aggregates and neurodegeneration. Since lysosomal function is impaired in PD, LRRK2 inhibition may potentially restore lysosomal homeostasis and modify disease progression in patients with a genetic LRRK2 mutation as well as those with sporadic PD. Restoration of lysosomal levels and function may represent a novel neuroprotective strategy in PD (Dehay et al., 2010). Indeed, several clinical studies are currently testing the value of a therapeutic approach directed at improving lysosomal function (Zhao & Dzamko, 2019).

1.2.7 LRRK2 mouse models

Transgenic animals overexpress human or mouse LRRK2 in the whole body or selectively in the brain, while knock-in mice harboring disease-linked mutations in their endogenous *Lrrk2* gene, which should be more relevant to the physiological condition (Araki et al., 2018). However, these mouse models do not generally show apparent histopathological changes relevant to PD, such as selective loss of DA neurons or motor dysfunction (Xiong, Dawson, & Dawson, 2017). There is evidence, however, of impaired DA neurotransmission upon amphetamine stimulation in R1441C knock-in mice suggesting impaired function in the dopamine D2 receptor (Y. Tong et al., 2009). Furthermore, mitochondrial abnormalities in the striatum of older homozygous G2019S knock-in mice were reported as well as a significant reduction in the extracellular dopamine induced by amphetamine, in addition to increased staining of microtubule-associated protein tau (MAPT) in the striatum, strengthening the link between *LRRK2* and *MAPT* (Yue et al., 2015).

Overall, although these results suggest that PD mutant forms of LRRK2 mice impair DA transmission, there is lack of manifestation of the significant PD hallmarks, suggesting that these mice may represent pre-symptomatic models of early pathological events.

Some transgenic mouse models overexpressing human LRRK2 with PD-associated mutations have been reported. For example, the progressive degeneration of dopaminergic neurons and reduced neurite complexity and autophagic abnormalities were reported by overexpression of human LRRK2 bearing G2019S mutation (Ramonet et al., 2011). Additionally, transgenic mouse model overexpressing R1441C pathogenic LRRK2 mutation displayed motor deficits by the age of 16 months and reported to exhibit the reduction in the number of substantia nigra DA neurons (Weng et al., 2016). Although those models artificially exaggerate the level of mutated LRRK2, they still provide an important insight into the pathogenic effects of familiar LRRK2 mutations.

Of interest, high levels of either LRRK2 WT or G2019S mutant in brainstem and cortical neurons did not alter endogenous α-synuclein or Tau levels and did not exacerbate or otherwise modify α-synucleinopathy (Lewy pathology) (Herzig et al., 2012).

Since none of the current LRRK2 animal models fulfills all the key features of PD and along with the evidences of incomplete penetrance of LRRK2 mutations in PD patients (Bonifati, 2007; Xiromerisiou et al., 2012), it is possible that additional genetic or environmental factors might be necessary for mutant LRRK2 to trigger nigral cell loss in short living animals such as mice (J. W. Lee & Cannon, 2015).

Up to date, animal models represent powerful tools in the reconstruction of the pathways that are physiologically relevant and potentially deregulated during pathology and probably will be in use for some time until substituted with models better recapitulating PD pathology.

1.3 LRRK2 and inflammation

1.3.1 Inflammation in PD

Inflammation has been closely associated with the pathophysiology and etiology of neurodegenerative diseases, including PD (N. L. Dzamko, 2017; Pradhan & Andreasson, 2013). Although it is still controversial whether inflammation represent a causative or a secondary effect of earlier pathological events of PD, there is an increasing recognition of neuroinflammation as a major player in the PD pathology (Isabella Russo, Bubacco, & Greggio, 2014).

Supporting evidence for a role of inflammation in PD has recently emerged from GWAS. Specifically, polymorphisms in genes encoding inflammatory cytokines such as TNF-α and IL-1β, and HLA (cell-surface human leukocyte antigen) are associated with a higher risk of developing PD (Bialecka et al., 2008; Hamza et al., 2010). These genes are expressed in peripheral immune cells and brain glial cells and are directly involved in the inflammatory process.

Supporting an important role of neuroinflammation in PD, increased number of activated microglial cells and reactive astrocytes surround the degenerating neurons of PD brain (McGeer, Itagaki, Boyes, & McGeer, 1988).

Widespread microglial activation was observed in PD, particularly in the striatum, but also in hippocampal and cortical regions (Imamura et al., 2003). Additionally, neuroinflammation is characterized by increased reactive oxygen species (ROS) production, elevated cytokine levels in the brain and CSF (Cerebrospinal fluid) and by infiltration of peripheral immune cells into brain's parenchyma (Kozina et al., 2018).

Microglia cells, the resident macrophages of the brain, mediate the innate immune response in the brain, and are considered to be key players during neuroinflammation

(Lenz & Nelson, 2018; Isabella Russo et al., 2014). A current hypothesis is that inflammation may play a role in the prodromal stages of the disease even preceding the onset of PD (J. Q. Li et al., 2014). Blocking the early phase of neuroinflammation by anti-inflammatory drugs or specific anti-cytokine inhibitors has been shown to attenuate the PD-like disease process, at least in preclinical models, as reviewed by (J. Q. Li et al., 2014), but additional studies need to confirm this preliminary findings.

1.3.2 Interaction of LRRK2 and α-Synuclein in the Immune System

It was reported in the literature that LRRK2 expression in myeloid cells is correlated to pro-inflammatory responses induced by α-synuclein overexpression in the SNpc and LRRK2 KO rats are protected from DA neurodegeneration induced by the potent myeloid cell agonist lipopolysaccharide (LPS) (Daher, 2017).

With regard to the association between LRRK2 and α-synuclein, it has been reported that LRRK2 knock-out (KO) attenuates the neuropathology induced by α-synuclein overexpression in mouse brain through a delay of neuronal death resulting from improved structure and function of the Golgi complex (Lin et al., 2009). Although the study was mainly focused on neurons, activation of microglia in the striatum of *A53T*/*LRRK2* mice was observed, suggesting the contribution of immune response.

Russo and colleagues demonstrated that LRRK2 kinase activity modulated the induction of pro-inflammatory mediators (i.e., IL-1β cytokine, protein kinase A, NF-κB p50) in primary microglia cultures treated with LPS or α-synuclein fibrils (I. Russo et al., 2015).

In the brain, microglial α-synuclein clearance is closely related to neuronal survival. A study investigating α-synuclein clearance showed that in LRRK2-KO microglia, α-synuclein was taken up in larger amounts and cleared from the supernatant more effectively than for microglia isolated from wild-type (WT) mice, accompanied by down-regulation of the endocytosis pathway. This suggests that LRRK2 negatively regulates the clearance of α-synuclein (Maekawa et al., 2016).

Overall, multiple studies indicate that LRRK2-mediated exacerbation of α-synuclein neuropathology might be cell type and brain region dependent (Daher, 2017). Since microglia and myeloid cells represent part of innate immune system, the interplay between LRRK2 and α-synuclein toward pro- or anti-inflammatory response might represent part of the defense function.

1.3.3 LRRK2 involvement in inflammatory response

Many early LRRK2 studies were focused primarily on its function in neurons. However, LRRK2 expression is not only limited to neural cells, but also can be expanded to antigen-presenting cells of the innate immune system including microglia, monocytes and B-cells, as well as in adaptive human immune cells (N. L. Dzamko, 2017; Hakimi et al., 2011).
An increasing number of publications suggest a role for LRRK2 in modulation of the neuro-immune response (N. L. Dzamko, 2017; Isabella Russo et al., 2014; Tansey & Goldberg, 2010).
Additionally, genetic evidence also links LRRK2 to disorders with a strong immune component. GWAS revealed a possible involvement of the *LRRK2* locus in the autoimmune Crohn's disease and *Mycobacterium leprae* infection (Fava et al., 2016; Umeno et al., 2011), raising the possibility that mutations in LRRK2 may modify immunogenic responses in PD (Schapansky, Nardozzi, & LaVoie, 2015).

It has been shown that LRRK2 is abundantly expressed in immune cells, such as microglia, BMDMs (Bone-marrow-derived macrophages) and B-cell lymphocytes and enhances NF-κB-dependent transcription, thereby suggesting a role within immune signaling (Kozina et al., 2018; Price, Manzoni, Cookson, & Lewis, 2018).
A number of studies have revealed a deficiency or alteration in the immune response upon knockdown of LRRK2 (B. Kim et al., 2012; Wandu et al., 2015) and additionally, LRRK2 has been shown to be a potential substrate for proteins such as the cytokine IFN-γ (Gardet et al., 2010), which is a critical regulator of immune responses and inflammation.

Recent studies of innate immunity, involving macrophages and microglia, have shown that endogenous LRRK2 expression is up-regulated upon cell activation (H. Lee, James, & Cowley, 2017). For example, some groups have reported significant up-regulation of LRRK2 protein expression by stimulation with LPS (a general inflammagen and TLR4-receptor agonist) in primary mouse microglia or in THP-1 cells (Gillardon, Schmid, & Draheim, 2012; Moehle et al., 2012), whereas others did not detect any changes in primary mouse microglia (I. Russo et al., 2015) or mouse bone marrow-derived macrophages (BMDMs) (N. L. Dzamko, 2017).
From a mechanistic point of view, LRRK2 kinase activity negatively regulates protein kinase A (PKA), impacting NF-κB p50 signaling and the inflammatory response in microglia cells. Interestingly, primary microglia carrying LRRK2 G2019S pathological mutation with overactive kinase exhibit an increased inflammation upon priming with α-synuclein pre-formed fibrils (I. Russo et al., 2018).
Recently, it was reported that intraperitoneal injections with LPS caused accelerated neuroinflammation in R1441G transgenic mice in comparison to WT, which was not mediated by dysfunctional microglia or monocytes, but rather by peripheral circulating cytokines and inflammatory proteins in leucocytes (Kozina et al., 2018).
In summary, these studies suggest that LRRK2 can play a role as a positive regulator of inflammation in the different cells of the innate and adaptive immune system. Additionally, LRRK2 mutations may alter the microenvironment of the brain to favor neuroinflammation which, in turn, may lead to predisposition to PD or modifying disease progression.

Overall, additional investigations are required to shed light into the conflicting results about the contribution of microglial LRRK2 to the pathogenesis of PD.
In the second part of the introduction, I will focus on microglial overview and its role in neuroinflammation.

1.4 Microglia

1.4.1 Discovery of microglia

In 1856, **Rudolf Virchow** introduced the concept of neuroglia ("Nervenkitt," meaning nerve-glue), defining glial cells as a population in the brain that is distinct from neurons [for historical review, see (Rezaie & Male, 2002)].
In the early 1870s a major discovery in neuroglia research was empowered by **Camillo Golgi** and his famous "Reazione nera" (Black reaction), that allowed him to obtain the best images so far of neurons and neuroglia tissue stained in black against a light yellow background (De Carlos & Borrell, 2007).
In the following decades, there was a debate regarding the neuroglia's cellular entity. These cells eventually received a new name: astrocytes. At the beginning of the 20th century, neuroanatomist **Santiago Ramón y Cajal** described a population of "apolar cells" in addition to neurons and astrocytes (known today as oligodendrocytes and microglia together). Using an improved staining method of Golgi's black reaction, he defined these cells as "corpuscles without processes" and called them a 'third element' of the central nervous system [reviewed by Sousa C. et al (Sousa, Biber, & Michelucci, 2017)].
Later, in 1919, **Pio del Rio Hortega** characterized the morphology of microglia cells (Figure 1-4), distinguishing them from oligodendrocytes using his silver-carbonate staining method. Moreover, Rio Hortega realized that what Ramon Cajal reported as "corpuscles without processes" was in fact a limitation of his gold chloride-sublimate method that did not allow the complete observation of these cell processes (Helmut Kettenmann & Verkhratsky, 2008).

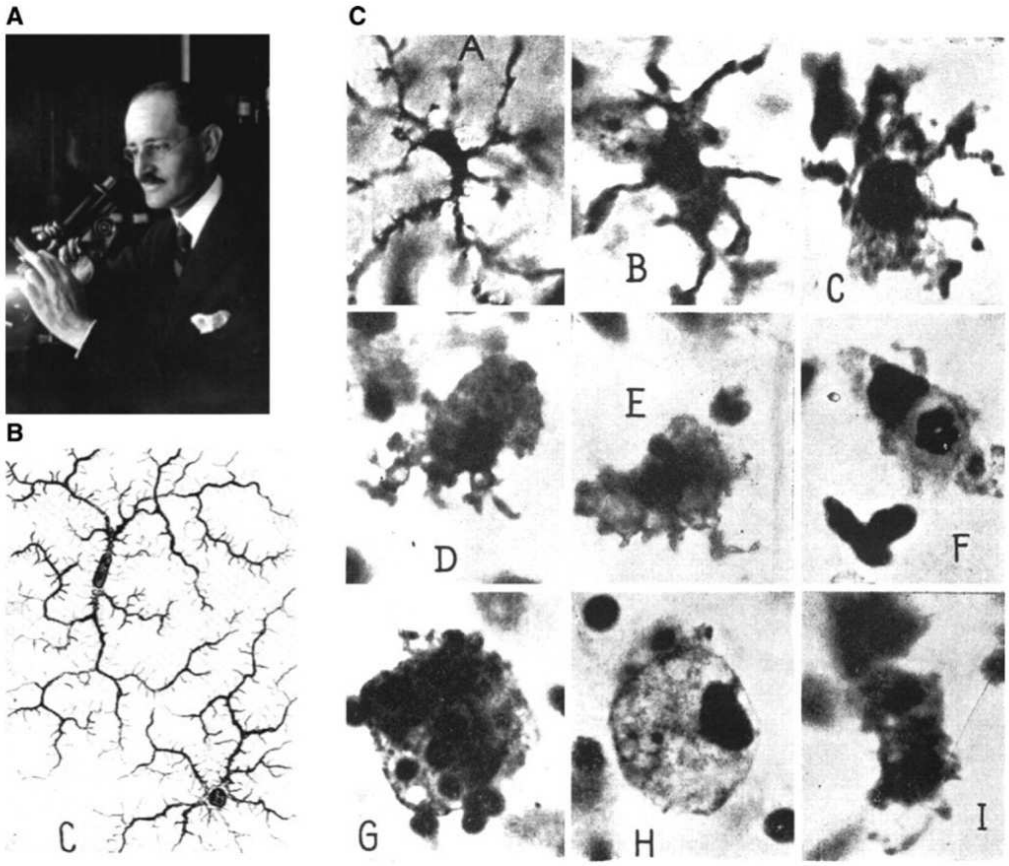

Figure 1-4. Microglial cells discovered by Pio del Rio-Hortega. *A*: Pio del Rio-Hortega (1882–1945). *B*: images of ramified microglial cells drawn by Hortega. *C*: evolution of microglia during its phagocytic activity. [Photomicrographs from del Rio-Hortega, 1932.] Image reproduced from (H. Kettenmann, Hanisch, Noda, & Verkhratsky, 2011)

In 1930, Isaac Costero introduced the first *in vitro* culture method of microglial cells from human brain and recorded their activity using time-lapse cinemicroscopy. This finding predicted microglial motility, which was confirmed in experiments almost one century later [for historical review, see (Rezaie & Male, 2002)].

In 1960s the pioneering work of George Kreutzberg's group discovered that microglia and astrocytes are implicated in the regenerative process after the disruption of the facial nerve **(Blinzinger & Kreutzberg, 1968)**. A major finding was that activated microglia physically interact with neurons by removing synaptic terminals, now known as "synaptic

stripping". These findings expanded the known microglial role in phagocytosis to the potential neuroprotective role in neuronal regeneration.
From the 1980s, microglial research was stimulated with the technical advances of immunohistochemistry and studies on the origin and identity of brain macrophages (Menassa & Gomez-Nicola, 2018).

1.4.2 Origin of Microglia

Microglia are the resident macrophages of the central neural system (CNS) parenchyma, which dynamically screen their surrounding for signs of infection or cell distress. Microglia are activated by either pathologic events or changes in brain homeostasis (Casano & Peri, 2015). In mice, microglia derive from the embryonic yolk sac myeloid progenitors and enter the CNS early in development (around embryonic day 9) before the blood-brain barrier is formed. This is in contrast to adult peripheral macrophages that arise from the fetal liver (Ginhoux et al., 2010). As development proceeds, microglia transition from an amoeboid to a highly ramified morphology with multiple fine processes that display a constant motility within neural tissues.

In humans, microglial-like cells can already be detected at 13 weeks of gestation, whereas ramified microglia are detected at week 21 (Wolf, Boddeke, & Kettenmann, 2017). Brain microglia are a self-sustaining population within the CNS. Recent findings have shown that it is critical for brain homeostasis that microglial cell numbers are stably maintained, because having reduced numbers results in behavioral and learning deficits (Parkhurst et al., 2013).

1.4.3 Microglial population in the brain

The microglial population in the adult rodent brain accounts for 5 to 12% of the total number of brain cells (Furube, Kawai, Inagaki, Takagi, & Miyata, 2018). In human brain, microglia show significant regional differences ranging from 0.5% to 16.6% of all cells in

the brain parenchyma with more microglia in white than in gray matter (Mittelbronn, Dietz, Schluesener, & Meyermann, 2001). The microglial density in both, mouse and human brain, remains remarkably stable, but microglia turnover several times during a lifetime (Askew et al., 2017).

Notably, human microglia, unlike most other hematopoietic lineages, renew slowly at a median rate of 28% per year. They have an average age of 4.2 years and some microglia last for more than two decades (Reu et al., 2017). Most immune cells do not live longer than a few days or weeks (Macallan et al., 2005), making microglia one of the slowest dividing immune cells described to date.

1.4.4 Physiological functions of microglia

Microglia represent an integral part of CNS network. Microglial processes constantly scan through their environment and establish frequent transient contacts with neighboring neurons and astrocytes (Figure 1-5).

Within their normal environment, microglia can interact with neurons, astrocytes and oligodendrocytes. They express transmembrane protein 119 (TMEM119), P2Y purinoceptor 12 (P2RY12) and Sal-like protein 1 (SALL1) as specific markers (M. L. Bennett et al., 2016; Buttgereit et al., 2016).

Microglia cells represent parenchymal macrophages and express low levels of $CD45^{(low)}$ and MHC $II^{(low)}$ markers, which distinguish them from three other major types of non-parenchymal brain-resident macrophages, namely meningeal, perivascular and choroid plexus macrophages. All brain macrophages, including microglia, maintain their populations by self-renewal under normal conditions, except choroid plexus macrophages that receive input from the circulation (Q. Li & Barres, 2018).

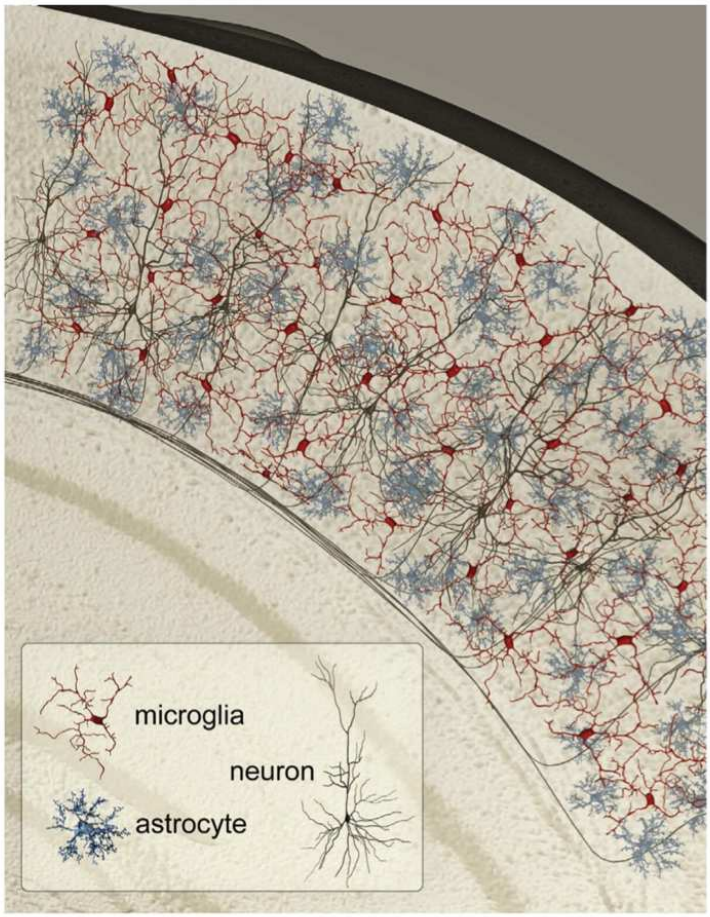

Figure 1-5. Distribution of microglia in the central nervous system, CNS. Throughout the central nervous system microglia (red) surveys neuronal networks (black) and astrocytes (blue). Both microglia and astrocytes tile the entire brain with the minimal overlap in the three-dimensional space. However, processes of one cell type can strongly overlap with territories of the other cell type. Image reproduced from (H. Kettenmann, Kirchhoff, & Verkhratsky, 2013)

During postnatal stages, microglia promote synapse maturation and remodel neural networks by pruning immature synapses. The receptors of the complement cascade have been identified as an important factors for controlling synaptic pruning in the nervous system (Stevens et al., 2007). Weak synapses are removed through a process that is

dependent on the complement components C1q and C3 and the microglial complement receptor 3 (CR3) (Brown & Neher, 2014; M. E. Tremblay et al., 2011).

In the adults, microglia modulate neuronal activity and phagocytose myelin, which is considered to be a mechanism for myelin turnover (Q. Li & Barres, 2018). Phagocytic recognition leads to the removal of neuronal structures or live cells, contributing to CNS homeostasis (Brown & Neher, 2014), (Figure 1-6).

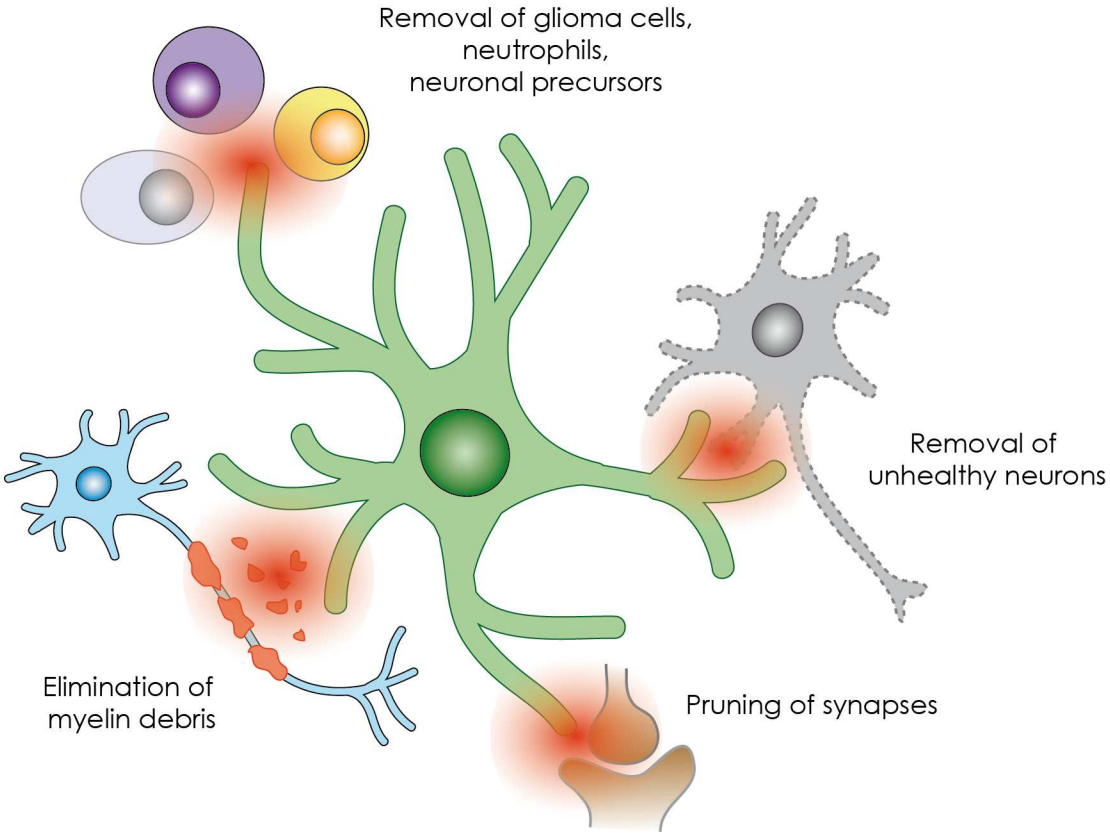

Figure 1-6. **Microglial phagocytosis of live cells and neuronal structures.** The figure illustrates situations in which phagocytic recognition leads to the removal of neuronal structures (synapses and neurites), live cells (glioma cells, neutrophils, neuronal precursors and stressed-but-viable neurons) and myelin debris in the CNS. Redrawn from (Brown & Neher, 2014).

Overall, there are no periods of inactivity for microglia and surveillance and phagocytic functions are important for the active maintenance of CNS homeostasis by microglia cells [reviewed by (H. Kettenmann et al., 2011)].

1.4.5 Microglial response to CNS injury and inflammation

In response to pathological stimuli or tissue damage, microglia undergo morphological changes and migrate toward the site of injury, where they play important roles in inflammatory reactions and neuronal damage. Within minutes of brain damage, microglial processes rapidly extend toward the injured site. The chemoattractive response is triggered by ATP released at the site of injury and the consequent activation of the purinergic receptor P2Y12R on microglia (Ohsawa & Kohsaka, 2011).

Upon activation, the shape of microglia shifts from a highly branched and ramified morphology to an amoeboid form becoming an active phagocyte. The activation process is highly diverse and depends on the context and type of stress. In the activated form, microglia release various substances such as reactive oxygen species (ROS), cytokines, chemokines or growth factors, which influence the pathological process during the acute and chronic phase as well as during subsequent regeneration. Microglia help to arrange the immunological response by interacting with infiltrating immune cells and can influence neuronal survival either in a positive or in a negative direction (H. Kettenmann et al., 2011; Wolf et al., 2017).

1.4.6 Impact of aging and neurodegenerative disease on microglia transcriptome

On one side, microglia influence neurodegenerative disease severity and progression in the aging brain and, on the other side, perturbation of brain environment deeply affects microglia phenotype and functionality (Crotti & Ransohoff, 2016).

In the last few years, genome-wide approached (RNA-seq and ChIP-seq) have been used to investigate transcriptomic and epigenomic profiles of microglia. Differences in the transcriptome between microglia and macrophages were recently reported (Butovsky et al., 2014; Hickman et al., 2013). It was shown, however, that microglia and other macrophages share many similarities, including the ability to phagocytose and secrete pro-inflammatory cytokines.

The characterization of cell surface molecules, termed the "microglia sensome" have been identified as enriched in microglia in comparison to the whole brain and included genes encoding receptors, clusters of differentiation markers and some secreted proteins (Hickman et al., 2013).

In summary, *Hexb, Tmem119, Olfml3, P2ry12, P2ry13, Crybb1, Cx3cr1, Fcrls, Itgb5, Rnase4, Slc2a5, Gpr34, Siglech, Gpr84 and Socs3* are genes that have been consistently reported to be distinctive for microglia among murine peripheral immune or brain cells [reviewed by (Crotti & Ransohoff, 2016)], although, some, for example, Cx3cr1 could be also expressed by monocytes infiltrating the brain.

In the aged brain, microglia have been described as "primed",i.e., more responsive and producing an exaggerated transcriptional and morphologic reaction to disturbance of homeostasis as result of persistent exposure to misfolded proteins or neuronal debris. Priming makes the microglia susceptible to a secondary inflammatory stimulus, which, in elderly individuals, most commonly arises from a systemic disease with an inflammatory component (Perry & Holmes, 2014).

Examination of age-related changes in the microglial transcriptome has shown downregulation of genes involved in perceiving endogenous ligands (such as *P2yr12*, *P2ry13*, *Adora3*, and *Siglech)* without changes in genes that sense microbial ligands. It has been hypothesized that aging microglia retain products associated in the periphery with defense against infectious pathogens, but progressively lose the components needed for sensing endogenous debris (Hickman et al., 2013).

Neurodegeneration triggers microglia reactivity with nonspecific changes in morphology and increased microgliosis. For example, microglial activation, has been shown in PD *post-mortem* studies and also most recently on *in vivo* PET imaging analysis of

prodromal (REM sleep disorder patients) and diagnosed PD patients (Gerhard et al., 2006; Stokholm et al., 2017).

RNA-seq analyses have been performed with microglia purified from mice with different neurodegenerative disease models, such as Multiple sclerosis (MS), Amyotrophic Lateral Sclerosis (ALS), Alzheimer's disease (AD). An overview of expression of mouse microglia signature genes in aging and various disease conditions has been reported by Crotti and Ransohoff (Crotti & Ransohoff, 2016).Overall, the authors observe that microglia acquire an inflammatory phenotype and simultaneously express neurotoxic and neuroprotective factors.

A recently identified subset of brain resident disease-associated microglia (DAM) was found at sites of neurodegeneration, but not in other regions in an AD mouse model (Keren-Shaul et al., 2017). DAM show a unique transcriptional and functional signature and are equipped with a dedicated sensory mechanism, which includes the Trem2 signaling pathway to detect damage within the CNS [reviewed by (Deczkowska et al., 2018)].

Genes expressions study in postmortem tissues of AD and ALS but not PD revealed significant changes among DAM genes according to single report from Bennet et al (J. P. Bennett, Jr., Keeney, & Brohawn, 2019). This may reveal that the genomic profiles of microglia can be unique in each neurological disease context.

1.4.7 Advanced tools to study microglia

For the last several years, the most widely used method for the isolation of microglial cells was the mechanical shake-off (Tamashiro, Dalgard, & Byrnes, 2012), which is based on differential adherence properties between microglia and astrocytes, producing microglia primary cultures. Recently, the introduction of a magnetic cell sorting (MACS-sorting) using CD11b microbeads improved the yield of microglial cells and allowed the accurate separation of microglia from astrocytes, reviewed by Sousa and colleagues (Sousa et al., 2017). This method has opened the possibility to isolate microglia cells directly from the adult mouse brain and to use the isolated cells in many downstream applications

including, but not limited to bulk or single cell RNA sequencing, ATAC-sequencing and in ex-vivo functional assays.

Generation of Human iPSC-Derived Microglia-Like Cells (*in vitro* pluripotent stem cell-derived MGLCs) have been described recently by several groups (Muffat et al., 2016; Pandya et al., 2017). This platform can serve as a valuable model to study microglial function and the impact of mutations, for example the immune receptor TREM2 on microglial cells, that confers an increased risk of developing neurodegenerative disorders (Garcia-Reitboeck et al., 2018).

Additionally, recent experiments modeling PD in midbrain-like 3D organoids derived from PD patients carrying the LRRK2-G2019S mutation have been shown to recapitulate disease-relevant phenotypes. Results have demonstrated a decrease in the number and complexity of midbrain dopaminergic neurons (mDANs) in LRRK2-G2019S compared to control organoids (Smits et al., 2019). The robust method to reproducibly generate 3D human midbrain organoids containing mDANs opens the possibilities of co-culturing them with the brain-derived microglia to explore the microglial-neuronal interaction and to investigate PD-relevant mechanisms.

In order to characterize microglia in vivo in their biological environment, Jung and colleagues developed the fractalkine receptor *Cx3cr1*^{GFP} knock-in mouse model with GFP-labeled microglia (Jung et al., 2000). Although *Cx3cr1* is also expressed by other mononuclear phagocytes and not exclusively restricted to microglia, the use of this animal model is still having a tremendous impact on the field of microglial study.

Lately, the discovery of the brain-specific microglial marker Tmem119 (M. L. Bennett et al., 2016), has led to the development of two new Tmem119 mouse lines: knock-in mice expressing EGFP for specific microglia labeling and CreERT2 mice for manipulation of microglia (Kaiser & Feng, 2019). These mouse models will serve as a valuable tool to specifically study the role of microglia in healthy brain environment as well as in neuroinflammatory and neurological disease.

Another field of study of microglia is related to gene therapy. Adeno-associated viruses (AAVs) are commonly used for *in vivo* gene transfer. Recently, the use of CD68 promoter

in combination with a novel capsid-modified AAV6 vectors, have demonstrated selective microglial transduction *in vivo (Rosario et al., 2016)*. Characterization of recombinant-AAVs that specifically transduce microglia would allow physiologically relevant disease modeling and development of glia-targeted immuno-biotherapies.

To fully understand the role of microglia in neurological disorders, it is critical to study human microglia from brain donors. Recent studies have demonstrated successful isolation method of pure microglia from human post-mortem brain tissue using density gradient and CD11b+ purification with magnetic beads (Mizee et al., 2017).

The recent advances in single cell technology, namely single cell RNA-sequencing, have raised the new horizons in transcriptome characterization of microglial cells. Numerous studies have been investigating mouse (Hammond et al., 2019; Keren-Shaul et al., 2017; Mathys et al., 2017) and human (Masuda et al., 2019; Olah et al., 2018) microglial states in association with neurological disorders and aging brain.

Overall, the described new approaches, will certainly contribute in our understanding of microglial complexity and their interaction with other brain cells. This will bring us a step closer to understanding of neurological disorders including PD.

Chapter 2

Aims of the project

The main goal of this PhD project was to investigate the contribution of microglial cells to the pathogenic mechanisms behind LRRK2-associated Parkinson's disease (PD).

This work is divided into to two main aims:

First: To perform RNA-seq analysis of primary microglia isolated from LRRK2 WT and KO mice treated with inflammatory stimuli (α-synuclein fibrils or LPS) and to validate the RNAseq data on primary microglia.
Second: To characterize resident microglia acutely isolated from the adult brains of LRRK2 WT, KO and knock-in mice carrying two PD-associated mutations (G2019S and R1441C) stimulated with the inflammagen lipopolysaccharide (LPS).

These specific aims can be broken down into the following sub-aims:

1. Perform RNA-sequencing of primary microglia isolated from LRRK2 WT and KO mice treated with α-synuclein pre-formed fibrils (PFFs) or with LPS.
2. Validate gene candidates at the transcript and protein level using qRT-PCR and western blot analysis.
3. Evaluate cytokine profile of α-synuclein PFFs and LPS-treated microglia.
4. Isolate and characterize resident microglia from adult mouse brain of LRRK2 WT, KO and mutant mice.
5. Perform a functional analysis of isolated resident microglia using ex-vivo phagocytic assay.
6. Perform morphological analysis of intrastriatally injected brain microglia from LRRK2 WT, KO, G2019S and R1441C mice.
7. Evaluate gene candidates in resident brain microglia using single cell RNA-seq analysis from WT and KO mouse brains.
8. Determine endogenous LRRK2 protein levels in resident isolated microglia.

Chapter 3

Material and Methods

3.1 Animal handling approach

3.1.1 Animals and ethical approval

All animal procedures were carried out in strict accordance with the recommendations issued in the guidelines for the Care and Use of Laboratory Animals of the National Institutes of Health (NIH) for animals housed at NIH and for the European Community Council Directive 2010/63/UE for animals housed at University of Padova. The protocols were approved by the Institutional Animal Care and Use Committees of the US National Institute on Aging (Approval number 463-LNG-2021) and by Ethics Committee of the University of Padova (Project ID: 1041/2016-PR), respectively. The mice were housed in a pathogen-free environment on a 12 hours light/dark cycles, food and water were provided *ad libitum*.

For Lrrk2 WT mice experiments were performed using C57BL/6J mice (NIH/NIA/ Bethesda, USA). Two different Lrrk2 Ko mice have been used in the experiments, both bred to be congenic on a C57BL/6J background. Lrrk2-KO mice with exon-2 deletion (Parisiadou et al., 2009) were used for the initial RNA-Seq experiment, for technical validation experiments and to confirm time course data at the mRNA level. Additionally, Lrrk2-KO mice with exon-41 deletion (Hinkle et al., 2012) were used to future validate time course data at protein level and differences between genotypes. Lrrk2 G2019S KI mice (Yue et al., 2015) was kindly provided by Dr. H.L.Melrose (Mayo Clinic, FL, USA) and was cross-bred to local C57BL/6J. Lrrk2 R1441C KI (Y. Tong et al., 2009) was kindly provided by Dr. Huabin Cai (NIH, Bethesda, USA) and was cross-bred to local C57BL/6J. *Cx3cr1*$^{GFP/+}$ and *Cx3cr1*$^{GFP/GFP}$ microglia-reporter mice (Jung et al., 2000), Jackson model B6.129P-Cx3cr1^{tm1Litt}/ J were backcrossed onto a C57BL/6J background.

3.1.2 Genotyping

For the characterization of the brain resident microglia, Lrrk2$^{+/+}$, Lrrk2$^{-/-}$, G2019S$^{+/+}$ and R1441C$^{+/+}$ mice were first cross-bred with *Cx3cr1*$^{GFP/GFP}$ mice to obtain heterozygous cohorts and then additionally intercrossed to produce homozygous Lrrk2$^{+/+}$, Lrrk2$^{-/-}$, G2019S$^{+/+}$ and R1441C$^{+/+}$ mice in Cx3cr1 heterozygous (Cx3cr1$^{GFP/+}$) background (Figure 3-1).

Figure 3-1. An overview of the microglia reporter mice cross-bred with homozygous Lrrk2 animals.

In general, genomic DNA was extracted from the mouse tails, amplified by PCR using specific primer pairs and visualized on agarose gel. For each animal, two sets of genotypings have been performed: one, to detect heterozygous Cx3cr1$^{GFP/+}$ and second, to confirm relevant Lrrk2 genotype. Genomic DNA was extracted by overnight incubation of 0.5 cm tail in DirectPCR Lysis Reagent (Tail, Viagen Biotech) with 1 mg/ml Proteinase K, resulting in crude tail lysates. The region of interest was amplified using specific pairs of primers and polymerases (Table 3-1).

Primer	Sequence	Polymerase for PCR reaction
G2019S_KI_F G2019S_KI_R	5'-CAGGTAGGAGAACAAGTTTAC-3' 5'-GGGAAAGCATTTAGTCTGAC-3'	2xTaq PCR (Qiagen, no.201445)
R1441C_KI_F	5'-CTGCAGGCTACTAGATGGTCAAGGT-3'	2xTaq PCR (Qiagen, no.201445)
R1441C_KI_F	5'-CTAGATAGGACCGAGTGTCGCAGAG-3'	
LRRK2_KO_F LRRK2_KO_R	5'-CTCTGAGAGCAGGAGCCGT-3' 5'-TGCCTTCCTGGACATTATTCAGCC-3'	Mega Blue (GelCompany, no.2MMB-5)
Cx3cr1-14276_F-WT	5'-GTCTTCACGTTCGGTCTGGT-3'	Mega Blue (GelCompany, no.2MMB-5)
Cx3cr1-14277-Het	5'-CCCAGACACTCGTTGTCCTT-3'	
Cx3cr1-14278_F-Mutant	5'-CTCCCCCTGAACCTGAAAC-3'	

Table 3-1. PCR primers for Lrrk2 and Cx3cr1 genotyping.

To genotype Lrrk2-G2019S or Lrrk2-R1441C, 2µl of crude lysate was combined with 10µl of 2xTaq PCR polymerase mix (Qiagen), 0.5 µM forward primer, 0.5 µM reverse primer and PCR-grade water to make up a total reaction volume of 20 µl. The PCR reaction for each genotype was performed under the cycling conditions outlined in Table 3-2**.**

To genotype Lrrk2-KO, 1µl of crude lysate was combined with 22µl of MegaBlue Mix polymerase kit (GelCompany), 0.4 µM forward primer, 0.4 µM reverse primer to make up a total reaction volume of 25 µl. The PCR reaction was performed under the cycling conditions outlined in Table 3-2**.**

To genotype Cx3cr, 1µl of crude lysate was combined with 21µl of MegaBlue Mix polymerase kit (GelCompany), and a combination of all three Cx3cr1 primers (Table 3-2), 0.4 µM of each to make up a total reaction volume of 25 µl. The PCR reaction was performed under the cycling conditions outlined in table 2. The $Cx3cr1^{-/-}$ corresponded to $Cx3r1^{GFP/GFP}$ and was present on agarose gel as a single upper band at 500bp. The $Cx3cr1^{+/+}$ (wild type, no GFP) was present as a single lower band at 410bp. The $Cx3cr1^{+/-}$ corresponded to $Cx3r1^{+/GFP}$ and was present as a double band, 410bp and 500bp respectively. The PCR reactions were performed under the cycling conditions outlined in table 3-2**.**

All PCR-amplified products were subsequently run on E-Gel EX 2% Agarose gel with SYBR Gold II (ThermoFisher Scientific, no.G402002) and the corresponding bands were visualized with E-Gel Imager (ThermoFisher Scientific).

	Lrrk2-G2019S			Lrrk2-KO			Lrrk2-R1441C and Cx3cr1		
Step	Temp	Time	Cycles	Temp	Time	Cycles	Temp	Time	Cycles
Initial Denaturation	94°C	3 min	1	95°C	2 min	1	94°C	5 min	1
Denaturation	94°C	45 sec		94°C	30 sec		94°C	45 sec	
Primer Annealing	60°C	45 sec	35	60°C	30 sec	38	60°C	30 sec	38
Extension	72°C	45 sec		72°C	30 sec		72°C	90 sec	
Final Extension	72°C	2 min	1	72°C	2 min	1	72°C	10 min	1
Hold	4°C	∞			∞		4°C	∞	

Table 3-2. PCR conditions for genotyping.

3.2 Primary microglia study

3.2.1 Primary microglia

Primary microglia were isolated from postnatal 1-4 days-old (P1-4) Lrrk2$^{+/+}$ and Lrrk2$^{-/-}$ mouse brains. Meninge-removed mice cortices were mechanically dissociated in cold DMEM/F12 medium and the cell suspension was settled for 5 min following by collection of the top fraction and centrifugation at 1000 rpm for 5 min. After discarding the supernatant, cell pellet was resuspended by fresh DMEM-F12, supplemented with 10 % FBS, 2 mM glutamine, 2 mM sodium pyruvate (Sigma-Aldrich), penicillin and streptomycin. Cell suspension obtained from 2 pups was plated on one T-75 poly-D-lysine (0.1 mg/ml, Sigma-Aldrich) coated flask. After 4 days, the cell culture medium was replaced and the mixed glial culture was maintained until day 14. At the end of incubation,

microglia cells were isolated by shaking 2 h at 160 rpm following by spinning down 5 min at 1000rpm and seeded onto PDL-coated cover slips or cell culture wells.

The purity of the obtained culture was verified by double immunofluorescence staining with rabbit anti-Iba1 antibody (Wako, no.19-19741) for microglia cells and with mouse anti-GFAP antibody (BD-Pharmigen) for astrocytes. The primary microglia yield was ~0.5×10^6 cells/flask, and the amount of astrocyte contaminants was negligible

3.2.2 Inflammatory stimuli and cell treatments

Human α-synuclein pre-formed fibrils (PFFs) were generated from recombinant α-synuclein produced by a lipid A mutant of Escherichia coli, BL21(DE3) with decreased endotoxin production. After purification, α-synuclein was incubated for 15 days to induce aggregation. α-Synuclein fibrils were then quantified in terms of monomer concentration. The equivalent monomer concentration in the fibrils preparation was calculated by the difference between the starting monomer concentration and the residual supernatant monomer concentration after fibrillation.

Microglia were treated with 25 μM α-synuclein PFFs or lipopolysaccharide (LPS) from Escherichia coli O111:B4 at 100 ng/ml (Sigma-Aldrich, L4391), both resuspended in phosphate-buffered saline (PBS). During treatments, primary microglia cells were cultured in medium (as described in Material and Methods) containing 1% FBS. Treatments and genotypes were randomized across batches of primary cell preparations.

3.2.3 RNA extraction (Trizol/Chloroform method)

RNA extractions from primary microglia were performed according to Trizol/Chloroform isolation method as described below. Cells were washed once with PBS and collected with 0.5 ml of ice-cold Trizol reagent (Invitrogen) and incubated for 15 min. 0.1 ml chloroform per 0.5 ml Trizol was added, tubes *were shaken* up *vigorously* by hand for 15 sec and incubated for 3 min at RT, followed by centrifugation at 12000 x g for 15 min at 4°C for phase separation. The resulting upper aqueous phase, containing RNA was transferred to a new tube and RNA was precipitated by mixing with 0.25 ml isopropyl

alcohol per 0.5 ml Trizol used and incubated at RT for 10min. Samples were centrifuged at maximum of 12000 x g for 10 min at 4˚C to form a gel-like RNA pellet and it was washed once with 0.5 ml of 75% ethanol per 0.5 ml Trizol used, followed by vortexing and 5 min centrifugation at maximum of 7500 x g at 4˚C.

The supernatant was discarded and the RNA pellet was air dried for 10 min and resuspended in 50 µl RNase-free water. The RNA concentration was measured using NanoDrop spectrophotometer (ThermoFisher Scientific) and diluted with RNAse-free water to a final concentration of 1 µg/µl. Resuspended RNA was incubated for 10 min at 55˚C and stored at -80˚C before proceeding to downstream applications.

3.2.4 RNA extraction (RNeasy Plus Mini kit)

RNA was isolated from resident brain microglia cells using RNeasy Plus Mini kit (Qiagen, no.74136). Isolated microglia cells were lysed in buffer RLT Plus containing ß-mercaptoethanol, vortexed for 30 sec and centrifuged on gDNA Eliminator spin column at 8000 g for 30 sec to remove genomic DNA. To purify total RNA, the collected flow-through was mixed with 70% ethanol and centrifuged on RNeasy spin column at 8000 g for 15 sec following by washes of the membrane-bound *RNA* with Qiagen buffers RW1 and RPE. Finally, the RNA was eluted from RNeasy spin column with 30µl of RNAse-free water by centrifugation at 8000 g for 1 min and analyzed on Bioanalyzer to determine RNA integrity.

3.2.5 RNA analysis and quantitation (RIN number)

The quality of the RNA was analyzed by the RNA integrity number (RIN). RNA measurements were prepared using either the RNA 6000 Nano Kit (Agilent, no.5067-1511) for RNA-seq experiment or the RNA 6000 Pico Kit (Agilent, no.5067-1513) for the RNA extracted from brain resident microglia. RNA 6000 nano (or pico) gel was added to the nano (or pico) gel matrix, loaded on an RNA nano (or pico) chip and primed using the priming station. RNA samples, RNA kit marker and a ladder were loaded and the nano (or pico) chip was inserted into the Agilent 2100 bioanalyzer to measure RNA integrity.

The bioanalyzer measures the RIN number based on the degradation of 18S and 26S ribosomal RNA.

3.2.6 cDNA library preparation for bulk-RNA-sequencing

cDNA libraries were generated from 1 µg total RNA using the TruSeq Stranded Total RNA Sample Prep LS (Illumina, RS-122-2301), according to manufacturer's instructions. RNA quality was measured using Agilent 2100 Bioanalyzer RNA 6000 Nano Chip (as described in Material and Methods) and samples had a mean RNA integrity number of 9.0. Ribosomal RNA was depleted from the RNA samples using paramagnetic RiboZero Deplete RNAClean XP Beads. RNA was subsequently fragmented using Fragment High mix. First strand cDNA was synthesized using superscript II reverse transcriptase following with the second cDNA-strand synthesis and RNA depletion. Double-stranded cDNA was purified using AMPure XP paramagnetic beads (Beckman Coulter, A63881) and 3' ends were polyadenylated. Indexing adaptors were ligated at both sides of the cDNA and the fragments with ligated adaptors were enriched by PCR amplification using adaptor targeting primers. PCR products were purified using AMPure XP paramagnetic beads. The quality and concentration of the cDNA libraries were subsequently analyzed using digital droplet PCR as described below.

3.2.7 Droplet digital PCR (ddPCR)

cDNA libraries were quantified prior to sequencing using ddPCR Library Quantification kit for Illumina TruSeq (Bio-Rad, no.186-3040). The cDNA library was subjected to serial dilution, with final dilutions of 10^{-6}, 10^{-7} and 10^{-8}. ddPCR master mix was prepared using 11µl of 2x ddPCR Supermix for Probes (no dUTP), 1.1µl of 20x ddPCR library quantification assay and 5µl of RNAase/DNAse free water. 17.6µl of the master mix was added into each well of 96-well blue semi-skirted ddPCR plate (Twin-Tech, no.951020362) and 4.4µl of diluted cDNA library was added per well for total volume of

22µl. Droplets were generated with a QX200 Droplet Generator (Bio-Rad) at the CCR Genomics Core facility at the National Cancer Institute, NIH and followed by thermal cycling according to manufacturer's instructions by ddPCR Library Quantification kit.

PCR reads were analyzed at the QX200 Droplet Reader (Bio-Rad) and the stock concentration of each library was calculated using the ddPCR values within the range of 100-5,000 copies/ul and the library quality was assessed using the QuantaSoft Software (Bio-Rad), followed by normalization for pooling.

3.2.8 Bulk RNA-sequencing

cDNA libraries were multiplexed with 4 samples per pool for final pools concentrations of 10 nM with Tris-HCl with 0.1% Tween20. 7pM of each pool was hybridized to a flow cell following cluster generation using the HiSeq Paired-End Cluster Kit v4 (Illumina) on the cBot cluster amplification system (Illumina) by grafting cDNA with annealed adaptors on the surface of the flow cell. The templates were copied from the adaptor hybridization primers and amplified using high fidelity DNA polymerase to create clonal clusters of ~1000 copies each. Clusters were subsequently sequenced using the HiSeq Sequencing by Synthesis Kit V4 (Illumina) reagents and the Illumina HiSeq2500 sequencer to generate ~35 millions of 100-bp single end reads per library.

3.2.9 Read mapping

Sequencing counts were mapped and quantified by Dr. Jinhui Ding. The standard Illumina pipeline was used to generate fastq files, Ensembl GRCm38 annotated transcript abundance were quantified using Salmon in a non-alignment-based mode, and gene level counts were estimated using tximport package (Patro, Duggal, Love, Irizarry, & Kingsford, 2017; Soneson, Love, & Robinson, 2015).

3.2.10 Differential expression analysis

Differential expression analysis of the cDNA reads resulting from the RNAseq experiment was performed by Dr. Mark Cookson. Preliminary inspection of the data identified

expression of the astrocyte marker GFAP, likely due to small numbers of contaminating astrocytes in the microglial preparations. The Population Specific Expression Analysis [PSEA - (Kuhn et al., 2012)] has been used to estimate the proportions of astrocytes per sample. The DESeq2 R package was used (Love, Huber, & Anders, 2014) to normalize data and estimate differential expression between groups using the generalized linear model:

Transcript Expression~Group + Shake + P-day + Astrocyte

In the model, Group represent the combined experimental variables of genotype and treatment, while the remaining terms are technical variables describing the batch of cells used (Shake), postnatal day of the animals in that batch (P-day) and the proportion of contaminating Astrocytes from the PSEA analysis. A table containing contrasts for all levels of group, ie for each treatment in each genotype was generated and any genes that have showed significant (uncorrected $p < .05$) association with astrocytes were filtered out from the future analysis.

3.2.11 qRT-PCR

In qRT-PCR, mRNA transcripts are quantified by reverse transcribing them into cDNA first, then qPCR is subsequently carried out. cDNA is amplified by 3 repeating steps: denaturation, annealing and elongation and fluorescent labeling enables the detection of a specific PCR product as it accumulates during PCR reaction progress.

3.2.12 cDNA synthesis

1 µg of RNA was used to generate cDNA using the SuperScript III First-Strand Synthesis SuperMix Kit (Invitrogen). For reverse transcription, 1 µg of Trizol-extracted RNA was mixed with 1 µl of 50 ng Random hexamers primers, 1 µl (10mM) dNTPs mix and DEPC treated water was added to make up a total volume of 10 µl. Reaction was incubated on a thermal cycler for 5' at 65°C and immediately placed on ice for 1 min. Then 8 µl of DNA synthesis mix (containing RT-buffer, MgCl2 and DTT) was prepared and combined with

2 µl of SuperScript III/RNaseOUT Enzyme Mix and 10 µl of RNA/primer mix for a total reaction volume of 20 µl. Reactions were incubated 10 min at 25˚C followed by 50 min at 50˚C and terminated by 5 min incubation at 85˚C. At the end of the procedure, 1µl of RNase H was added and incubated for 20 min at 37C to break down the RNA molecules in RNA-DNA hybrids. cDNA was stored at -20˚C until used for downstream applications.

3.2.13 qPCR

To analyze cDNA expression of the RNA-seq top hits, I used the Applied Biosystems 7900HT Real-time PCR system with the TaqMan probes containing a FAM™ dye label and the fast advanced master mix (Applied Biosystems/Thermo Fisher Scientific). 5 ng of cDNA was mixed with 5 µl of TaqMan Master Mix(2x), 0.5 µl TaqMan probe and water was added to make up a total reaction volume of 10 µl. Each reaction was carried in quadruplicates on 384-well plate. Data was analysed using QuantStudio 6 Flex Real-Time PCR System with supplementary Software (Thermo Fisher Scientific).

The following TaqMan probes have been used: *Lrrk2* (ID: Mm01304127_g1), *Il-1β* (ID: Mm00434228_m1), *Sod2* (ID: Mm01313000_m1), *C5ar2* (ID: Mm01267981_s1), *H2-M2* (ID: Mm01279077_g1), *Irg1* (ID: Mm01224532_m1), *Txnip* (ID: Mm01265659_g1) and *NFκBiz* (ID: Mm00600522_m1). We used *Ppid-Cyclophillin* (ID: Mm00835365_g1) as a reference gene for genes with the low level of expression and *Gapdh* (ID: 99999915_g1) as a reference for genes with the high level of expression. The selection of suitable housekeeping genes for expression analysis was based on the level of expression of our top hits genes (Valente et al., 2009).

3.2.14 Western blot

Cells were lysed in CSL lysis buffer (Cell Signalling, no.9803S) - 20 mM Tris-HCl pH 7.5, 150 mM NaCl, 1 mM Na_2EDTA, 1 mM EGTA, 1% Triton, supplemented with Halt 1x protease inhibitor cocktail and Halt 1x phosphatase inhibitor cocktail (Thermo Fisher) for 30 min on ice. Protein lysates were subsequently cleared (10’ centrifugation at 4˚C at

14000 g) and protein concentrations were determined using a 660 nm protein assay (Pierce).

Protein samples were boiled in 1x Laemli Sample buffer (Bio-Rad) and loaded on pre-cast 4-20% TGX polyacrylamide gels (Criterion, Bio-Rad) along with a protein standard (Precision Plus Protein Dual Color Standards, Bio-Rad). Electrophoresis was performed in 1x pre-mixed electrophoresis buffer (10 mM Tris, 10 mM Tricine, 0.01% SDS, pH 8.3, diluted with water) and were run at 200 V for 45' using the Criterion Vertical Electrophoresis Cell (Bio-Rad). Following gel electrophoresis, samples were transferred to 0.45 µm pore-size nitrocellulose membranes (Bio-Rad) using the Trans-Blot Turbo Transfer System (Bio-Rad).

The membrane was blocked in a 1:1 solution of phosphate buffered saline (PBS) and Odyssey Blocking Buffer (Li-Cor) for 30 min and incubated with primary antibodies diluted in antibody buffer (1:1 of Tris buffered saline (TBS) with 0.1% Tween and Odyssey Blocking Buffer (Li-Cor)).

The following primary antibodies have been used:

rabbit anti-SOD2 (1:20000, Prestige Sigma Aldrich),

goat anti-IL-1β (1:2000, R&D system),

rabbit anti-phospho Ser935 LRRK2 (1:300, Abcam),

rabbit-anti total LRRK2 (1:300, Abcam),

mouse anti-GAPDH (1:20000, Prestige Sigma Aldrich),

mouse-anti-GFAP (1:5000, BD Pharmigen),

rabbit anti-Iba1 (1:1000, Wako).

Following primary antibody incubation, membranes were washed 3 times for 5 minutes in TBS with 0.1% Tween. Membranes were then incubated with fluorescent secondary

antibodies (IRDye, Li-Cor) diluted 1:15000 in antibody buffer for 40 min at room temperature (RT) under gentle agitation. Secondary antibody incubation was followed by 3 washes of 5' each in TBS with 0.1% Tween. Western blots were imaged using the Odyssey CLx system (Li-Cor) and quantified using Image Studio software.

3.2.15 ELISA-multiplex

Primary microglia were prepared as described above (see Material and Methods, 3.2.1). The cells were seeded at 150 x 10^3 per well in 96-well tissue culture plates and treated with either 100ng/ml LPS or 25μM α-synuclein fibrils (PFFs) for an amount of times indicated in the experiment, in DMEM/F12 medium supplemented with 1% FBS, 5% Pen/Strep. At the end of the incubation time, the supernatant (2x40μl) was collected and saved at -80C for future multiplex-ELISA experiment.
ELISA was performed by Dr. Heather Kalish, NIBIB, NIH Core-Facility.
Cytokines released into the supernatant of primary microglia were analyzed according to manufacturer's instructions (Quansys Biosciences, Mouse Cytokine 16-plex kit, no.110949MS), measuring IL-1α, IL-1β, IL-2, IL-3, IL-4, IL- 5, IL-6, IL-10, IL-12p70, IL-17, MCP-1, IFNγ, TNFα, MIP-1α, GMCSF, RANTES by quantitative ELISA-based chemiluminescent assay. Screening was performed at 96-well plate and signal was detected using Quansys™ imaging system.

3.3 Adult brain resident microglia study

3.3.1 Acute isolation of resident microglia from adult mouse brain by CD11-labeling (MACS-sorting).

Adult microglia were isolated from 3-month-old and 1 year-old wild-types (for quality evaluation), from 1.5 years-old WT, KO and mutants LRRK2-C57BL/6J (for phagocytosis assay) or 1 year-old LRRK2-*Cx3cr1*$^{GFP/+}$ mice (for single cell western blot and single cell RNA-sequencing) using a protocol adapted from Adult Brain Dissociation kit, ABDK (Miltenyi, 130-107-677). Mice were perfused and whole or half-brains were quickly dissected and placed in ice-cold Hank's balanced salt solution (HBSS), following with enzymatic and mechanical dissociation with Dissociator program 37C_ABDK_01 for 30

min. After brief centrifugation at 300g for 1 min, cells were resuspended with HBSS and tissue debris was removed by passing the cell suspension through HBSS pre-wetted 70µm cell strainer and centrifugation at 300g for 5 min. Myelin was removed using a discontinuous Percoll gradient (Sigma, GE Healthcare, 17-0891-02). The osmolality of undiluted Percoll was adjusted with 9 parts(v/v) of Percoll and 1 part(v/v) of HBSS to make Percoll isotonic solution.After centrifugation cells were resuspended in 70% Percoll and layered under 30% Percoll, following by centrifugation 1000g for 30 min at 10C with free deceleration, break 0 (soft stop). The supernatant containing white myelin was removed and the “ring of cells” was collected at the 30-70% Percoll interface, washed with ice-cold HBSS and centrifuged at 300g for 10 min with full break.For the next step of CD11b magnetic labeling, washed cell pellet was resuspended with 90µl of ice-cold solution of 0.5% BSA in HBSS and 10µl of anti-CD11b-coated microbeads (Miltenyi, 130-093-634) were added for 15 min at 4C, following with two washed with BSA/HBSS buffer. After last wash cell pellet was resuspended with 400µl of BSA/HBSS buffer and loaded onto pre-washed MS columns (Miltenyi, 130-042-201) and CD11b-positive cells were enriched and eluted as the positively selected cell fraction using MACS separator.

Each half-brain extraction yielded approximately $0.5x10^6$ $CD11b^+$ viable cells from unstimulated brains and approximately $4x10^6$ cells from LPS-injected animals (10 time more CD11b positive cells compare to PBS-injected brains).

3.3.2 Immunocytochemistry (ICC)

Acutely isolated brain microglia cells were plated, depending on assay, on 24-well plates containing poly-D-lysine coated glass coverslips or on poly-D-lysine coated 8-wells Lab-Tek II removable Chamber slides (Nunc, no.154534).
Cells were fixed with 4% paraformaldehyde (PFA) in PBS pH 7.4 for 20 min and blocked for 30 min with 5% FBS (heat inactivated fetal bovine serum) in 1xPBS containing 0.1% Triton X-100. Cells were incubated with primary rabbit anti-Iba1 antibody (Wako, no.019-19741), mouse anti-GFAP antibody (BD Pharmigen, no.556329) for 1 h at room temperature. All antibodies were diluted 1:500 in blocking solution. Cells were washed for 10 min three times with PBS followed by incubation with secondary antibody donkey anti-

rabbit Alexa-fluor 488 (1:500, ThermoFisher, A32790) and donkey anti-mouse Alexa-fluor 568 (1:500, ThermoFisher, A10037) for 40 min at room temperature, followed by 3 washes with PBS and counter-stain with DAPI for 5 min (at 1:10,000 dilution). Coverslips were mounted on microscope slide using ProLong Gold Antifade Mountant (TheroFisher) and dried overnight at room temperature in the dark.

3.3.3 Ex vivo microglia phagocytic assay

Adult microglia were isolated from 1.5 years-old WT, KO and mutants LRRK2-C57BL/6J mice. The myelin was removed by a two-layer density gradient, followed by the labeling of microglia with CD11b immunomagnetic beads and magnetic separation of CD11b-positive microglia from the remaining brain cell suspension (see Material and Methods, section 3.3.1).

Isolated microglia were resuspended in DMEM/F12 supplemented with 10% fetal bovine serum (FBS) and plated at $0.15x10^6$ cells/well on poly-D-lysine coated, 8-wells Lab-Tek II removable Chamber slides (Nunc, no.154534) at 37C, 5% CO_2 for 24 h before an experiment.

Neural apoptotic cells have served as phagocytic target and were prepared from primary neuronal culture by exposure to 254nm ultraviolet (UV) irradiation (UV lamp) for 15 min. Apoptosis was verified with trypan blue stainig. UV-exposed cells were labeled with 5µl of 5(6)-TAMRA stain (ThermoFisher, 5(6)-TAMRA Succinimidyl ester, C1171) and washed twice with cold PBS. Chamber-seeded isolated brain microglia cells were fed with the 2x amount of neuronal apoptotic debris ($0.3x10^6$) in culture media. After 1 h at 37C, 5% CO_2, media was removed and microglia cells washed with PBS and fixed with 4% PFA for 15 min. Next, cells were washed with PBS and immunostained (see Material and Methods) with primary anti-Iba1 antibody (Wako, 019-19741) and secondary donkey anti-rabbit Alexa-fluor 488 antibody (ThermoFisher, A32790). Fluorescence of 5(6)TAMRA stain was detected by laser excitation at wavelength of 568nm.

A phagocytic index was calculated using Particle analysis (ImageJ software) by dividing the total area of phagocytosed TAMRA-labeled apoptotic cells by the total area of Iba1-positive microglial cells.

3.3.4 Transmission electron microscopy (TEM)

Acutely isolated CD11b magnetically-sorted microglia cells were seeded onto Poly-D-lysine coated 24 wells plate (Sarstedt). After 24 h cells have been fed with neuronal debris for 1 h (as described in Materials and Methods, Phagocytic assay) following with two washes with PBS. After PBS was removed, the Fixative buffer (glutaraldehyde 2.5% in 0.1M sodium cacodylate buffer) was added to cells for 1 hours at 4°C.
After 1 hour, the samples were post-fixed with 1% osmium tetroxide plus potassium ferrocyanide 1% in 0.1M sodium cacodylate buffer for 1 hour at 4°. After three water washes, samples were dehydrated in a graded ethanol series and embedded in an epoxy resin (Sigma-Aldrich). Ultra thin sections (60-70 nm) were obtained with an Ultrotome V (LKB) ultramicrotome, counterstained with uranyl acetate and lead citrate and examined by Tecnai G2 (FEI) transmission electron microscope (TEM) operating at 100 kV. Images were captured with a magnification 9800x, using a Veleta (Olympus Soft Imaging System) digital camera.

3.3.5 Stereotaxic surgery for LPS stimulation in vivo

All experimental procedures performed were approved by the NIH/ NIA Animal Care & Use Committee. Stereotaxic surgeries were performed by Dr. Natalie Landeck, NIA, NIH.

For LPS stimulation by stereotactic injection, 6-month old mice were initially anesthetized by 5% isoflurane and kept under anesthesia using 1–2% isoflurane. The tooth bar was adjusted to −5.0 mm. Mice were placed into a stereotaxic frame and eyes were covered with ointment. The top of the head was shaved and sterilized using 70% Ethanol. An incision was made above the midline and skull was exposed using cotton tips. At anteroposterior +0.2 mm, mediolateral ± 2.0 mm from bregma (bi- lateral injection), a hole was drilled into the skull and the last thin layer was removed using a forceps to not

damage the dura. A pulled glass capillary (blunt) attached to a 5 µl Hamilton syringe was used for injection. First, an air bubble of 1 µl was pulled in followed by 1 µl of either PBS or 5mg/ml LPS solution. The capillary was lowered to dorsoventral −3.2 mm from bregma into the dorsal striatum. The solution was delivered at a rate of 0.1 µl per 10sec. After the injection, the capillary was held in place for 2 min, retracted 0.1 µm and another 1 min was waited before it was slowly withdrawn from the brain. The head wound was closed using surgical staples. Ketoprofen solution at 5 mg/kg was administered subcutaneously as analgesic treatment for the following 3 days.

3.3.6 Histology

Animals were sacrificed 3days after surgery. Mice were deeply anesthetized with an intraperitoneal injection of 200ul of 10% ketamine and the thoracic cavity was opened to expose the heart. Blood was flushed out using 10 ml of 0.9% NaCl for 2 min. Brains were removed, the left hemisphere was used for single-cell RNA-Seq (scRNA-Seq) and the right hemisphere was fixed in 4% PFA for 48 h. After 2 days, brains were transferred to 30% sucrose solution for cryoprotection and sectioning was started once brains had sunk to the bottom. The brains were then cut into 30 µm thick coronal sections - 6 series - and stored in antifreeze solution (0.5 M phosphate buffer, 30% glycerol, 30% ethylene glycol) at −20 °C until further processed. Sections were washed with PBS, mounted on glass slides and coverslips applied using Prolong Gold Antifade mounting media (Invitrogen). GFP expressing microglia were imaged using a Zeiss LSM 880 microscope and 20x objective.

3.3.7 Immunohistochemistry (IHC)

To increase GFP-microglia signal for the purpose of detailed morphological analysis, brain sections were stained with GFP antibody as described below.
Free-floating brain sections were blocked in 10% NDS - normal donkey serum solution in 1xPBS, 1% BSA, 0.1% Triton X-100 for 30 minutes followed by a 24 hours incubation with primary antibodies (chicken anti-GFP 1:1000, Millipore AB16901; rabbit anti-Tmem119, 1:500, Abcam ab209064, rat antiCD68-APC, 1:500, Biolegend no.137007)

diluted in 1% NDS (in 1xPBS, 1% BSA, 0.1% Triton X-100). Brain sections were washed 3 times with PBS, followed by 1 hour incubation with Alexa Fluor secondary antibodies (donkey anti-rabbit-Alexa-488, 1:500, A32790; donkey anti-rabbit-Alexa-568, 1:500, A10042 ThermoFisher Scientific, donkey anti-rat-Alexa-594, 1:500, A-21209) diluted in 1% NDS (in 1xPBS, 1% BSA, 0.1% Triton X-100) and washed 3 times with PBS. Washed slices were mounted on slides using ProLong Gold Antifade Mountant (ThermoFisher Scientific), dried overnight at room temperature in the dark and kept at 4C for image acquisition.

3.3.8 Image acquisition

For morphological assay, GFP-stained brain coronal sections were scanned on a laser scanning confocal microscope (LSM 880, Zeiss) with 20x magnification Objective. 11 optical sections with 1um intervals were captured from the middle of 30µm-thick tissue with an image matrix of 1024x1024 pixels and a depth of 16 bit. The Z-stack 16-bit images were condensed into a maximum intensity projection images (MIPs).

3.3.9 General morphological analysis

Manual morphological analysis of brain sections with GFP expressing microglia was performed using Volocity Image Analysis Software (Perkin Elmer, version 6.0) and FIJI software (version 2.0) with the Sholl analysis plugin (T. A. Ferreira et al., 2014; Schoenen, 1982) and with the AnalyzeSkeleton plugin (Fiji).

General morphological parameters related to cell shape included cell area, cell perimeter length (the length around the periphery of each cell), circularity (4π x area/cell perimeter length^2) and soma size (the area contained within the soma mask not including branches). Total 160 images from three different brain areas (cortex, striatum and substantia nigra) have been collected. To date, about 80 to 120 cells per striatum area have been analyzed for cell shape and branch morphology.

3.3.10 Skeleton analysis

Skeletonization is a process of morphological thinning for reducing foreground regions in a binary image to a skeletal remnant that largely preserves the extent and connectivity of the original region while throwing away most of the original foreground pixels.
A skeleton analysis method was used to quantify microglial branching morphology in immunofluorescent confocal images of fixed brain tissues. The maximum intensity projection of the GFP positive channel was enhanced to visualize microglia processes. Thresholded binary images were skeletonized using FIJI software and data regarding amount of branches, process length and number of endpoints per cell were collected by AnalyzeSkeleton plugin.

3.3.11 Sholl analysis

Maximum intensity projection images (MIPs) have been thresholded to generate binary images and to create ROI (region of interest) in FIJI software.
Center of each cell was defined manually using Fiji straight line tool and extended to the most distal point of the longest branch. Then Sholl plugin created a series of concentric shells (circles) beginning at 5.0-um radii and increasing 1um with every circle (radius step size=1).
Sholl analysis (Sholl, 1953) was performed for each cell by counting number of intersections between microglia branches and each increasing circle. Branches have been analyzed and color coded according to their Sholl profile with warmer colors indicating higher number of intersections. Schoenen ramification index (RI) was calculated based on Sholl analysis as number of end branches divided by number of primary branches, that originated at the cell's soma (Schoenen, 1982).

3.3.12 Single cell RNA-sequencing

Single cell RNA quantification technology allows high-throughput single cell transcriptomics profiling. We have used 10xGenomics expression profiling GemCode platform, which combines microfluidics with molecular barcoding to enable 3' mRNA counting from thousands of single cells.

Single cells, reagents and a single gel bead containing barcoded oligonucleotides are encapsulated into nanoliter-sized GEMs (Gel Bead-in-Emulsions). Lysis and barcoded reverse transcription of RNAs from single cells are performed inside each GEM. High quality next generation sequencing libraries are finished in a single bulk reaction (Figure 3-2).

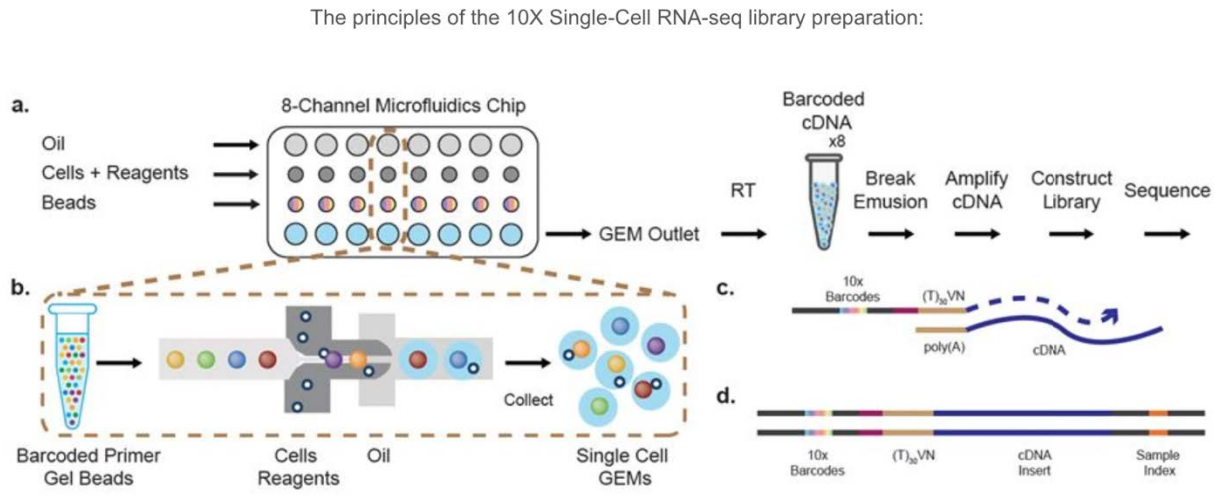

Figure 3-2. 10xGenomics GemCode single cell platform. a) Formation of GEMs**.** Reverse transcription takes place inside each GEM, which is then pooled for cDNA amplification and library construction in bulk. b) Formation of single-cell GEMs. c) Barcoded oligonucleotides inside GEMs. d) Final library molecules. Image reproduced from 10xGenomics/Chromium™ Single Cell Solution.

3.3.13 Single cell preparation

Single cell solutions were generated from the half-brain samples and prepared by isolation of resident brain microglia cells with enzymatic dissociation and CD11b-positive magnetic beads (as described in Materials and Methods, section 3.3.1). Cell concentration and viability was determined on LunaFL cell counter (Logos Biosystems). Cells with more than 80% viability were used and kept on ice for single cell RNA-seq analysis.

3.3.14 Single cell encapsulation, library preparation and sequencing

Single cell encapsulation, library preparation and sequencing was performed at the NCI, NIH Bethesda Core facility by Dr.Michael Kelly and Zachary Rae.

Droplet-based single-cell partitioning and single-cell RNA-Seq libraries were generated using the Chromium Single-Cell 3′ Reagent v2 Kit (10× Genomics, PN-120737) based on the 10× GemCode proprietary technology (Zheng et al., 2017). A single-cell suspension at a density of some 2000 cells/µl was mixed with RT-PCR master mix and loaded together with Single-Cell 3′ Gel Beads and Partitioning Oil into a Single-Cell 3′ Chip. The Gel Beads were coated with unique primers bearing 10× cell barcodes, unique molecular identifiers (UMI) and poly(dT) sequences.

The chip was then loaded onto a Chromium Controller (10× Genomics) for single-cell GEM generation and barcoding. RNA transcripts from single cells were reverse-transcribed within droplets to generate barcoded full length cDNA using Clontech SMART technology.

After emulsion disruption, cDNA molecules from one sample were pooled and pre-amplified. Finally, amplified cDNAs were fragmented, and adapter and sample indices were incorporated into finished libraries which were compatible with Illumina next-generation sequencing technologies. The size profiles of the pre-amplified cDNA and sequencing libraries were examined by Agilent Bioanalyzer 2100 using a High Sensitivity DNA chip (Agilent).

Individually indexed libraries were evenly pooled based on molarity and sequenced on an Illumina NextSeq 500 sequencer using a NextSeq v2.5 150 cycle High Output Kit. The recommended read structure of 26 bp for Read 1, 98 bp for Read 2 and 8 bp for i7 index was used. Using proper cluster density, a coverage around 250 M reads per sample (3000–5000 cells) was obtained corresponding to at least 50,000 reads/cell.

3.3.15 Data processing and clustering

The sequencing data was analyzed using the Cell Ranger Pipeline (version 2.0.1) to perform quality control, sample demultiplexing, barcode processing, alignment and single-cell 3′ gene counting.

Samples were demultiplexed with bcl2fastq Conversion Software v2.19. based on the 8-bp sample index, 10-bp UMI tags, and the 16-bp GemCode barcode. The 98-bp-long read 2 containing the cDNA sequence was aligned using STAR against the Genome Reference Consortium Mouse Build 38 (GRCm38-mm10) Mus musculus reference transcriptome. “Fraction Reads in Cells” was determined by the fraction of cell-barcoded, confidently mapped reads with cell-associated barcodes to check the background of cell-free (ambient) RNA in cell suspension. Clustering, filtering, variable gene selection and dimensionality reduction were performed using R package Seurat version 3 (Butler, Hoffman, Smibert, Papalexi, & Satija, 2018). Single cell data from PBS or LPS treated animals were combined into a single Seurat object and filtered for cells that had > 800 but < 6000 features and had < 0.1% of reads mapped to the mitochondrial genome. After log-normalization and scaling, data were reduced using the first 50 principal components, then cells were mapped to two-dimensional space using t- distributed stochastic neighbor embedding (tSNE).

3.3.16 Single-Cell Western Blot

Single cell (sc) immunoblotting was performed using the Milo sc-Western Blotting device (from ProteinSimple) according to the manufacturer's instructions. Milo scWest chips (small or standard size) were rehydrated in 1xSuspension Buffer (ProteinSimple) for 15 minutes, at room temperature. Freshly CD11b-isolated mouse brain microglia cells were

loaded on rehydrated Milo scWest chip with the polyacrylamide gel side up. Cell concentration was ~100,000 cells in 1ml of Suspension Buffer. The cells were allowed to settle into pre-cut acrylamide microwells for 10-15 min to achieve single-cell occupancies of the wells. Cell settling was monitored by brightfield microscopy and then gently washed with 1xSuspension Buffer to remove unsettled cells. Cell-loaded chips were then inserted into the Milo instrument for lysis, electrophoresis, and fixing. The conditions were set as following: for the first experiment with non-injected microglia cells: lysis time 0 sec, electrophoresis time 150-170 sec at 240V and UV capture 4 min. For the next experiments with LPS/PBS-injected brain microglia, the lysis time was adjusted to 10 sec.

Primary antibody probing and washing were performed following the manufacturer's protocols. Namely, the chips were incubated with primary antibody for 2 hours at room temperature - rabbit anti-LRRK2 antibody (1:15 dilution, Abcam c41-2, ab133474 or 1:15 dilution, Cell Signalling D18E12, cat.13046) and loading controls antibody mouse anti-Vinculin (1:20, R&D, mab6896) or rabbit PKC-delta (1:80, Abcam, ab182126) diluted in the antibody dilution buffer.

After 3 washes x 5 min washes with Wash buffer (ProteinSimple), fluorescently labeled secondary antibodies were applied for 1 hour at room temperature protected from light exposure donkey anti-mouse IgG Alexa 555 (1:40 Invitrogen, A-31570), donkey anti-rabbit IgG Alexa 555 (1:40 Invitrogen, A-31572) or donkey anti-rabbit IgG Alexa 647 (1:40, Invitrogen, A-31573). After 3 × washes with the Wash Buffer, the chip was briefly rinsed with water and centrifuged to remove the remaining liquid. Stained and dried scWest chip was scanned on a two-color microarray scanner - InnoScan 710 with the resolution setting at 3 µm/pixel and analyzed by Scout 2.0 Software (Milo System, Protein Simple).

3.3.17 Statistical analysis

All quantitative data are expressed as mean ± SEM and represent at least three independent sets of experiments. Statistical significance was assessed using two-way ANOVA followed by Bonferroni's post-hoc test for the comparison of the two variables (genotype and treatment) and by one-way ANOVA followed Tukey's post-hoc test for

comparison of multiple groups in the time course experiments. Data were analyzed using Prism (GraphPad) and the statistical significance was taken at $p < .05$.

For the bulk RNA-sequencing and single cell RNA-sequencing, data were analyzed by DSEQ2 package (Love et al., 2014) and Seurat package v.3 (Butler et al., 2018) respectively and plotted using R version 3.4.3. (R Core Team, 2016, http://www.rstudio.org/) as described in details in specific sections in Material and Methods.

Chapter 4

Transcriptome analysis of LRRK2 WT and KO primary microglia stimulated with LPS or α-synuclein fibrils

4.1 Introduction

Microglia are immune cells in the brain, playing critical roles during the innate inflammatory response (Perry & Holmes, 2014). Among the genes mutated in familial PD, those encoding LRRK2 and α-synuclein play major roles in neuroinflammatory processes. Specifically, α-synuclein can be secreted by neurons to cause activation of glia cells and LRRK2 has been suggested to play a role in mediating pro-inflammatory responses in activated microglia (Maekawa et al., 2016; Marques & Outeiro, 2012).

Activated microglia release pro-inflammatory and reactive oxygen species (ROS) components to mediate the inflammatory response and to remove foreign materials or pathogens by phagocytosis (Garden & Moller, 2006).

An inflammatory response is essential for tissue repair and brain integrity, however excessive and prolonged inflammation can lead to significant tissue and cellular damage and contribute to neurodegeneration (Gao & Hong, 2008). Increased numbers of reactive microglia have been observed to surround DA neurons in the SNpc of PD post-mortem brains (McGeer et al., 1988; Mogi et al., 1994).

LRRK2 was proposed to contribute to PD pathogenesis via altered neuroinflammatory signaling (Isabella Russo et al., 2014; Tansey & Goldberg, 2010). Additionally, aggregated forms of α-synuclein released by degenerating neurons or actively secreted through exosomes by stressed neurons can trigger microglial activation and initiate the inflammatory process (Bliederhaeuser et al., 2016; C. Kim et al., 2013). However, the molecular pathways by which α-synuclein induces microglial activation require additional investigations.

To gain insights into the role of LRRK2 in α-synuclein-mediated neuroinflammation, we performed an RNA sequencing (RNA-seq) analysis of primary microglia cells isolated from LRRK2 wild-type (WT) and knock-out (KO) mice, treated with α-synuclein pre-formed fibrils (PFFs) or with the more general inflammagen lipopolysaccharide LPS.
Following the identification of differentially expressed genes by RNAseq, we also validated top candidates at the RNA-level using quantitative PCR (qPCR). In addition, gene ontology was performed to analyze differentially expressed genes between LRRK2 genotypes and inflammagen treatments.

4.2 Results

4.2.1 Experimental design

Primary microglia cells, isolated from LRRK2 WT or KO animals, under basal conditions (untreated) or stimulated with either α-synuclein pre-formed fibrils (PFFs) or lipopolysaccharide LPS were analyzed through RNA sequencing (RNAseq) (Figure 4-1), after RNA extraction and cDNA-library preparation, as described in Material and Methods.

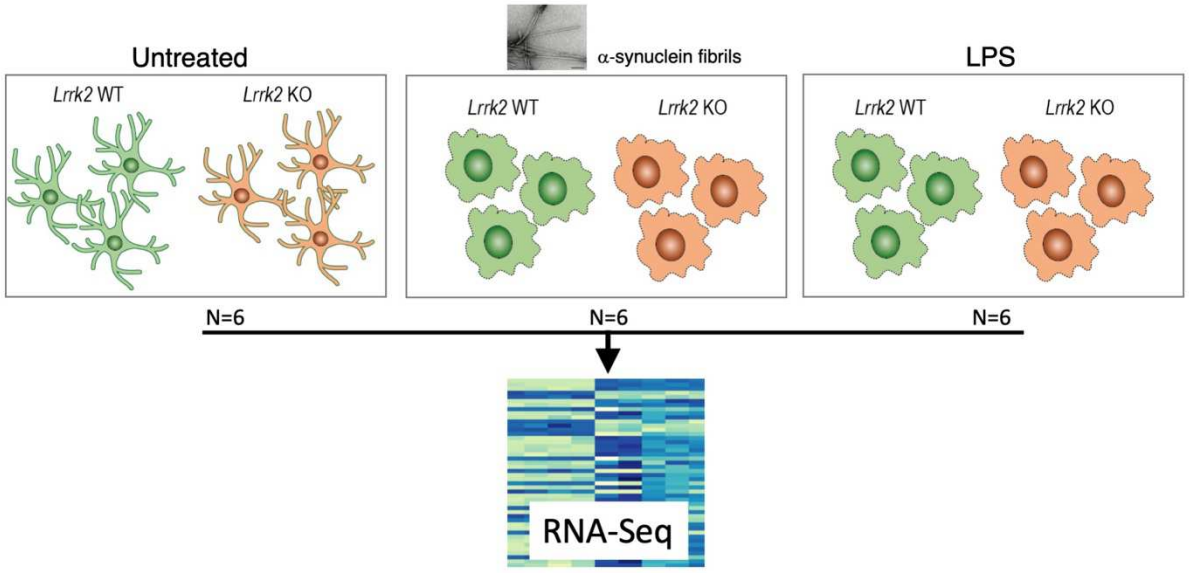

Figure 4-1. Design of RNAseq experiment for differential gene expression analysis. Primary microglia cells from LRRK2 WT and KO mice were untreated or stimulated with α-synuclein pre-formed fibrils (PFFs) or LPS and subjected to RNA-seq analysis.

4.2.2 Differential gene expression after inflammatory treatments

RNA-sequencing was generating a high-resolution transcriptome profile of LRRK2 WT and KO microglia cells. The obtained RNA-seq dataset had an average of 30,902,421 uniquely mapped reads (range 22,388,606-44,910,295) per sample.

Hierarchical clustering of the aligned and normalized read counts indicated that the three treatments, including untreated control, LPS and α-synuclein PFFs, have separated the microglia samples into different groups (clusters), whereas genotype had a subtler effect on overall differential gene expression.

Clustering has been presented for the four experimental variables which included two technical variables (P-day, for postnatal day of the pups that were used for making primary microglia cultures and shake-Date, for the date when the microglia were isolated from initial mixed glia cultures), and two biological variables, treatment and genotype (Figure 4-2, top part)**.** The colors of the heatmap represent the Euclidean distance between samples in a pairwise manner with the yellow-blue scale (Figure 4-2, low part) and show that samples are separating mostly by treatment.

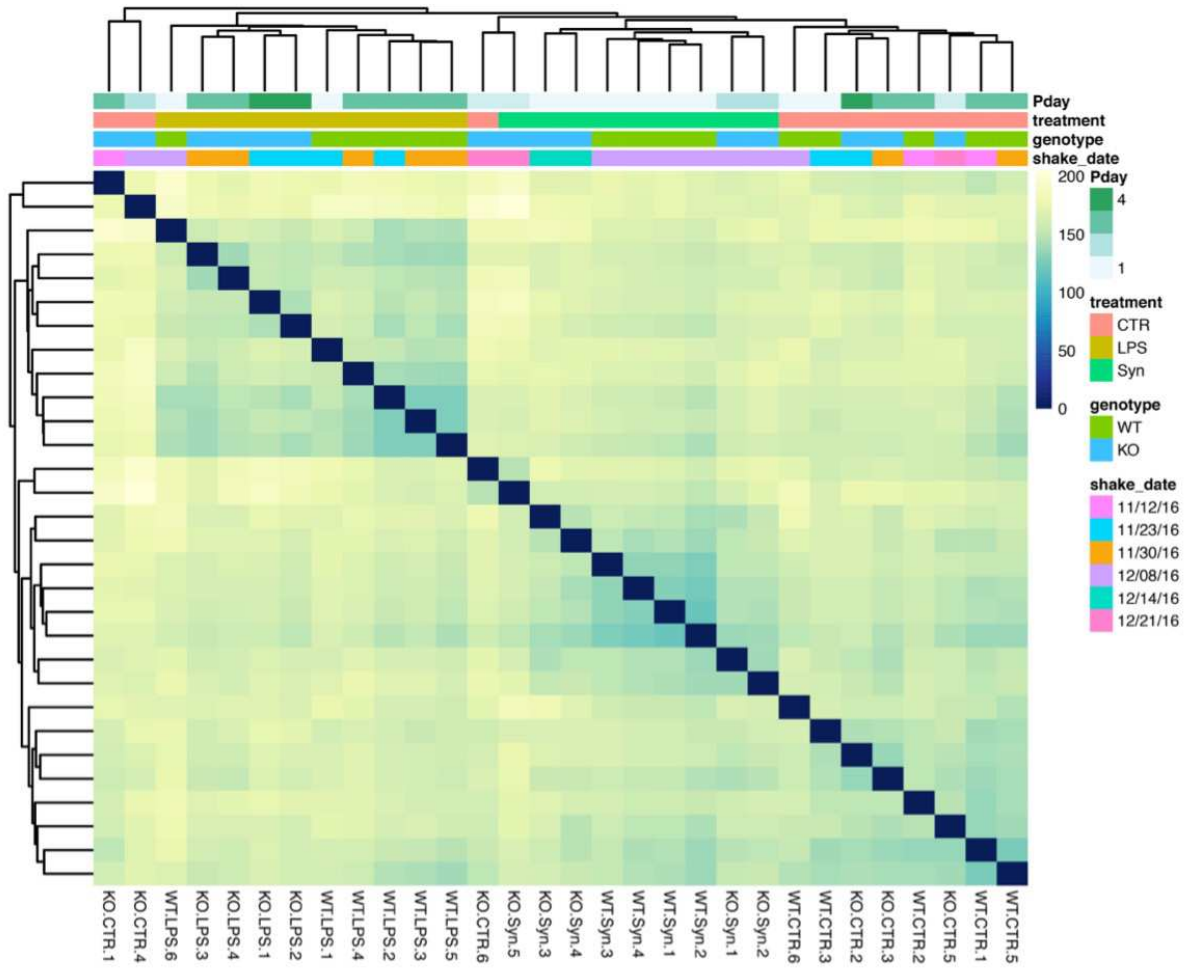

Figure 4-2. RNA-Seq profiling of WT and LRRK2 KO microglia after inflammatory stimulation. Hierarchical clustering and heatmap of the Euclidean distance for all the samples from the study. The samples separated largely by treatment (CTR=untreated cells, LPS or α-synuclein treatment) and to a lesser extent by genotype (WT and KO samples).

Principal component analysis (PCA) was performed to analyze the source of variation between samples. The first principal component of the overall gene expression profile, driving 24% of variation between samples, separated LPS treated group from the other two treatment groups. The second principal component, driving 8% of variation, separated α-synuclein PFFs treated samples from the controls (Figure 4-3). These results demonstrate that both α-synuclein PFFs and LPS induce gene expression responses but that these differ from each other.

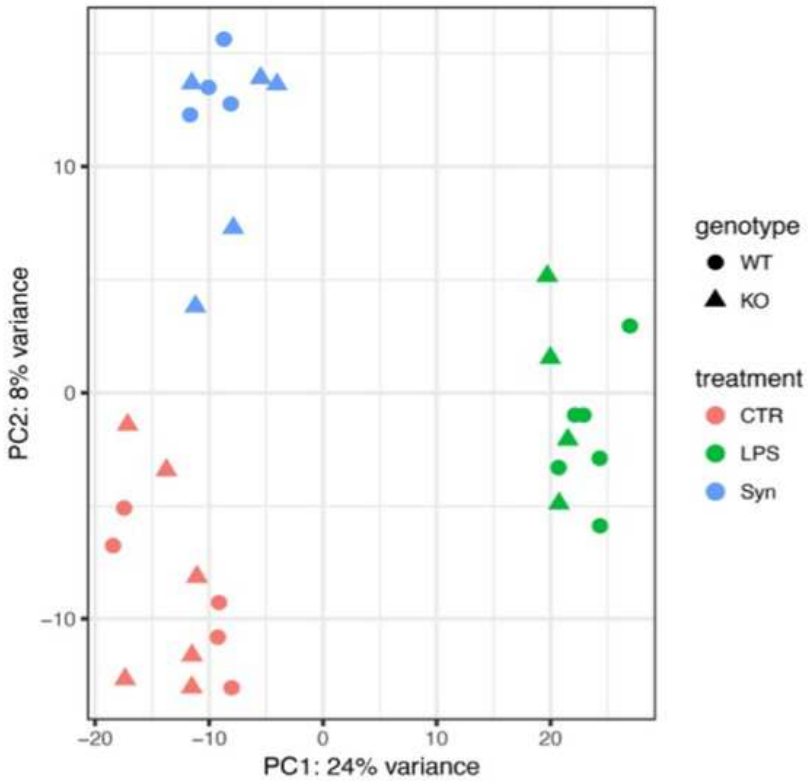

Figure 4-3. Principal component analysis (PCA) of RNA-sequenced samples. First two principal components of the same data from LRRK2 WT and KO samples, confirms separation of the three treatment groups (with designated colors) but less efficient separation by two genotypes (with designated shapes).

As a next step, we looked at differential gene expression in three major experimental settings of our model, specifically the genotype (Figure 4-4a), treatments with α-synuclein PFFs (Figure 4-4b) or LPS (Figure 4-4c). The z-score (normalized standard deviations from the mean) of the 50 most significantly differentially expressed genes for each setting were plotted on a heat map and subjected to unsupervised hierarchical clustering. Each gene on the right side of each heatmap is colored by Z-score for expression relative to the overall mean expression for that gene and samples are listed in each heatmap. Dendrograms are scaled to the Euclidean distance between samples based on the top 50 differentially expressed genes.

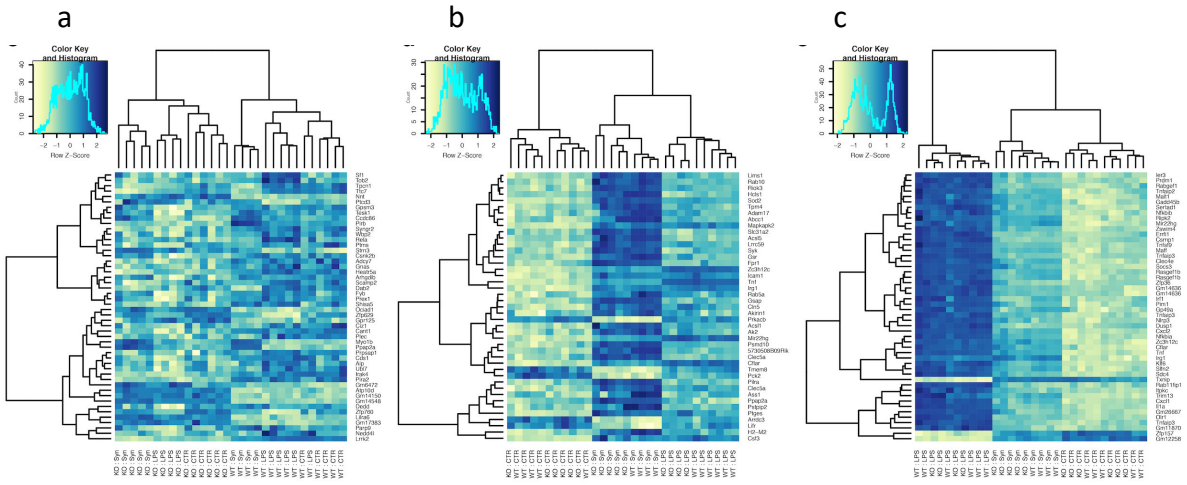

Figure 4-4. Heatmaps for the top 50 differentially expressed genes from RNA-seq analysis. Heat map of the z-score of top fifty most statistically significant genes associated with genotype (**a**) or treatments with α-synuclein PFFs (**b**) or LPS (**c**). Colors indicate the z-score per gene per sample and dendrograms are scaled to the Euclidean distance between samples based on the top 50 differentially expressed genes. (For the enlarged version of each heatmap, please refer to the web version of the published article PMID: 31102768)

While the inflammatory stimulation of the cells provided clear separation between all three experimental settings, the effect of genotype was subtle, although, as expected, LRRK2 was recovered as differentially expressed. However, within treated groups, gene expression separated out by genotype (Figure 4-4b,c). This data suggests that while Lrrk2 genetic deletion has only a subtle influence on basal gene expression in untreated samples, it might have measurable effects on inflammatory activated microglia.

4.2.3 Gene ontology

To gain further insights into the pathways associated with differentially expressed genes between LRRK2 WT and KO genotypes and inflammatory treatments, the top 50 genes were subjected to gene ontology (GO) analysis. One of the main uses of the GO is to perform enrichment analysis on gene sets to find which GO terms are over (or under)-represented using annotations for that gene set. Functional enrichment analysis is a key step in interpreting gene lists discovered in diverse high-throughput experiments

(Reimand et al., 2016). Enrichment analysis for GO term biological process was performed using the Fisher exact test, with Benjamini and Hochberg post hoc analysis and was conducted for genes that were significantly differentially expressed (adjusted p < .05 and 2-fold difference) for each factor in the experimental model (Figure 4-5). For each plot, the top 10 GO categories by p-value are shown with –log10 adjusted p on the y axes and GO term.id on the x axes. Each point is scaled to overlap size, ie the number of genes in the dataset also found in a given GO category (Figure 4-5a-c).

For genotype (Figure 4-5a) the most enriched categories included GO:0031982 for the GO term "vesicle" ($p = 2.96 \times 10^{-5}$). Other terms in this enrichment included extracellular exosomes (GO:0070062, $p = 3.7 \times 10^{-4}$) and regulation of response to stimulus (GO:0048583, $p = 5.5 \times 10^{-4}$).

The enrichment of this pathways might suggest that although LRRK2 deficiency had a subtle effect on gene expression in unstimulated microglia, there are still some differences between genotypes that suggest the role of LRRK2 in the endo-lysosomal system, as was recently reviewed by (Araki et al., 2018; Roosen & Cookson, 2016).

The separation of GO categories in inflammatory stimulated microglia was more notable. Although, as expected, both treatments showed the GO terms related to inflammation (Figure 4-5b for α-synuclein PFFs and Figure 4-5c for LPS), each set had unique elements. LPS treatment has demonstrated many more identified GO categories as shown by Euler diagram that illustrates the relationships between two tested groups of treatments (Figure 4-5d). Specifically, LPS treatment resulted in alterations of categories including GO:0051171 "regulation of nitrogen compound metabolic process" ($p = 3.56 \times 10^{-16}$) that contained the Thioredoxin Interacting Protein (Txnip), which is known to regulate metabolism and ER stress.

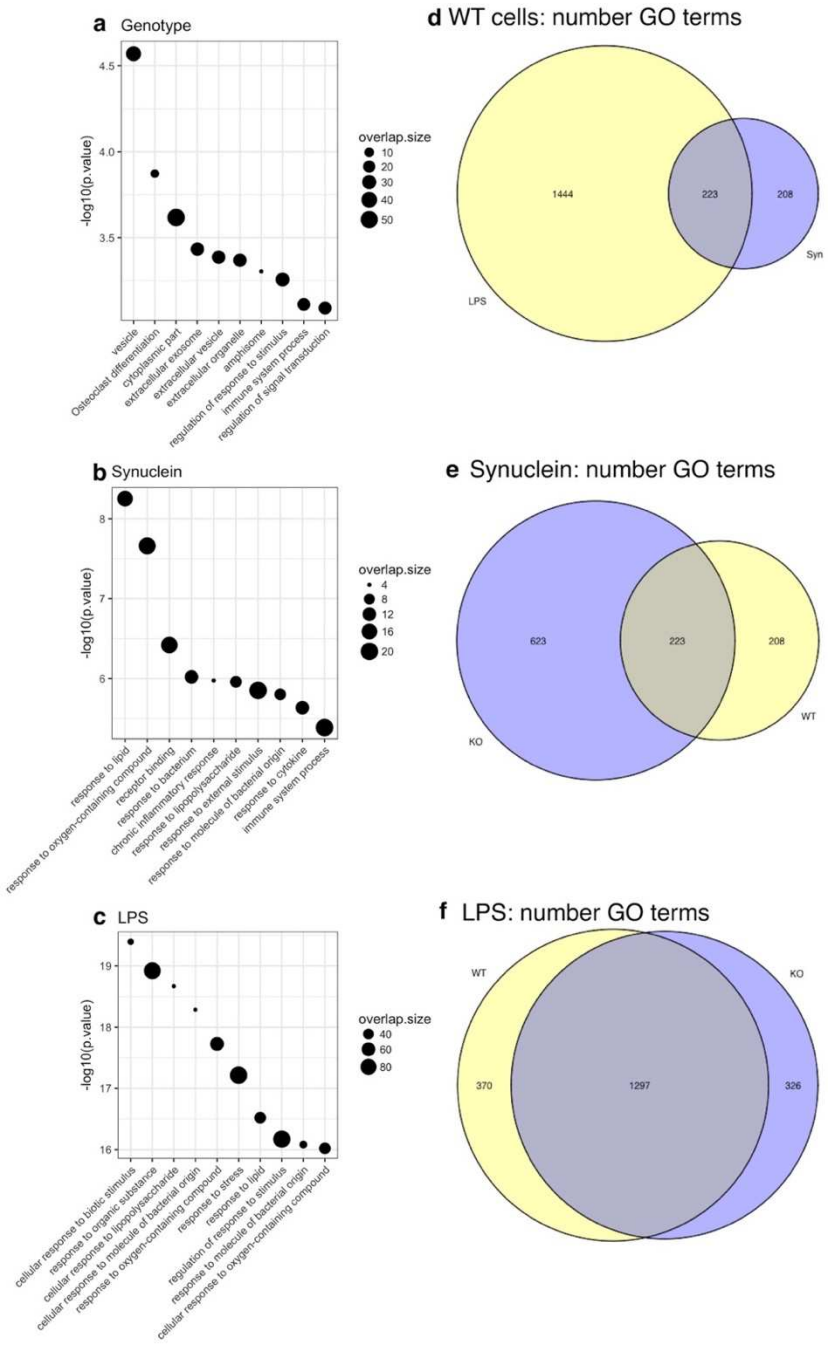

Figure 4-5. Gene ontology (GO) analysis of differentially expressed genes between LRRK2 genotype and inflammagen treatments. (a-c) Plots of top 10 significant GO terms associated with LRRK2 in untreated cells (**a**) or after exposure to α-synuclein PFFs (**b**) or LPS (**c**) in wild type cells. (**d-f**) Euler diagrams of significant (p adjusted < 0.05) GO terms comparing the treatments in WT cells (**d**) or genotypes (**e-f**) treated with either α-synuclein PFFs (**e**) or LPS (**f**).

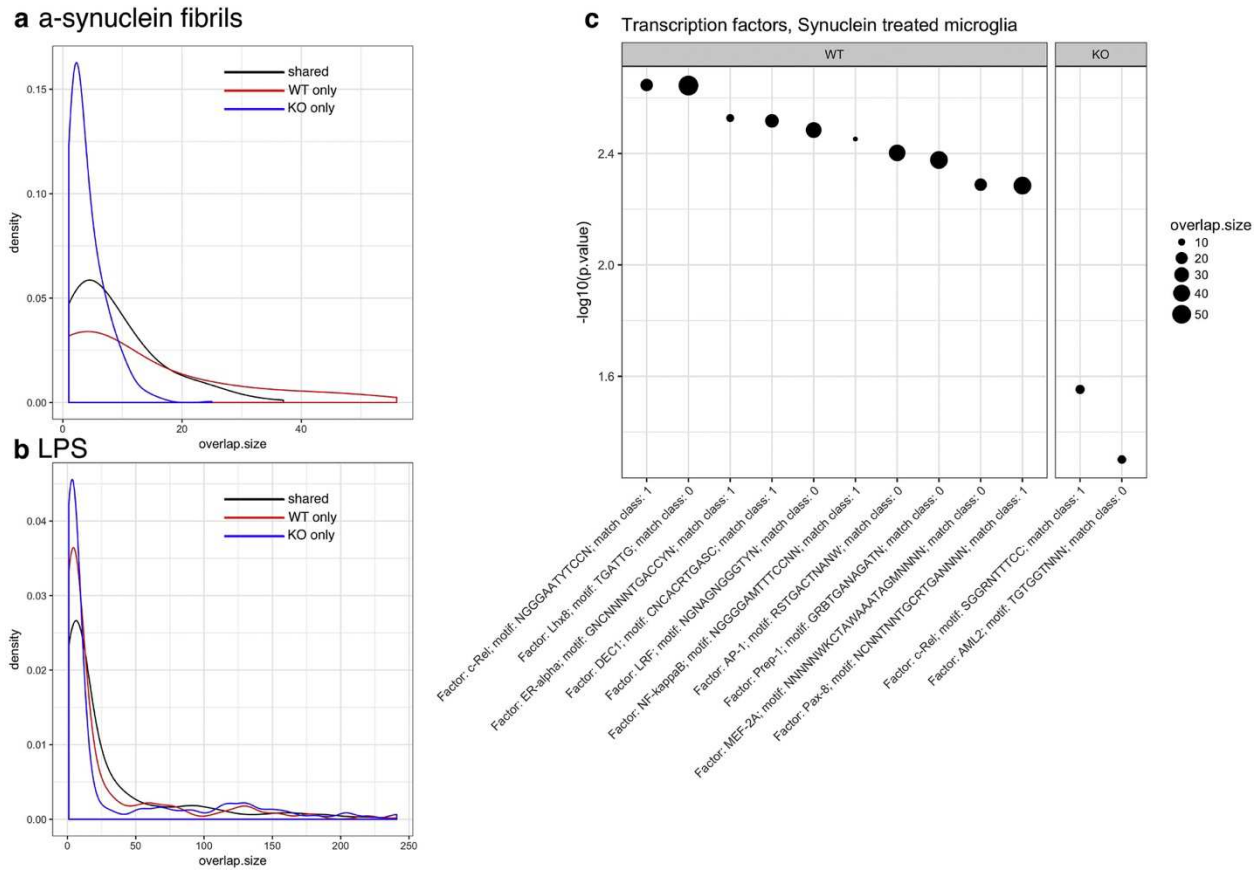

Figure 4-6. Total evaluation of GO terms between LRRK2 WT and KO genotypes.
(**a, b**) Density plots of overlap size (number of differentially expressed genes in the dataset in a given GO category) for all significant GO terms after exposure to α-synuclein PFFs (**a**) or LPS (**b**) in either both genotypes (black), only in WT cells (red) or only in LRRK2 KO (blue). KO cells have more GO categories but with fewer genes in each category. (**c**) Top GO terms in the domain of transcription factors. Top 10 transcription factor GO terms for WT cells (left) and only 2 significant transcription factor terms in KO cells (right).

On the other hand, the GO:200037 category “regulation of reactive oxygen species metabolic process” was present uniquely in the α-synuclein PFFs-exposed cells(p=0.000359) and included the mitochondrial anti-oxidative enzyme dismutase Sod2. (The full list of enriched GO categories can be accessed through the web version of the published article, PMID: 31102768).

Additionally, while comparing the GO enriched pathways in LRRK2 WT and KO genotypes, we noticed that KO cells, had a greater number of identified GO terms than WT after exposure to α-synuclein PFFs (Figure 4-5e), but that LPS induced similar pathways in both genotypes (Figure 4-5f).

To understand the differences in GO categorization, the density plots of overlap size (number of differentially expressed genes in the dataset in a given GO category) of all significant GO terms have been evaluated for WT and KO cells or for total amount of cells. We found that distribution of overlap size for differentially expressed genes after α-synuclein exposure showed a peak at lower overlap size in KO cells compared to WT (Figure 4-6 a-b). The data revealed that although KO cells have more GO categories they contain fewer genes in each category.

After looking in more depth at the subsets of GO terms in the WT and KO cells, we noted that in WT, but not in KO cells, there was an enrichment of the genes regulated by the transcription factors c-Rel and NFκb, both associated with inflammation. Graph shows the top 10 transcription factor GO terms for WT cells and only 2 significant transcription factor terms in KO cells (Figure 4-6c). This data suggests that regulation of transcription may be influenced by LRRK2 upstream of NF-κB and other transcription factors through unknown regulatory pathways that needs to be evaluated in the future.

Overall, the GO profiling data suggest that exposure to LPS or α-synuclein PFFs induce distinct and specific effects on gene expression with new genes and pathways underlying those differences.

4.2.4 Technical validation of differential gene expression from RNA-seq top hit

Next, I performed a technical validation of the data obtained in the RNA-seq experiment using qRT-PCR as an alternative method of evaluation of gene expression changes at the mRNA level. First, the LRRK2 expression was confirmed in WT samples in comparison to KO animals in all, treated and untreated samples (Figure 4-7a). Next, I

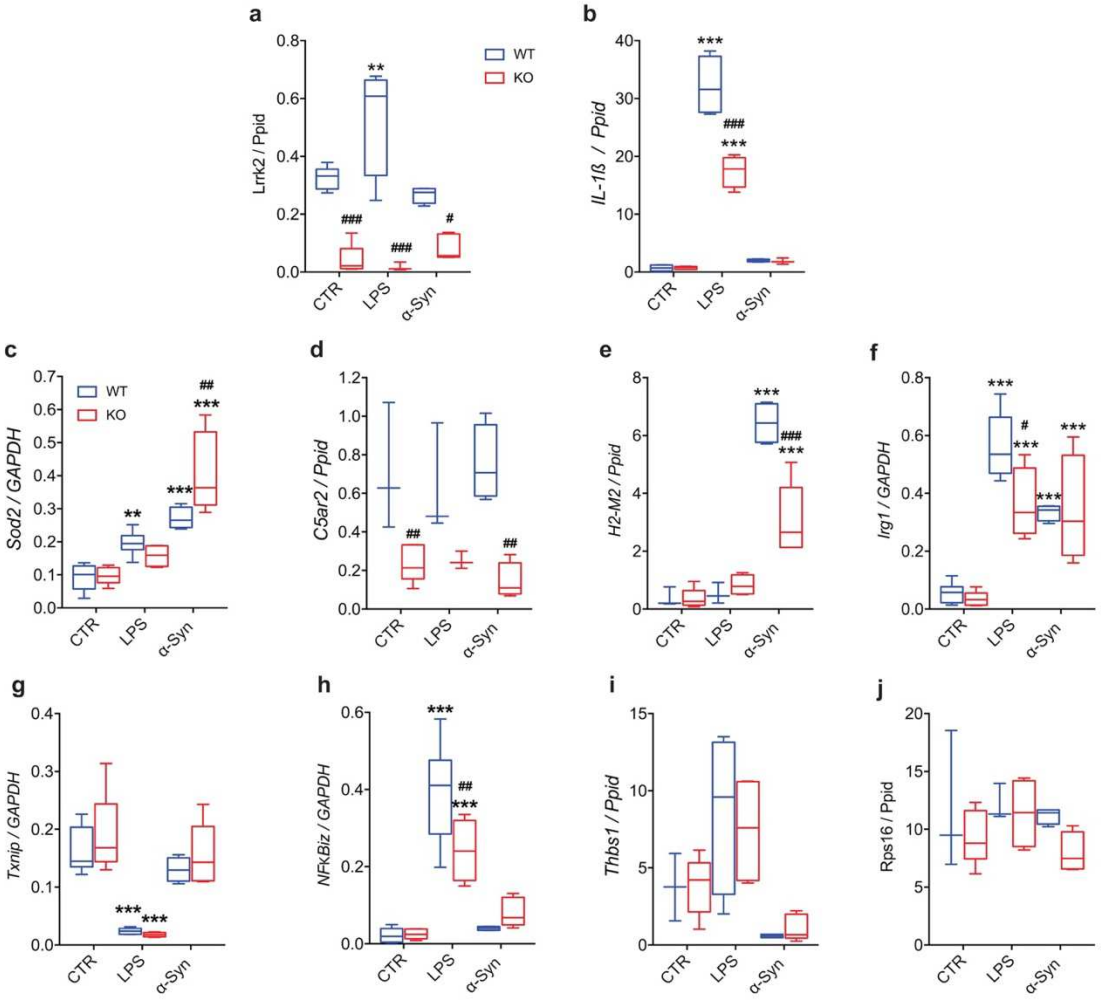

Figure 4-7. Technical validation of RNA-Seq top hits by qRT-PCR. Quantification of relative gene expression of RNA-seq top hits in LRRK2 WT and KO microglia cells unstimulated or stimulated with α-synuclein PFFs or LPS. Two-way ANOVA followed by Bonferroni's post-hoc test, with *** p-value < 0.001 for treatments with LPS or α-synuclein and with $^{###}$p <0.001 for WT vs. KO.

measured the changes in expression level of pro-inflammatory cytokine IL-1β. In our laboratory, its expression was recently reported to be attenuated in LRRK2 KO primary microglia cells and increased after LPS treatment of microglia (I. Russo et al., 2015). In agreement with the reported data, I was able to confirm an increased expression of IL-1β

following LPS treatment and its lower mRNA level in microglia from LRRK2 KO animals (Figure 4-7b).

Additionally, the Lrrk2 KO mice with exon-2 deletion that have been used in this study (see Material and Methods) are different from the Lrrk2 exon-41 KO animals, reported in our previous study (Russo et a., 2015). Our data confirm that responses to LPS are conserved across two different KO models and, therefore, are genuinely due to Lrrk2 deficiency.

We next attempted to validate a set of gene candidates that showed a range of expression levels with an enrichment for genotype or for two inflammatory stimuli with > 2-fold differential expression and adjusted p value < 0.05 based on the RNA-Seq dataset.

During validation, we grouped the selected genes by the level of expression, with the high expression genes of ***Txnip*** (downregulated by LPS in WT cells), ***Sod2*** (upregulated by both LPS and α-synuclein PFFs), ***Irg1*** (upregulated by LPS and α-synuclein PFFs) and ***NFKBiz*** (upregulated after LPS treatment). For a moderately expressed gene, **Thbs1** (upregulated by LPS) and the two low expressed genes, **C5ar2** (lower in Lrrk2 KO cells after α-synuclein treatment) and **H2-M2** (upregulated by α-synuclein PFFs).

The p-adjusted values for each gene candidate were the following: Txnip: p adjusted = 3.6×10^{-26} in WT cells and 1.0×10^{-26} in KO cells; Sod2: p adjusted = 1.64×10^{-13} by LPS and 4.35×10^{-51} by α-synuclein treatment; Irg1: p adjusted = 2.64×10^{-24} by LPS and 1.38×10^{-15} by α-synuclein; NFKBiz: p adjusted = 2.05×10^{-41} by LPS; Thbs1: p adjusted = 2.66×10^{-6} by LPS; C5ar2: p adjusted = 0.0262 by α-synuclein; H2-M2: p adjusted = 3.0×10^{-12} by α-synuclein treatment.

The results were expressed as the mean ± SEM (WT-CTR n = 4, WT-LPS n = 5, WT-α-synuclein n = 4, KO-CTR n = 5, KO-LPS n = 4 and KO-α-synuclein n = 5). Data were analyzed using two-way ANOVA followed by Bonferroni's post-hoc test as reported in the figure legend (Figure 4-7c-j).

Ppid was used as reference gene for lowly and moderately expressed genes, while GAPDH for highly expressed genes (see Material and Methods).

Six out of the seven assayed genes (Sod2, C5ar2, H2-M2, Irg1, Txnip and NFKBiz) were detected by qRT-PCR in the identical pattern as determined by RNA-Seq (Figure 4-7c-

h). However, despite the expression trend of Thbs1 and Rps16 genes that was in the same direction with RNA-seq experimental data, the qRT-PCR differences were not statistically significant (Figure 4-7i-j), resulting in an overall validation rate of 75%.

4.2.5 Biological validation and time-course of microglial responses to α- synuclein PFFs

4.2.5.1 Timecourse of SOD2 mRNA and protein expression in response to α-synuclein PFFs stimulation

As discussed above, LPS and α-synuclein PFFs induce overlapping as well as distinct effects on gene expression profile of WT microglia cells. However, in order to maximize the responses to each inflammagen, we used different timepoints for LPS (1 hour) and α-synuclein PFFs (8 hours of treatment), based on previous observations (Russo et al. 2015).

To ensure that the observed differences in gene expression between LPS and α-synuclein PFFs were not due the differential time of treatments used for the RNA-Seq experiment (LPS 1 h and α-synuclein PFFs 8 h), we performed a time-course experiment where microglia cells were treated for 0, 1, 4, 8 and 16h with α-synuclein PFFs or LPS. This set of experiments was performed on independent cohort of samples.

We choose the mitochondrial antioxidant enzyme SOD2, one of the most differentially expressed genes in WT cells in response to α-synuclein PFFs stimulation (2.5-fold, adjusted $p = 4.3 \times 10^{-51}$) as a candidate gene for the biological validation of RNA-seq data.

Using qRT-PCR, we found that α-synuclein PFFs trigger a robust induction of SOD2 mRNA starting at 1h, which continues to significantly increase at 8 h and 16 h of treatment compared with untreated cells (Figure 4-8a; 35-fold at 8 h vs. control, ***p < 0,001, to 60-fold at 16 h vs. control, ***p < 0,001; 1,7-fold 8 h vs. 16 h, $^{\#}p < 0,05$).

As expected, LPS also induce an increase in SOD2 mRNA at 16 h of treatment (31-fold at 16h vs. control, ***p < 0,001). However, SOD2 levels are half of the amount expressed by microglia in response to α-synuclein PFFs at matched treatment times (~2-fold α-synuclein PFFs vs. LPS at 16 h, §§p < 0,01). GAPDH was used as reference gene in this experiment. The results are expressed as the mean ± SEM (0h n=8, LPS1h n=5, LPS 4h n=5, LPS 8h n=5, LPS 16h n = 4, α-synuclein 1h n = 5, α-synuclein 4h n = 5, α-synuclein 8h n = 5, α-synuclein 16h n = 4).

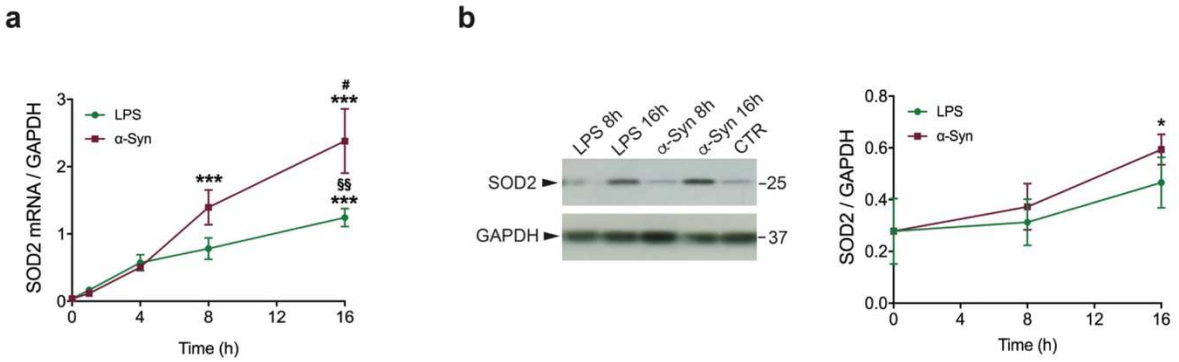

Figure 4-8. Timecourse of SOD2 mRNA and protein expression in response to α-synuclein PFFs stimulation in LRRK2 WT microglia cells. (a) α-synuclein PFFs trigger a robust induction of SOD2 mRNA compare to LPS. One-way ANOVA followed by Tukey's post-hoc test, with ***p-value < 0.001 for LPS or α-synuclein treatments, #p < 0.05 for α-synuclein 16 h vs. α-synuclein 8 h and §§p < 0.01 for LPS treated vs. α-synuclein treated cells. **(b)** Time course of SOD2 protein expression of WT microglia cells treated with α-synuclein PFFs or LPS priming. The results are expressed as the mean ± SEM (n = 3 per each group), one-way ANOVA followed by Tukey's post-hoc test. *p < 0.05, α-synuclein 16 h vs. untreated cells (0 h).

These data therefore confirm that there are quantitative differences – not just time shifted responses - in SOD2 gene expression between cells exposed to LPS or α-synuclein PFFs.

To investigate whether the changes in SOD2 mRNA expression also present at the protein level, we performed a timecourse experiment where microglia were treated for 0, 8 and 16h with α-synuclein PFFs or LPS (Figure 4-8b). The Western blot data show that although both inflammatory insults induce an increase in SOD2 at the protein level, the increase was higher with α-synuclein PFFs (~2-fold α-synuclein PFFs 16 h vs. control, *p < 0.05), confirming the mRNA data.

4.2.5.2 LRRK2 phosphorylation after inflammatory stimuli

Previous research demonstrated that inflammatory stimuli result in increased LRRK2 Ser935 phosphorylation in microglia (Puccini et al., 2015; Schapansky et al., 2015). Based on this observation, we investigated the effect of LPS and α-synuclein PFFs on LRRK2 phosphorylation after 8h and 16 h of α-synuclein PFFs or LPS treatment (Figure 4-9).

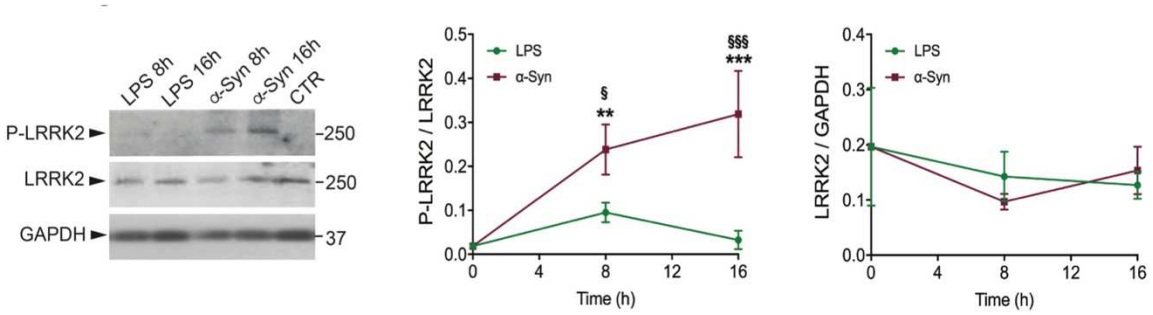

Figure 4-9. pS935-LRRK2 and total LRRK2 protein expression in WT microglia cells treated with α-synuclein or LPS. GAPDH was used ad reference gene for LRRK2 expression. The results are expressed as the mean ± SEM (n = 3 per each group). Data were analyzed using one-way ANOVA followed by Tukey's post-hoc test. **p < 0.01 and ***p < 0.001, α-synuclein treated vs. untreated cells (0 h). §p < 0.05 and §§§p < 0.001, α- synuclein treated vs. LPS treated cells.

According to our results, α-synuclein PFFs trigger a robust increase of pS935-LRRK2 at 8 h (12-fold, 8 h vs. control, **p < 0,01) and 16 h of treatment compared to untreated cells (16-fold, 16h vs. control, ***p < 0,001). Although LPS priming caused a mild increase of pS935-LRRK2 after 8 h of treatment, the increase was not statistically significant. Moreover, LPS and α-synuclein PFFs do not induce significant changes in LRRK2 total protein levels up to 16 h of treatment as shown at (Figure 4-9).

This data are in agreement the previous findings (I. Russo et al., 2015), although we noted that other studies have seen an increase of total LRRK2 protein expression after LPS stimulation (Moehle et al., 2012), leaving the effect of LPS on LRRK2 protein levels still unclear. Overall, these results confirm the RNA-Seq data showing that α-synuclein PFFs trigger a microglial response that is distinct from that induced by LPS.

4.2.5.3 Inflammatory cytokine profile of stimulated microglia

Cytokines constitute a significant portion of the immuno and neuromodulatory messengers that can be released by activated microglia (Hanisch, 2002; Y. S. Kim & Joh, 2006). As discussed above, LPS and α-synuclein PFFs induce overlapping as well as distinct effects on gene expression profile of WT microglia cells. To evaluate the profile of inflammatory cytokines released by microglia stimulated with two different inflammagens, I performed the multiplex enzyme-linked immunosorbent assay (ELISA), which allows simultaneous detection of 16 different mouse cytokines (Figure 4-10).
The microglia cells were stimulated with LPS or α-synuclein PFFs for different time points up to 24 hours and the culture medium with the released cytokines was subjected to ELISA analysis.
The results showed that seven out of sixteen cytokines were actively released from the activated microglia cells, representing mostly pro-inflammatory cytokines. Additionally, the data showed differential cytokine response between LPS stimulated (Figure 4-10a) or α-synuclein PFFs (Figure 4-10b) stimulated cells. Specifically, IL-1β, IL-6, and TNF-α cytokines secretion was attenuated upon α-synuclein PFFs treatment, while MCP-1 was slightly elevated (Figure 4-10c).

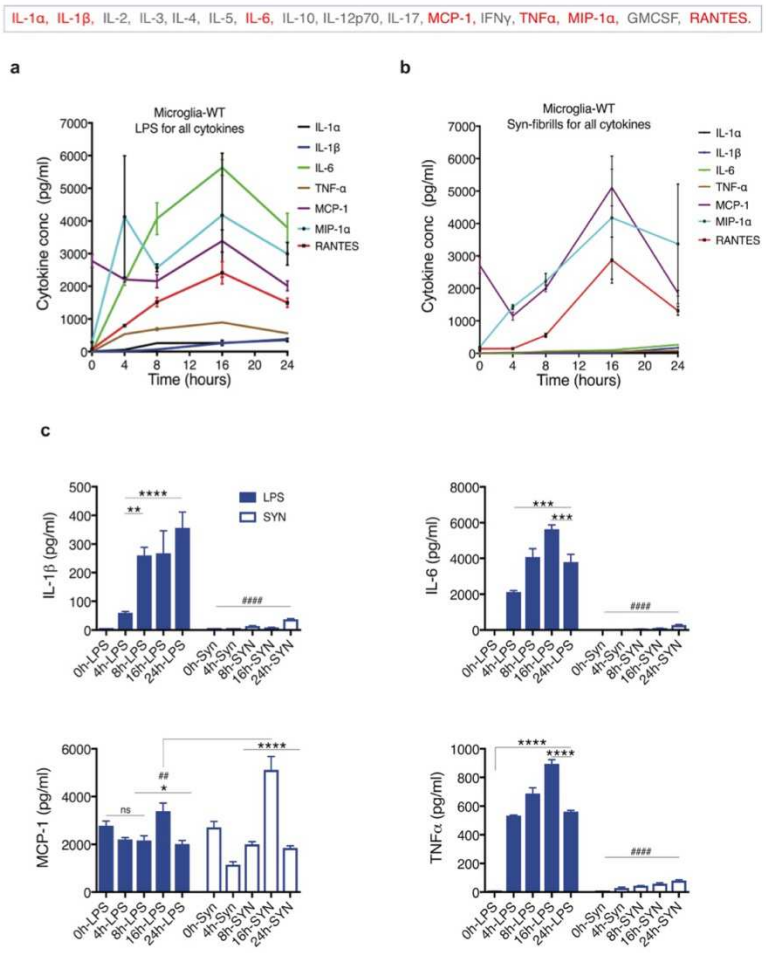

Figure 4-10. Inflammatory cytokine profile of microglia stimulated with LPS or α-synuclein PFFs. 7 out of 16 cytokines were activated (red color, top panel), after LPS (**a**) or α-synuclein PFFs (**b**) stimulation of microglia for different timepoints. Cytokine secretion was detected by ELISA-multiplex (Quansys). (**c**) IL-1β, IL-6, and TNF-α cytokines secretion was attenuated upon α-synuclein PFFs, while MCP-1 was slightly elevated. One-way ANOVA followed by *Tukey's post-hoc test* with $*p < 0.05$ for different time points and $^{\#\#}p < 0.01$ for different treatments; n=4.

The results are expressed as the mean ± SEM ($n = 4$ per timepoint). Data were analyzed using one-way ANOVA followed by *Tukey's post-hoc test*. $*p < 0.05$, ***p < 0.001 and ****$p < 0.0001$, α-synuclein or LPS treatment between different exposure times. $^{\#\#}p < 0.01$ and $^{\#\#\#\#}$p < 0.0001 α-synuclein vs. LPS treated cells.

Overall, ELISA experiments showed different response between treatments, confirming that the two inflammagens produce different cytokine profiles.

4.2.6 α-Synuclein PFFs-mediated SOD2 induction in LRRK2 KO microglia

Multiple studies support the hypothesis that LRRK2 is one of the key modulators of microglial-associated inflammation, although the detailed molecular mechanisms are unresolved (B. Kim et al., 2012; Ma et al., 2016; Moehle et al., 2012). It has been shown that activated microglia secrete multiple toxic factors, including pro-inflammatory cytokines IL-1β, tumor necrosis factor-α as well as reactive oxygen species, ROS (Y. S. Kim & Joh, 2006; Lull & Block, 2010), suggesting that inflammation strongly correlates with an oxidative stress response. In our RNA-Seq data, we noted upregulation of the mitochondrial antioxidant SOD2 in response to inflammatory treatment.

To validate this observation at the protein level in LRRK2 WT and KO microglia, we treated cells with α-synuclein PFFs at 0, 8 and 16 h (Figure 4-11). Cell lysates were subjected to immunoblotting and probed with LRRK2, SOD2, IL-1β and GAPDH antibodies. First, we confirmed LRRK2 protein deletion in LRRK2 KO microglia cells (Figure 4-11a,b). Next, we analyzed SOD2 expression in LRRK2 WT and KO cells, treated with inflammatory stimuli. While α-synuclein PFFs induced a significant increase of SOD2

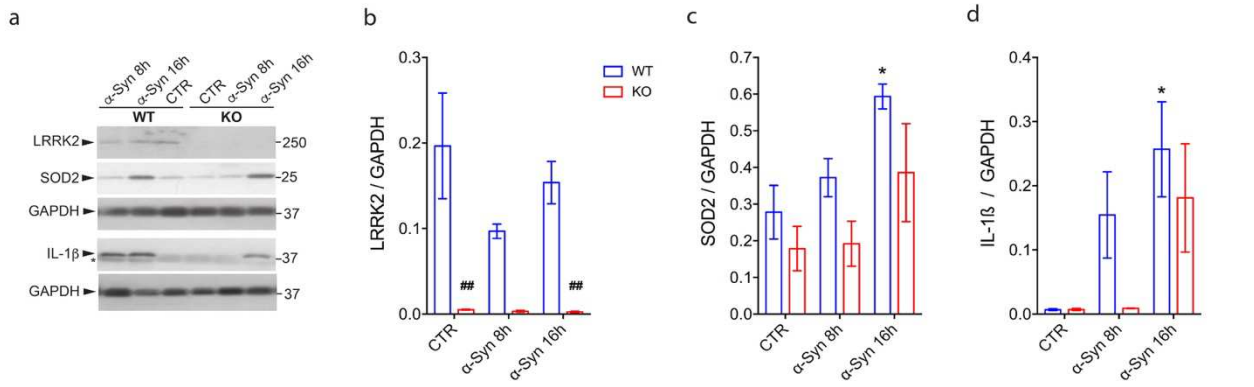

Figure 4-11. LRRK2 controls α-synuclein PFFs–mediated SOD2 induction. (a) LRRK2 WT and KO microglia cells were treated with α-synuclein PFFs for 0, 8 and 16 h. Quantification of LRRK2 **(b)**, SOD2 **(c)** or IL-1β **(d)** is normalized for GAPDH house-keeping protein. Two-way ANOVA followed by Bonferroni's post-hoc test, with * p-value< 0.05 for α-synuclein treated vs. untreated cells (0 h). ##$p < 0.01$ for LRRK2 WT vs. KO cells (for untreated and α-synuclein treated cells).

protein level after 16h treatment in WT cells (~2-fold at 16 h vs. control, *p < 0.05), the increase of SOD2 expression after 16 h of treatment in KO cells was not statistically significant, suggesting an attenuated response under Lrrk2 deficiency (Figure 4-11a, c). In the same experiment, we measured pro-inflammatory cytokine IL-1β levels and found that α-synuclein PFFs cause an increase of IL-1β protein expression in WT cells (~38-fold, 16 h vs. control, *p < 0.05) and this response is delayed in LRRK2 KO cells at both 8h and 16h of PFFs treatment (Figure 4-11a, d). The results are expressed as the mean ± SEM (n = 3 per genotype/timepoint). Data were analyzed using two-way ANOVA followed by Bonferroni's post-hoc test.

Taken together these data suggest a delayed response of LRRK2 KO microglia after an inflammatory stimulus compared to WT cells and reveal that LRRK2 contribute to α-synuclein PFFs-mediated SOD2 induction.

4.2.7 Summary

In this chapter we used RNA-Sequencing to examine transcriptomic profiles of LRRK2 wild-type (WT) and knock-out (KO) primary microglia cells under basal conditions and after treatment with two inflammatory stimuli, α-synuclein pre-formed fibrils (PFFs) or with more general inflammagen lipopolysaccharide (LPS).

We found that the separation between the treatments was stronger than the separation between LRRK2 WT and KO genotypes.

We further observed that, although α-synuclein PFFs and LPS mediate overlapping gene expression profiles in microglia, there are also distinct responses to each stimulus.

We found that α-synuclein PFFs trigger alterations of oxidative stress-related pathways with the mitochondrial antioxidant enzyme dismutase SOD2 as a strongly differentially regulated gene. We validated SOD2 at mRNA and protein levels. Furthermore, we found that LRRK2 KO microglia cells reported attenuated induction of mitochondrial SOD2 in response to α-synuclein PFFs, indicating a potential contribution of LRRK2 to oxidative stress-related pathways. Additionally, we found that two different inflammatory stimuli

cause different response in LRRK2 phosphorylation status (which is increased upon stimulation with α-synuclein PFFs) and resulted in a different cytokine profile. Overall, these results suggest that microglial LRRK2 may contribute to the pathogenesis of PD via altered oxidative stress signaling.

In the next chapters I will present the work related to inflammatory stimulation of acutely isolated brain microglia. Current gene candidates, obtained from the primary microglia experiment, will be evaluated in vivo in resident brain microglia using single-cell RNA-Sequencing analysis.

Chapter 5

Characterization of the resident microglia isolated from adult brains of LRRK2 WT, KO, G2019S and R1441C knock-in mice

5.1 Introduction

Microglial cells are the professional phagocytes of the central nervous system (CNS). Upon detection of signs for brain injury or nervous system dysfunction, microglial cells undergo a complex, multistage activation process that converts them into the "activated microglial cell." This cell form has the capacity to release a large number of substances that can act detrimental or beneficial for the surrounding cells. Activated microglial cells can migrate to the site of injury, proliferate, and phagocytose cells and cellular compartments (H. Kettenmann et al., 2011).

This phagocytic function is important for the normal brain, during brain development, and in pathology and regeneration (Neumann, Kotter, & Franklin, 2009). During development, microglial cells play a specific role in phagocytosis of apoptotic cells, and considered to be involved in synapse removal and in pruning synapses in the postnatal brain (Stevens et al., 2007). Phagocytosis represents a part of a host-defense mechanism of the innate immune system and there is a possible implication of phagocytic dysfunction in neuronal degeneration (Janda, Boi, & Carta, 2018).

Since pathogenic protein accumulation is a key feature in PD, altered phagocytic clearance (compromised or uncontrollably enhanced) might participate in PD pathogenesis or contribute to synaptic degeneration, as reviewed by (M.-E. Tremblay, Cookson, & Civiero, 2019).

It has been previously shown that brain-resident microglia are predominantly implicated in the removal of DA cell debris *in vivo* in the MPTP mouse model of PD (Depboylu et al., 2012).

Multiple lines of evidence suggest that aggregated forms of α-syn released from dying neurons can activate microglia (C. Kim et al., 2013; Zhang et al., 2005) and TLR2/4 receptor mediated microglial phagocytic activity has been reported in α-synuclein-induced microglia (Fellner et al., 2013). Additionally, defective function of TREM-2 receptor in PD may lead to incomplete removal of apoptotic cells and debris and accumulation of toxic products that may chronically stimulate microglia to release cytotoxic species, as reviewed in (Janda et al., 2018).

Microglial activation in response to injury and pathogens can lead to neuroinflammation, which, in turn, is known to contribute to worsening of neuropathology in animal models of PD (Cebrian, Loike, & Sulzer, 2015).

Since microglia is actively involved in clearing debris generated by dying neurons or membrane shedding (Neumann et al., 2009), we were interesting to investigate, whether this crucial activity is present in acutely isolated brain microglia cells and whether phagocytosis is altered upon activation with α-syn fibrils. Additionally, the important question is whether phagocytic activity differs between LRRK2 WT, KO and mutant mice.

5.2 Results

5.2.1 Acute isolation and characterization of resident microglia from the adult mouse brain using Cd11b

To investigate the role of Lrrk2 in inflammatory response of microglia under conditions closest to those seen *in vivo*, I established a method for the direct isolation of a pure population of resident microglia cells from the adult mouse brain. My objectives here

were to obtain sufficient cell numbers for analysis with minimal impact on the microglial gene signature. The isolated resident microglia from Lrrk2 WT, KO and mutant adult mouse brains were characterized morphologically and functionally to determine if the cells would be suitable for subsequent analyses in chapter 7.

Magnetic-activated cell sorting (MACS) is a method for separation of various cell populations depending on their surface antigens. MACS first labels cells with 50nm non-toxic, biodegradable paramagnetic microbeads. These microbead particles are conjugated to a specific antibody against a cell surface antigen and are inert, which allows for the preservation of the functional status of the labeled cells.
To isolate resident microglia cells from adult mouse brains, tissues were gently mechanically and enzymatically dissociated (Figure 5-1).

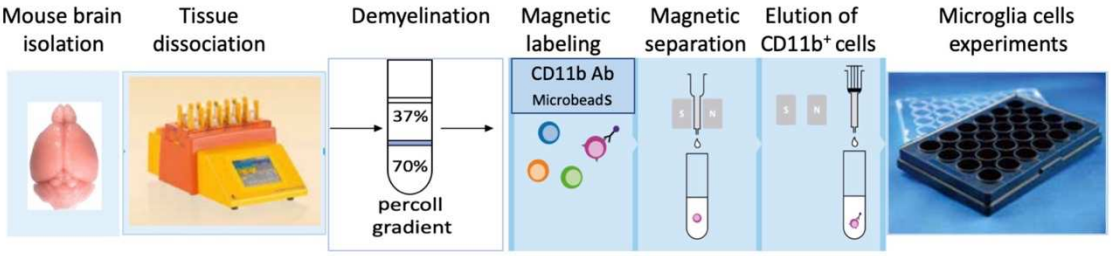

Figure 5-1. Isolation of resident microglia from adult mouse brain (MACS technology).
After tissue dissociation and demyelination by percoll gradient, cell mixture was labeled with CD11b-magnetic beads and isolated using magnetic separation following by elution of CD11b-positive cells.

Typically, myelin debris is generated during the dissociation procedure. In mice, myelination begins around birth in the spinal cord and is completed in the brain during the first postnatal month (Simons & Trotter, 2007). Removal of myelin debris by Percoll density gradient is therefore a necessary step to obtain a higher purity and recovery of target cells. The cell mixture was then labeled with magnetic beads conjugated with the pan-microglial marker CD11b and isolated using magnetic separation (see Materials and Methods).

5.2.2 Quality assessment of acutely isolated adult mouse brain microglia

As relatively long preparation time of isolation and sorting of brain microglia might introduce cell stress and influence gene expression data, it was critical to evaluate the quality of the isolated cells prior to their use in experiments. I therefore performed immunostaining for established microglial markers, RNA integrity number, LRRK2 expression and phagocytic activity as well as transmission electron microscopy (TEM).

5.2.2.1 Immunostaining of brain isolated microglia

Microglia were isolated directly from the whole brains of either young (postnatal day 4 pups) or adult (3 month old) wild type mice, magnetically sorted with CD11b-labeled beads and seeded on coated tissue culture plate for visual and immunofluorescent

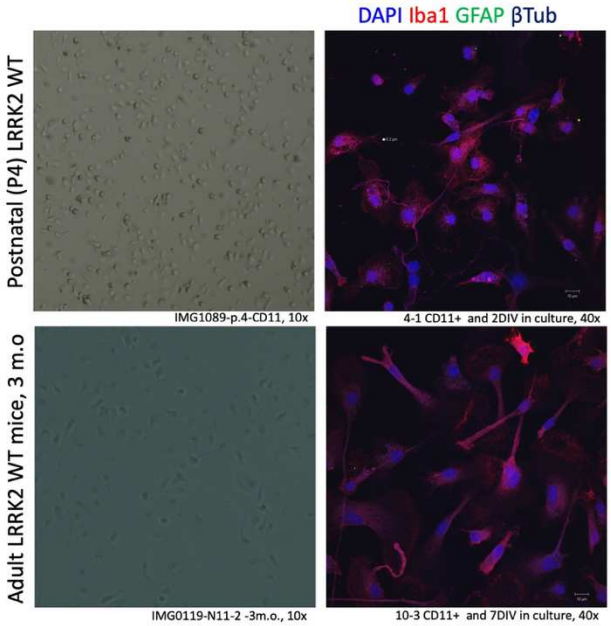

Figure 5-2. **Immunohistochemistry (ICC) of an acutely isolated brain resident microglia from adult mouse brain.** Magnetically sorted, CD11b-positive microglia cells, isolated from young postnatal pups (top) or from adult mice (bottom) show normal morphology and no contamination with astrocytes or neuronal cells. Representative light microscopy images (10x objective) and immuno-stained images from confocal microscopy (40x objective).

evaluation. To evaluate the purity of the isolated microglia, cells were immunostained with the microglial marker Iba1, the astrocyte marker glial fibrillary acidic protein (GFAP) and the neuronal marker ß-III-tubulin. After culturing for up to seven days (7DIV), the microglial population had no detectable contamination with either astrocytes or neuronal cells (Figure 5-2). In addition, intact DAPI nuclear staining was reflective of a healthy, viable cell status and Iba1, distributed throughout the whole cell, demonstrated normal microglia cell shape, with the presence of cellular processes.

5.2.2.2 RNA integrity of brain isolated microglia

Since my goal was to use acutely isolated microglia in several downstream applications, including single cell RNA-seq experiment, I wanted to assess the RNA quality of the freshly isolated adult mouse brain microglia as the critical point for this type of experiments. For this purpose, the total RNA was isolated using RNA-easyPlus mini-kit and the RNA integrity (RIN) was measured on Bioanalyzer (see Material and Methods section). As shown in Figure 5-3a, high quality, intact RNA with RIN=9.3 (out of 10) without signs of degradation could be extracted from the freshly prepared cells. Thus, these cells can be safely used for the sequencing library preparation for scRNA-seq experiment.

5.2.2.3 LRRK2 protein expression in brain isolated microglia

To investigate LRRK2 protein expression in acutely isolated adult mouse brain microglia, total amount of CD11b-separated cells from one brain of either 1.5 month old or 18 month old mouse was prepared for western blot analysis. Although, as shown in Figure 5-3b, left panel, the cells were positive for microglial protein Iba1 and negative for astrocyte marker GFAP, the level of LRRK2 protein expression was below detectable levels. In an additional experiment with increased amount of isolated cells, performed by combining CD11b-positive microglia from 5 brains it was possible to detect LRRK2 at the correct protein size of 280 kDa from a total of ~3x10^6 brain microglial cells (Figure 5-3b, right panel). Given the limited amount of isolated microglia from unstimulated mouse brain as well as limited mouse resources in general, I will approach a novel method for measuring

protein expression, single cell western blot (scWB) technology, that will be discussed in chapter 8 of this thesis.

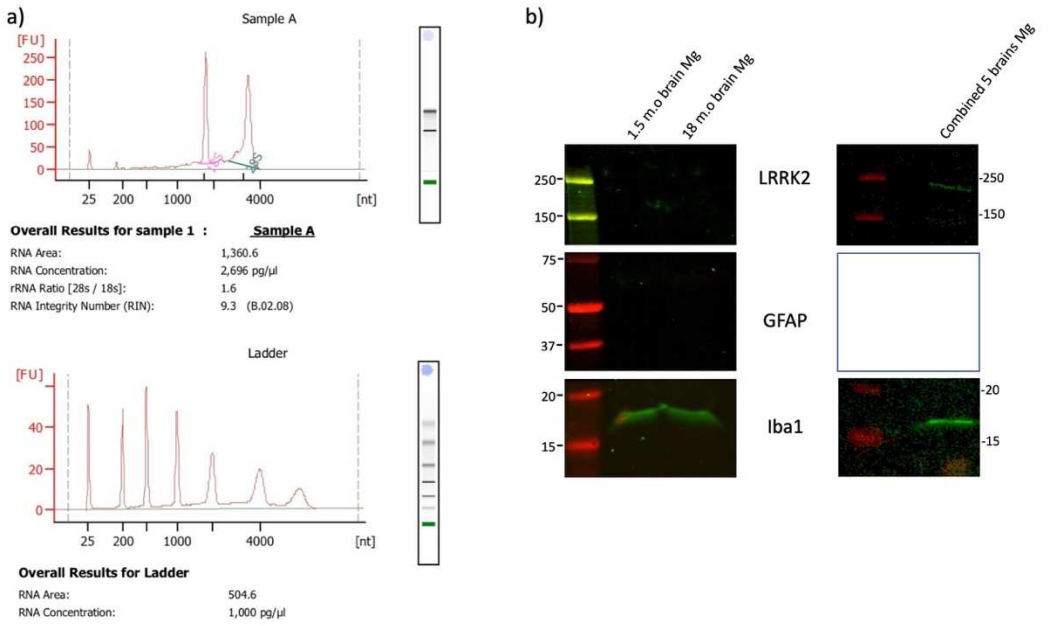

Figure 5-3. Evaluation of brain isolated microglia at RNA-level and protein expression level. (**a**)brain isolated microglia preserves RNA high quality with RNA integrity (RIN)=9.3. (**b**)Western blot analysis of brain isolated microglia shows LRRK2 protein expression and confirms purity of microglial extraction with Iba1-positive and GFAP-negative markers.

Overall, the data above show that microglia acutely extracted from adult mouse brain preserve the morphological features, have high RNA quality and express classical microglial protein markers. The use of resident brain microglia cells provides a potential advantage over culture-based protocols by avoiding transcriptional reprogramming of primary microglia as reported in the literature (Butovsky et al., 2014).These cells may therefore be a valuable tool for future *in vivo* investigations.

5.2.2.4 Functional characterization of resident microglia: ex-vivo phagocytic activity

Although the above data supports the contention that acutely isolated microglia are reasonable models for microglia *in vivo*, they do not prove that these cells are functionally active. In order to investigate the phagocytic properties of resident brain microglia and compare phagocytic activity between different LRRK2 genotypes ($Lrrk2^{+/+}$, $Lrrk2^{-/-}$, $G2019S^{+/+}$ and $R1441C^{+/+}$), CD11b-positive microglia were acutely isolated from 1.5 years-old animals (as described in Material and Methods). To evaluate phagocytic properties of resident microglia in the activated state, cells were stimulated with α-synuclein pre-formed fibrils (PFFs) that were reported to initiate the inflammatory process in microglial cells (Hoffmann et al., 2016; I. Russo et al., 2015). The phagocytic assay was then performed by feeding isolated microglia with fluorescently labeled neuronal debris (Figure 5-4).

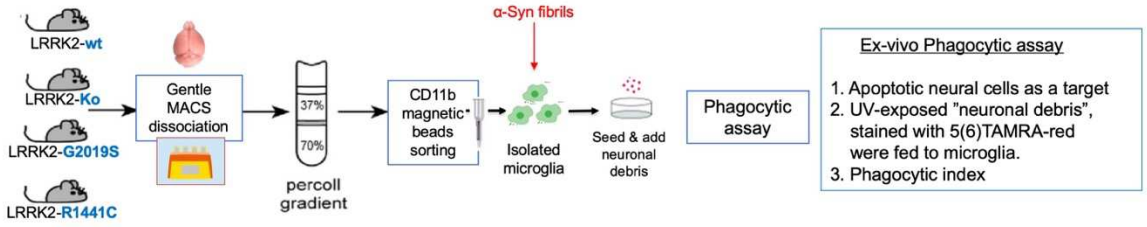

Figure 5-4. Schematic of acute isolation of brain microglia cells and phagocytic assay. To characterize phagocytic activity of microglia isolated from the adult brains of 1.5 y.o. LRRK2 WT, KO, G2019S or R1441C mice, cells were isolated with CD11b magnetic sorting, treated with α-Synuclein fibrils and fed with TAMRA-stained neuronal debris to evaluate a phagocytic index.

I choose to use apoptotic primary neurons as a targets, because they should closely approximate natural neuronal targets of microglial phagocytosis *in vivo* (Lehmann, Cooper, Maric, & Herkenham, 2016). Isolated microglia were seeded overnight at $0.15x10^6$ cells/well on PDL-coated, 8-well Lab-Tek II removable chamber slides to adhere. The next day cells were treated with freshly prepared UV-irradiated and TAMRA-labeled neuronal debris at double amount of the seeded microglia. Phagocytosis was

conducted for 1 hour following by extensive washing and cell fixation with 4% paraformaldehyde (PFA). Engulfed neuronal debris were detected in Iba1-immunolabeled microglia as shown in representative confocal images (Figure 5-5).

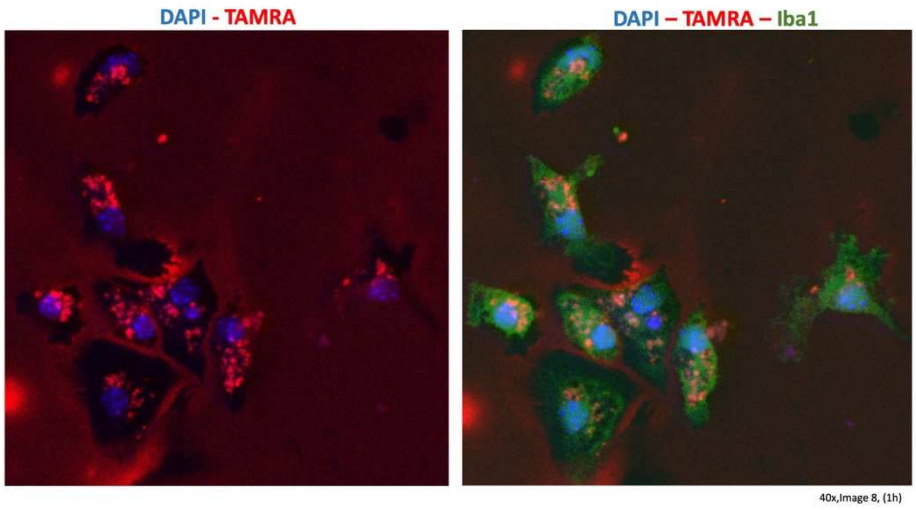

Figure 5-5. Phagocytic activity of isolated brain resident microglia. Representative confocal image of immunostained acutely isolated brain microglia (Iba1), that have been fed with the fluorescently 5(6)-TAMRA-labeled neuronal debris and counter-stained with DAPI (40x objective).

To quantify the phagocytic ability of microglial cells, the phagocytic index was calculated using particle analysis on thresholded images in the ImageJ software package. As shown in Figure 5-6, the total area of phagocytosed TAMRA-labeled apoptotic cells (in the red channel) was compared to the total area of microglial cells (in the green channel) to evaluate the level of phagocytosis in these cells (Lehmann et al., 2016)

Next, I wanted to investigate the dynamics of the phagocytic process in order to choose the optimal phagocytic time for subsequent experiments. For the time course experiment of *ex vivo* phagocytosis, isolated CD11b-positive LRRK2 WT microglia cells were exposed to TAMRA-red labeled neuronal debris for 30 min, 1, 2 and 3 hours (Figure 5-7). The results indicate that the phagocytosis is a quick process in these cells, and, under these experimental conditions, microglia are able to engulf the neuronal debris within 30 min and debris are still detectable within the cells at 3 hours after exposure.

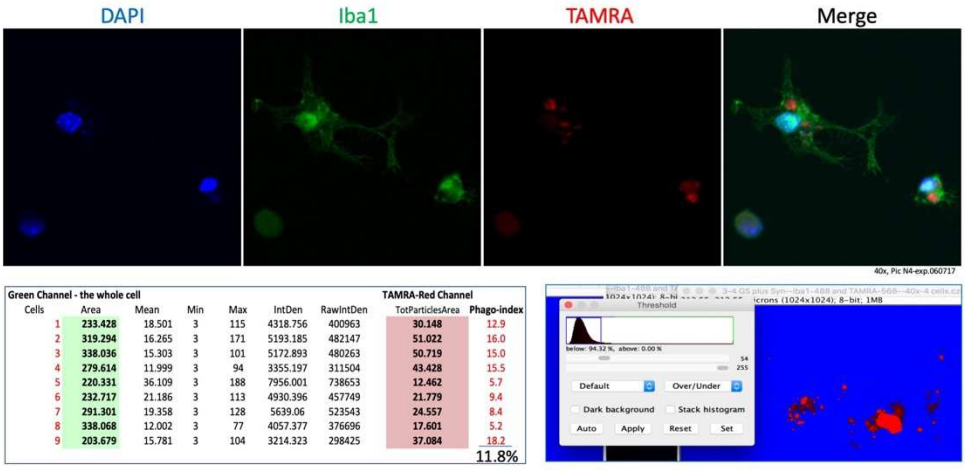

Figure 5-6. Quantitative evaluation of ex vivo phagocytic assay. Phagocytic index was calculated using Particle analysis by Fiji (ImageJ) software, dividing the total area of phagocytosed TAMRA-labeled neuronal apoptotic cells(red-positive) by the total area of microglial cells (Iba1-green positive).

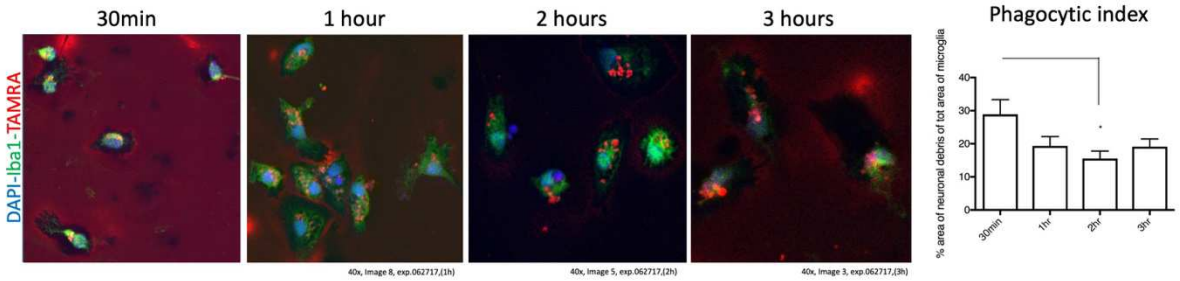

Figure 5-7. Time course experiment of ex vivo phagocytic activity. Isolated brain microglia cells (Iba1, green), were fed with TAMRA-red stained neuronal debris for different time points to evaluate time-dependency of phagocytic activity. (1-way Anova with Tukey's multiple comparisons test. *p<0.05).

In order to investigate the phagocytic activity of microglia acutely isolated from the adult brains of LRRK2 WT, KO, G2019S or R1441C knock-in mice, cells were simultaneously isolated from 1.5 year old animals, treated with 25μM α-synuclein PFFs to stimulate

microglial activation and fed for 1h with neuronal debris. (Figure 5-8). The cells were analyzed by immunostaining (Figure 5-8a) and confirmation of engulfed debris is provided by orthogonal projections of confocal z-stacks (Figure 5-8b).

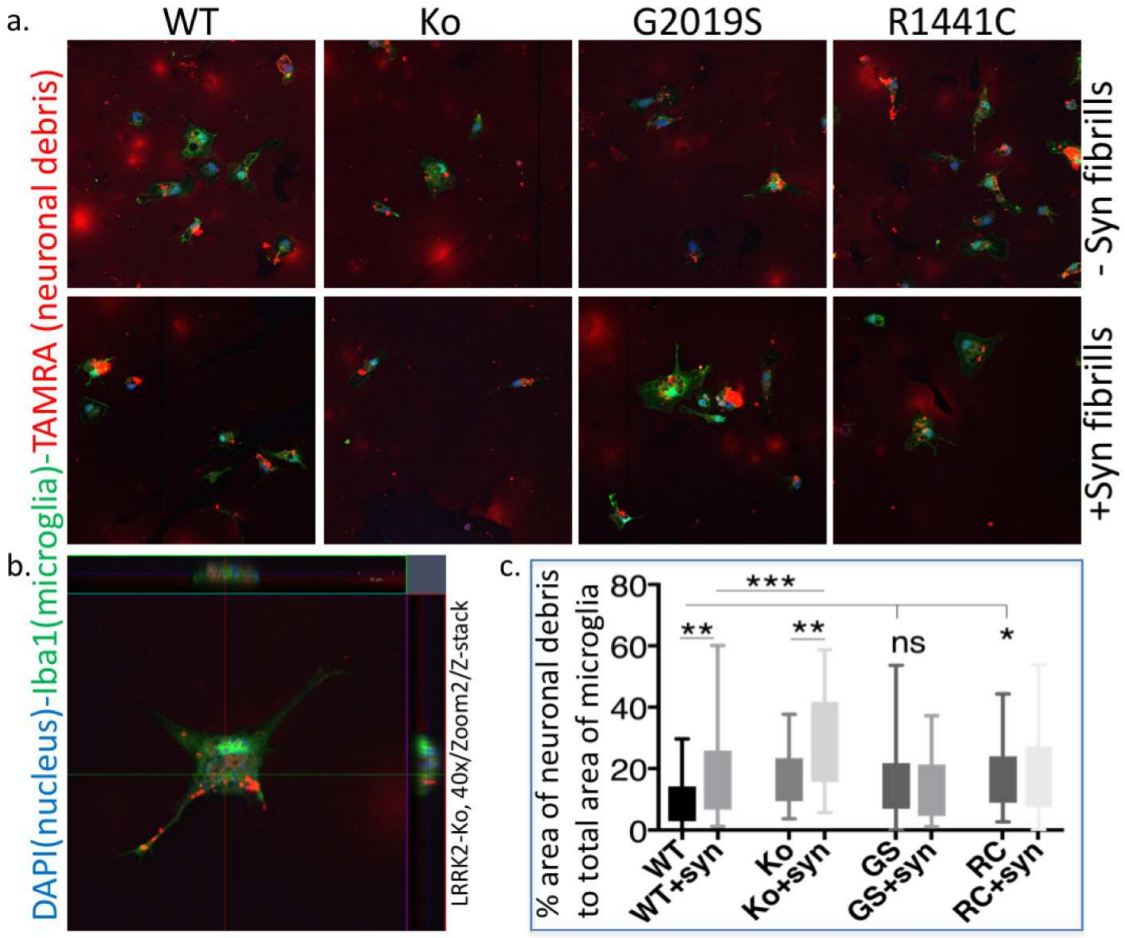

Figure 5-8. Ex vivo phagocytosis of LRRK2 WT, KO, G2019S and R1441C brain microglia. (**a**) Phagocytic activity of acutely isolated brain microglia from adult LRRK2 WT, KO and mutant mice (1.5y.o.) treated with α-synuclein fibrils. (**b**) Example of confocal z-stacks of the brain-isolated microglia engulfing neuronal debris. (**c**) Phagocytic assay quantification, 1-way Anova with Tukey's multiple comparisons test.

Additionally, the phagocytic index was calculated for LRRK2 WT, KO and mutants (Figure 5-8c). I found that the highest phagocytic activity was in LRRK2-KO cells stimulated with α-synuclein PFFs and this effect was not present in G2019S and R1441C mutant

microglia cells. These results implicate LRRK2 as a negative regulator of phagocytosis in the context of α-synuclein stimulated inflammation.

To test whether phagocytic activity of endogenous brain microglia can also be stimulated *in vivo*, brain sections from vehicle or LPS-injected mice were stained with CD68, a lysosomal protein associated with phagocytic activity in microglia. Elevated immunoreactivity of CD68 in LPS-activated brain sections indicates that inflammatory-stimulation changes the activation state of microglia and confirms an elevated phagocytic activity *in vivo* (Figure 5-9). Future experiments will determine whether CD68 marker is elevated specifically in acutely isolated microglia stimulated with α-synuclein PFFs and whether or not, its level varies among LRRK2 WT, KO and mutant microglia.

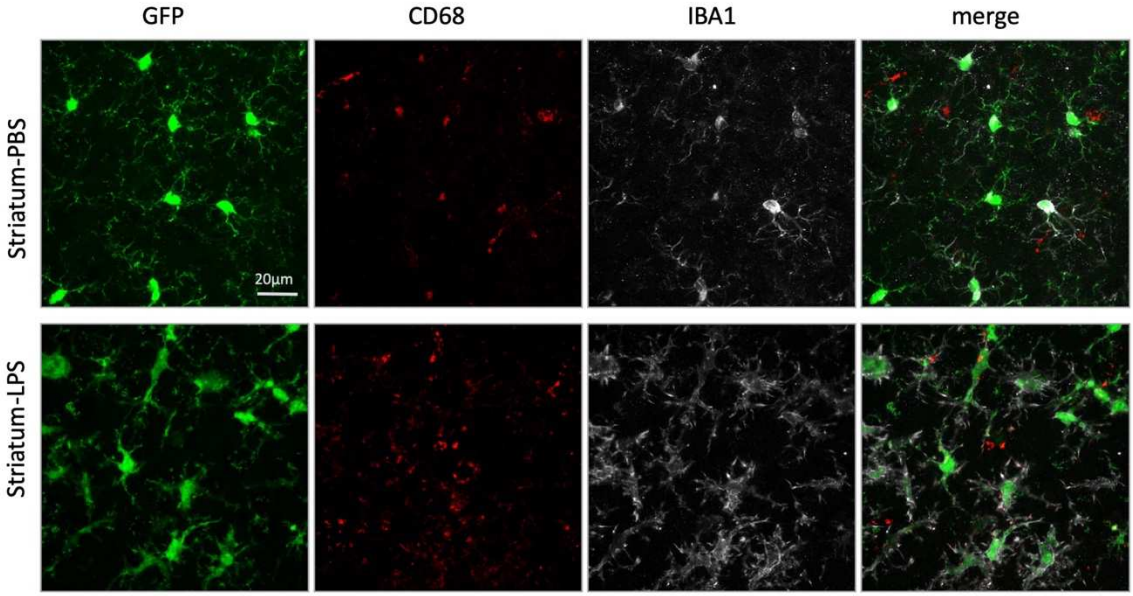

Figure 5-9. LPS-activated resident microglia shows elevated CD68 immunoreactivity *in vivo*. LRRK2 WT-Cx3cr1$^{GFP+/-}$ mice (with GFP-labeled microglia) were intrastriatally injected with general inflammagen LPS and stained with lysosomal marker CD68. Scale bar represents 20 µm.

5.2.2.5 Electron microscopy

To confirm microglial phagocytic activity, brain isolated microglial cells were imaged using transmission electron microscopy (TEM) to confirm the localization of neuronal debris

within the phagocytotic cells (Figure 5-10). Although the data from electron microscopy showing ingulfed debris after phagocytosis, the control image (microglia only) also showed some debris making the two images difficult to distinguish from each other. A possible explanation is that during the microglia isolation process, the microglia might phagocyte its neighboring cells, so specific staining is needed to distinguish between the two engulfed targets, detecting neuronal debris separately. For example, neuronal debris labelled with a photooxidizable dye may be exploited to distinguish neuronal debris from neighboring cells.

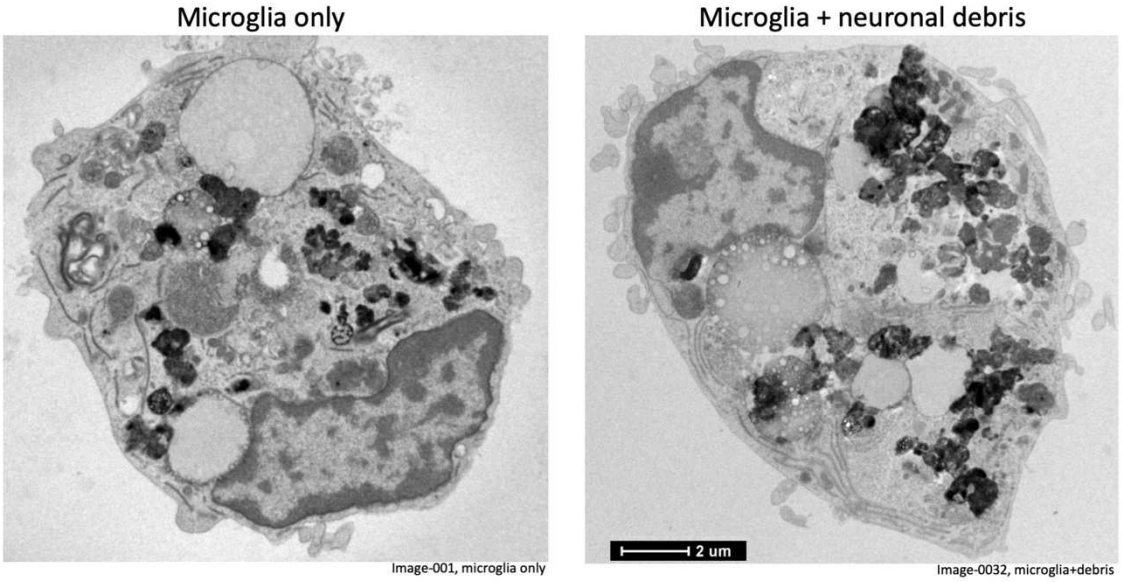

Figure 5-10. Transmission Electron Microscopy (TEM) of the resident microglia from 1.5 y.o. LRRK2-WT mice.

5.3 Summary

Overall, the data from *ex vivo* phagocytosis experiments show that isolated brain microglia have preserved functional properties of resident brain microglial cells in that they are capable of ingesting other cells or particles. Moreover, once activated with α-

synuclein PFFs, microglia show an increased phagocytic ability. These results identify these preparations as a useful tool for the future *ex vivo* experiments.

Based on my results, the highest phagocytic activity was found in LRRK2-KO cells stimulated with α-synuclein and this effect was not present in G2019S or R1441C mutant microglia cells. This result might implicate LRRK2 as a negative regulator of phagocytosis in the context of α-synuclein stimulated inflammation. My findings contrast with the report of Kim et al. (K. S. Kim et al., 2018), who observed that macrophages from LRRK2–G2019S PD patients and mouse microglia display a WAVE2-mediated increase in phagocytic response and LRRK2 loss results in the opposite effect. The discrepancy might be explained by the use of different experimental settings, namely phagocytosis of beads or apoptotic cells, as well as the different type of microglial stimulation. In addition, since the phagocytic index in my experiments is measured based on the number of particles detected in each cell, there is a possibility that the difference I see between LRRK2-WT and KO microglia is related to the degradation level of the engulfed debris through the lysosomal pathway, which is known to be impaired in LRRK2-KO animals (Pellegrini et al., 2018; Y. Tong et al., 2012) . Hence, the elevated phagocytic activity in stimulated LRRK2-KO microglia might actually represent the delayed lysosomal degradation. Future studies will be needed to evaluate the lysosomal degradation rate in LRRK2 KO and PD-mutant microglia in comparison to wild type cells. Better understanding of the involvement of lysosomal pathway and the implication of PD pathological mutations in the context of microglial phagocytosis might be helpful to understand the molecular basis of neurodegeneration in PD.

Chapter 6

Morphological analysis of inflammatory stimulated brain resident microglia from Lrrk2-Cx3Cr1$^{GFP/+}$ mice

6.1 Introduction

Microglia, as a resident brain immune cells, have a surveillance function that is characterized by the continuous monitoring of their surrounding microenvironment. Recent studies demonstrate microglia to be highly dynamic and to have an immediate and diverse morphological response to alterations in brain physiology (Nimmerjahn, Kirchhoff, & Helmchen, 2005); (M. E. Tremblay et al., 2011).

During the response to brain injury, microglia rapidly transform from a ramified to an amoeboid morphology. Ramified microglia represent the normal or resting state, composed of long branching processes and a small cellular body, actively sensing the surrounding microenvironment via dynamic fine cellular processes. Activated amoeboid microglia are hypertrophic, typically have a less dendritic shape, and participate in many functions including phagocytosis and cytokine release (H. Kettenmann et al., 2011).

Although these two states represent two extreme morphological outcomes, microglial morphology is not strictly limited to either ramified or amoeboid shape, but can present as a range of subtle morphological changes (Stence, Waite, & Dailey, 2001). Since microglia are finely tuned to their microenvironment through continuous cell-to-cell cross-talk and in vivo motility, microglia morphologies may reflect a diverse cell functions in the normal and pathological brain tissues (Ohsawa & Kohsaka, 2011).

In order to better understand the role of LRRK2 in microglia and the possible impact of mutated LRRK2 on microglial morphology in adult mouse brain, I studied several morphological properties of microglia in fixed brain slices from *Cx3cr1-Lrrk2* mice with GFP-labeled microglia. For this purpose I cross-bred *Cx3cr1*$^{GFP/GFP}$ mice (Jung et al., 2000) with LRRK2 WT, KO and mutant animals to generate a cohort of homozygous Lrrk2$^{+/+}$, Lrrk2$^{-/-}$, G2019S$^{+/+}$ and R1441C$^{+/+}$ mice in Cx3cr1 heterozygous (Cx3cr1$^{GFP/+}$) background.

Cx3Cr1, a fractalkine receptor, is expressed on monocytes, tissue macrophages, NK cells, activated T cells and microglia. Its ligand, fractalkine, is a membrane-bound glycoprotein expressed on neurons and endothelial cells and acts as a potent adhesion molecule. A targeted deletion Cx3Cr1 and replacement with the gene encoding green fluorescent protein renders brain microglia and other expressing cells endogenously fluorescent in mice (Jung et al. (2000). Heterozygous mice with one copy of CX3CR1 retain receptor function and have been used in our study, whereas homozygous mice have no functional CX3CR1. In summary, each animal in the present study had a single GFP copy and a double copy of the relevant LRRK2 gene, allowing to visualize changes in microglia morphology in situ across different Lrrk2 backgrounds in LPS injected brains.

6.2 Results

6.2.1 Experimental overview

In order to investigate whether LRRK2 plays a role in the morphological changes of brain resident microglia, four different groups of GFP-microglia reporter mice with homozygous LRRK2 genotypes (Lrrk2$^{+/+}$, Lrrk2$^{-/-}$, G2019S$^{+/+}$ or R1441C$^{+/+}$) were injected in the striatum with lipopolysaccharide (LPS) or with PBS as a vehicle control. Confocal images from coronal sections from 3 different brain regions, namely cortex, striatum and substantia nigra, were collected 48 hours after injection, as shown in Figure6-1. In this work I focused the morphological analysis on striatum, being a relevant region in PD pathology.

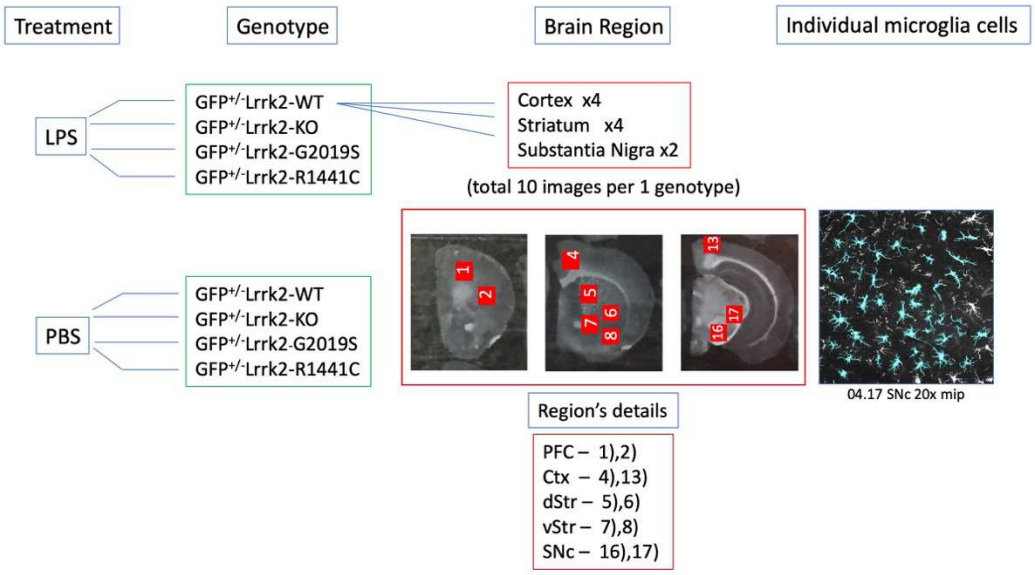

Figure 6-1. Visual schematics of an experimental design. Four different homozygous Lrrk2 genotypes of Cx3Cr1$^{GFP+/-}$ mice were striatally injected with LPS or PBS. Three different brain regions per each Lrrk2 genotype have been confocally imaged and future analyzed for morphometric parameters (30 to 45 cells per image). Ctx=cortex, Str=striatum, SNc=substantia nigra pars compacta, PFC=prefrontal cortex…

6.2.2 LPS injections and regional expression of brain microglial marker Tmem119

As shown in a representative image (Figure 6-2), in LPS-treated GFP$^{+/-}$Lrrk2 animals, microglia have an obviously bigger soma size and thicker processes in comparison to PBS-treated animals. To confirm specificity of GFP-microglia signal in our brain slices, I stained resident microglia with the recently characterized microglia brain specific marker Tmem119, which has been shown to be expressed on resident microglia but not on recruited macrophages or on infiltrating leukocytes (M. L. Bennett et al., 2016). Tmem119 mostly overlaps with GFP signal from Cx3Cr1-mice, but its expression varies depending on distance from striatal injection site, with higher expression in striatum and lower expression in the cerebral cortex (Figure 6-3).

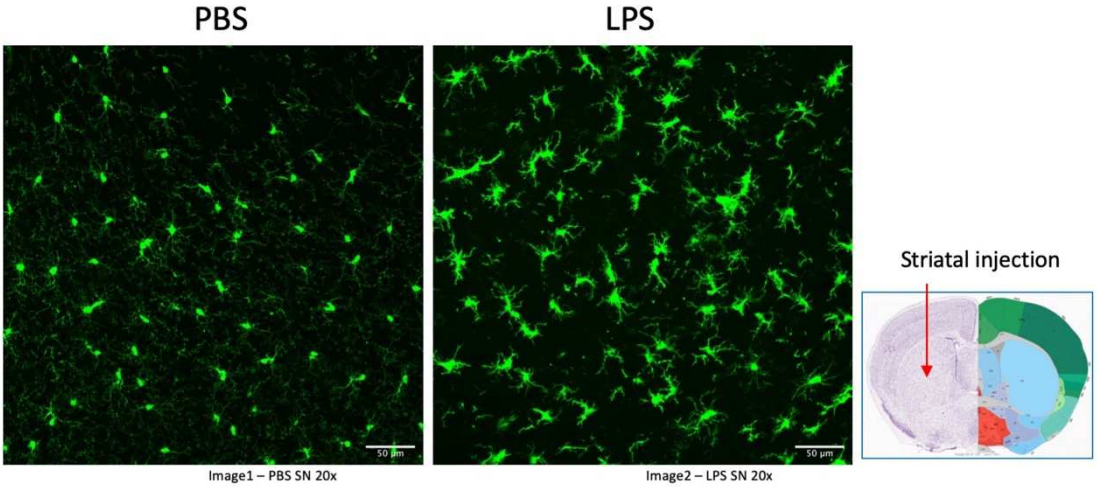

Figure 6-2. Endogenously labeled brain microglia from Cx3Cr1-GFP$^{+/-}$ Lrrk2$^{+/+}$ mice. Resident brain microglia of Cx3Cr1-GFP$^{+/-}$ Lrrk2$^{+/+}$ mice that were striatally injected with inflammatory stimulus LPS or PBS as a control. Confocal images show representative maximum intensity projections of image stacks at SNc 72 hours after injection.

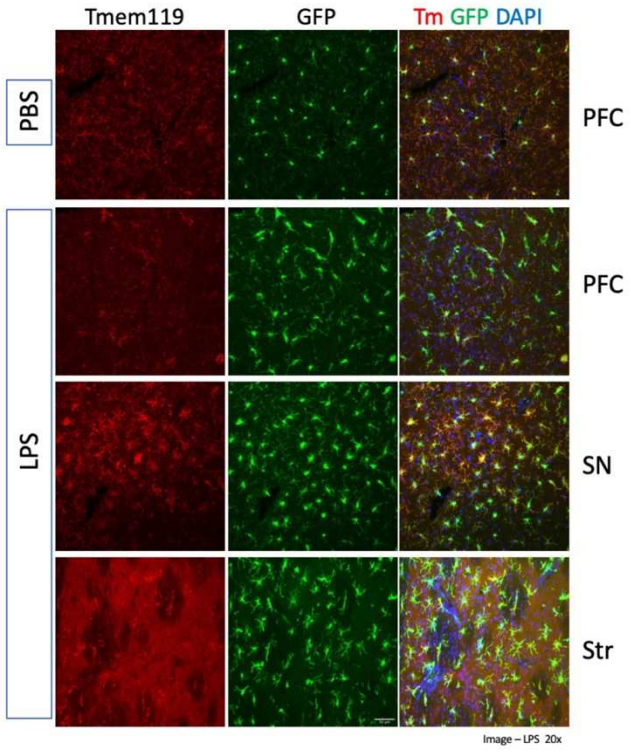

Figure 6-3. Expression of Tmem119, microglia brain specific marker, in three different brain regions: prefrontal cortex (PFC), substantia nigra (SN) and striatum (Str) from Cx3Cr1-GFP$^{+/-}$ Lrrk2$^{+/+}$ mice 48 hours after injection with LPS or PBS. Scale bar is 50µm.

To perform morphological characterization of microglia, we choose GFP-signal from coronal sections of LRRK2-Cx3Cr1$^{GFP/+}$ animals (Figure 6-4) as our detection and measurement method rather than Iba1 staining. Iba1 is strongly expressed by activated microglia, but its signal is reported to be weaker in resting microglia (Ito, Tanaka, Suzuki, Dembo, & Fukuuchi, 2001), (Norden, Trojanowski, Villanueva, Navarro, & Godbout, 2016), therefore GFP staining of the entire cell might better reflect subtle changes in brain microglia cells. In this study, I evaluated LPS-activated microglia morphology 48 hours after intrastriatal injections in 1year old animals.

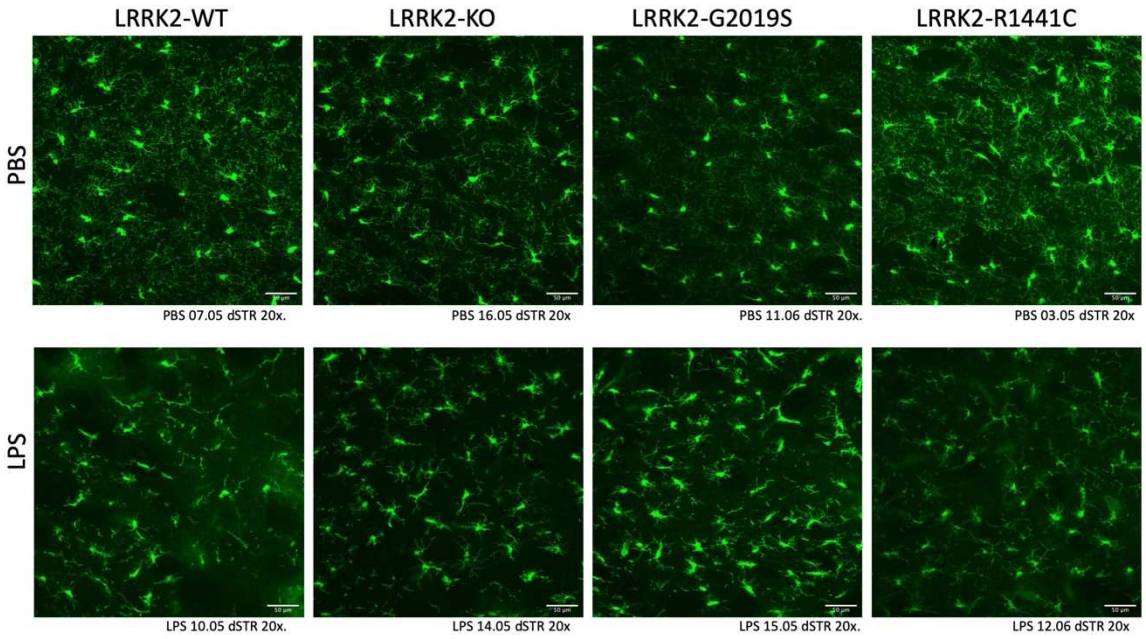

Figure 6-4. Microglia from Cx3Cr1$^{+/GFP}$ Lrrk2 WT, KO, G2019S and R1441C mice injected with PBS or LPS. Representative confocal images of 1 years old Cx3Cr1$^{+/GFP}$ Lrrk2$^{+/+}$ WT and mutant mouse striatal brain slices 48 hours after PBS or LPS injections. Brain slices immunostained with GFP antibody and analyzed for different morphometric parameters. Scale bar is 50µm.

To describe morphological parameters of microglia, features were selected from the three main types of analysis: 1) basic shape descriptions, based on cell surface area, soma area, perimeter and circularity index 2) skeleton analysis in order to characterize specific properties of microglia and get detailed information about branches and 3) Sholl analysis

to quantify cell branching density represented by Schoenen ramification index. Each of these analyses will be presented independently.

6.2.3 Basic shape analysis of LRRK2 WT, KO, G2019S and R1441C striatal microglia stimulated with LPS

For the cell shape analysis, maximum intensity projections of the cells were used as a threshold to create a binary mask using the ImageJ software package (Figure 6-5). The circularity index (roundness) was calculated from the measurement of the whole cell area (black within the blue outline) and the perimeter (blue) from the binary mask.

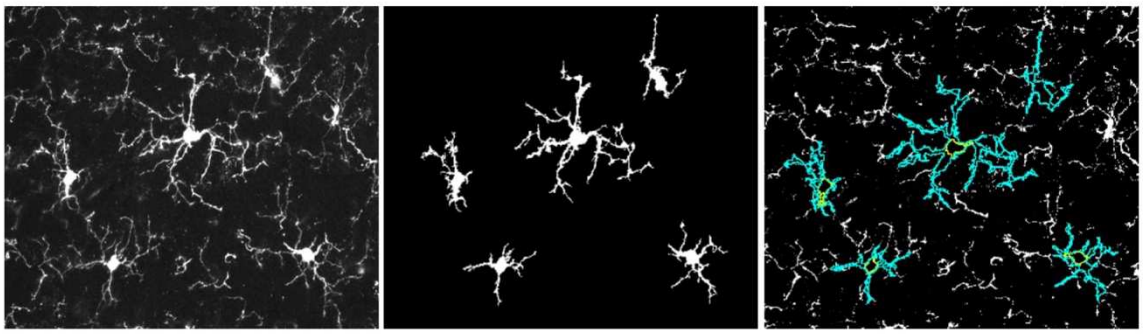

Figure 6-5. Representative image for cell shape analysis with ImageJ software. Original confocal images of striatal brain resident microglia (left) have been thresholded to create a binary mask(middle) and analyzed to measure different morphometric parameters (right): cell soma area (outlined in yellow), cell perimeter (outlined in blue) and whole cell area (black within the perimeter outline). The circularity index has been calculated based on whole cell area and cell perimeter.

As shown in Figure 6-6, LPS significantly altered microglial cell shape towards a more circular appearance. Additionally, the soma size was elevated in comparison to PBS-treated animals. No significant differences were detected between the four LRRK2 genotypes, although there was a trend of higher changes in R1441C brain microglia.

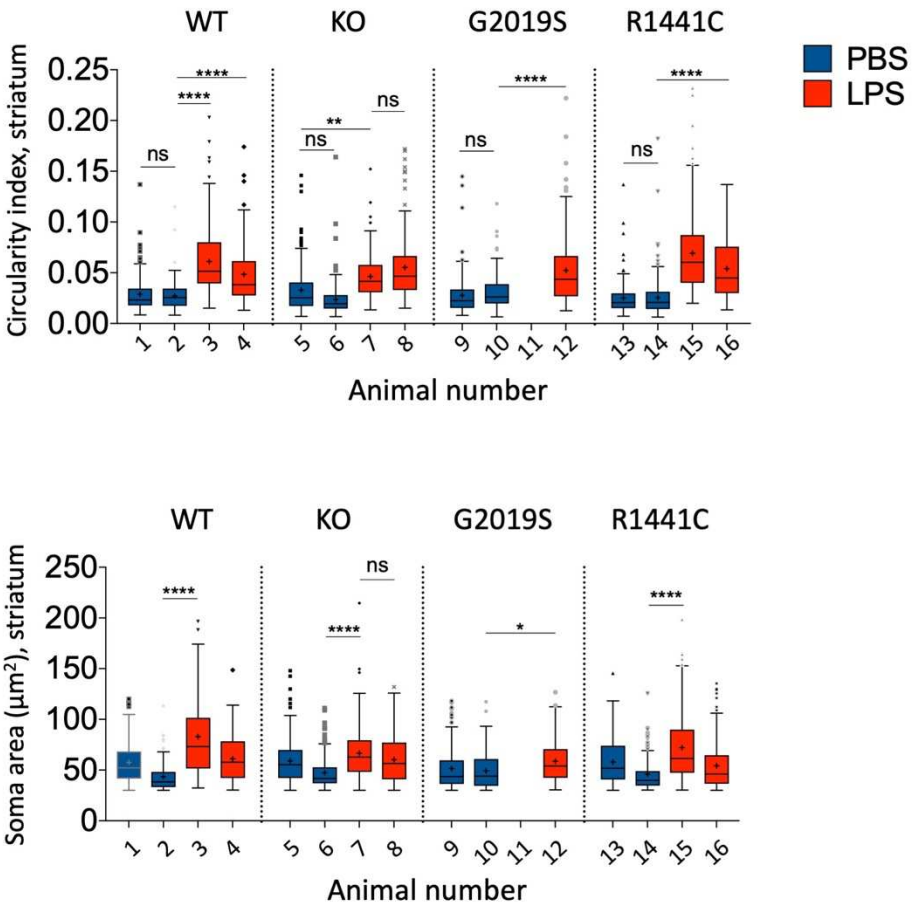

Figure 6-6. Changes in striatal microglia cell shape morphology of 4 different genotypes of Cx3Cr1$^{GFP+/-}$ Lrrk2 mice. Significant increase in microglial shape, circularity and soma area, occur in mice exposed to LPS compare to PBS brain injections and not between different LRRK2 genotypes. One-way ANOVA followed by Bonferroni's correction for multiple comparisons test has been used to analyze the data. ****p<0.0001, **p<0.01, *p<0.05 indicate statistical significance. 120 to 180 cells have been analyzed per sample with n=2 set of animals. Results from two separate animals shown separately to explore animal to animal variability.

6.2.4 Branch morphology analysis of LRRK2 WT and mutants brain striatal microglia stimulated with LPS

Next, I used the Skeleton ImageJ plugin and Sholl analysis to quantify branch complexity of the stimulated resident brain microglia cells. As shown in Figure 6-7, thresholded binary

images were skeletonized to collect data on the number of endpoints and branches as well as process length. These morphometric parameters were first analyzed in the test experiment of Cx3Cr1$^{GFP/+}$Lrrk2$^{+/+}$ which showed reduced microglia process branching complexity and process length in response to LPS treatment. This result is in agreement with literature regarding microglial response to injury (Morrison & Filosa, 2013) and inflammatory stimulation (Lehmann et al., 2016).

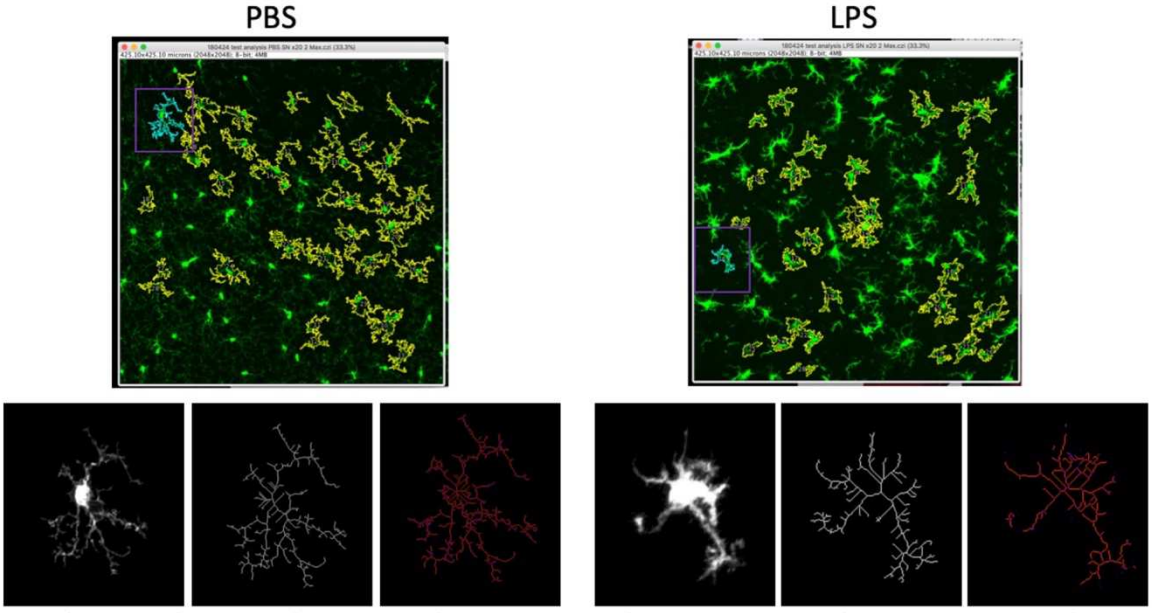

	soma area	# branch	# end-point voxels	avg branch length	max branch length(µm)
PBS	34.17	243	134	10.28	47.0
LPS	65.45	144	79	8.322	29.9

Figure 6-7. Skeleton analysis of the branching complexity of Cx3Cr1$^{GFP+/-}$ Lrrk2$^{+/+}$ mice. Characterization of the branching complexity in Cx3Cr1-GFP$^{+/-}$ Lrrk2$^{+/+}$ non-activated (PBS) and LPS-activated brain injected microglia by Skeleton plugin analysis (Fiji). Example of different morphological parameters, including the average number of microglia process endpoints and branch length are summarized showing increased soma area and reduced microglial branching complexity in LPS-activated cells (test-analysis based on 100 cells).

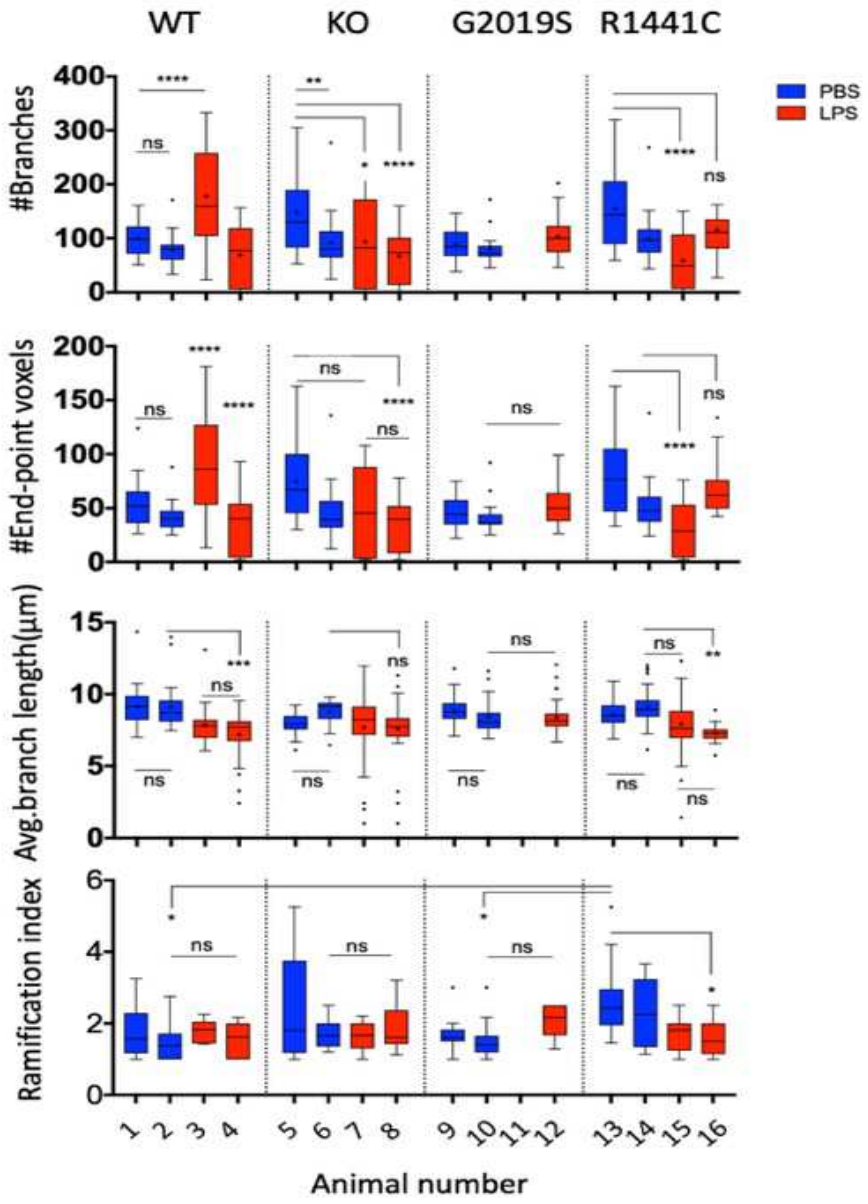

Figure 6-8 Changes in striatal microglia branch morphology in 4 different genotypes of Cx3Cr1$^{GFP+/-}$ Lrrk2 mice. Number of branches, process end-points and average branch length were partially reduced in LPS injected animals with stronger effect in Lrrk2-KO and R1441C genotypes and less response in G2019S animals. Schoenen ramification index was significantly reduced for R1441C striatal microglia.
One-way ANOVA followed by Bonferroni's correction for multiple comparisons test has been used to analyze the data. ****p<0.0001, **p<0.01, *p<0.05 indicate statistical significance. Results from two separate animals shown separately to explore animal to animal variability.

In addition, I have analyzed microglia branch morphology on a cell-by-cell basis using Sholl analysis, which is a well-established technique to quantitatively analyze branching complexity. Schoenen ramification index, derived from the Sholl analysis, was calculated as a ratio between the number of end branches and the number of the primary branches that are originating at the cell's soma. Branch morphology was quantified in striatal brain area for 4 different LRRK2 genotypes (Figure 6-8). I found that LPS-injections caused most of the branch parameters to be significantly reduced for LRRK2 KO and R1441C, although the effects were too variable. Microglial average branch length/cell was significantly decreased for LRRK2 WT and R1441C after LPS stimulation. Surprisingly, G2019S mutant was the less responsive to the LPS-stimulation based on tested branch morphology parameters. Ramification index did not change significantly between LPS and PBS-stimulated cells, except for R1441C that was more ramified in the control PBS condition compare to WT and other mutants and its de-ramification was significantly reduced in response to LPS. Representative confocal images of LPS or PBS-stimulated microglia with enlarged skeletonized and Sholl-analyzed cells are shown in Figure 6-9 for LRRK2 WT and the most responsive mutant R1441C.

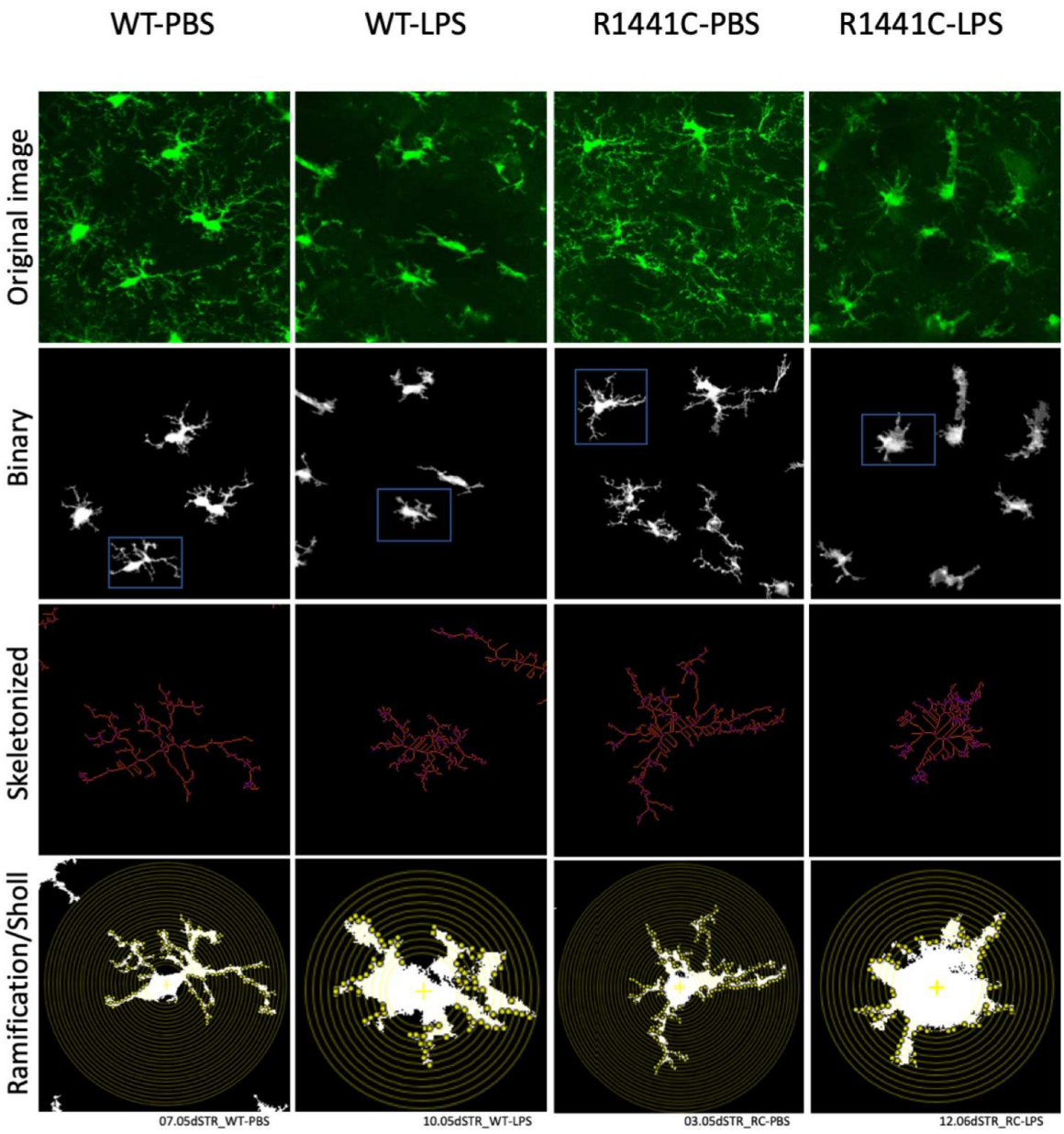

Figure 6-9 Representative confocal images of striatal branch morphology in LPS or PBS-injected Cx3Cr1$^{GFP+/-}$ Lrrk2 WT or R1441C mice.
An example images of fluorescent, skeletonized and Sholl-analyzed cropped cells corresponding to the blue boxes of Lrrk2-WT and R1441C brain microglia. Branch morphology and Schoenen ramification index were analyzed by Skeleton Fiji plugin and Sholl analysis (ImageJ) respectively.

6.3 Summary

Overall, these data suggest that resident brain microglia responded classically to an inflammatory stimulation with LPS by increasing the soma size and cell roundness and by reduction of branching complexity.

There are subtle differences between LRRK2 genotypes in response to inflammatory stimulation, with a trend to higher response in R1441C mutant and almost no response in G2019S in terms of branch complexity. I could speculate that kinase overactive G2019S LRRK2 mutant might represent an elevated basic level of activated microglia and so masking an overall inflammatory response in these cells.

The morphometric analysis described here is related to the striatal area of the mouse brain microglia. The regional heterogeneity of microglial responses has been reported in the literature (Lehmann et al., 2016) and suggests that an immune response can be influenced by the local microenvironments within specific brain regions. Additional brain areas, relevant to PD, namely substantia nigra (SN) and cortex might show different level of response to the inflammatory stimuli as well as differential LRRK2 genotyping response. Analysis of these areas will be addressed in the future study.

To date, there is only a limited set of tools to properly quantify microglia morphology. My current results were obtained through manual image analysis with Image and based on two-dimensional projections of microscopic images, similar to other recent studies (Morrison & Filosa, 2013); (Fernandez-Arjona, Grondona, Granados-Duran, Fernandez-Llebrez, & Lopez-Avalos, 2017).This type of analysis has limitations as it might miss some valuable information when analyzing complex three-dimensional cell shapes. However, more intensive evaluations such as three-dimenional analyses demand high time investment and are not applicable for analysis of large cell numbers. Additional methods that employed a fully automated algorithm for morphological analysis of microglia have been recently published (Heindl et al., 2018) and might be used to distinguish morphological changes of microglia in future studies.

Chapter 7

Global gene expression changes in inflammatory stimulated brain microglia using single-cell RNA sequencing

7.1 Introduction

Activated microglia is a general term accounting for the biochemical and physical changes from an original homeostatic state in response to alterations in the brain microenvironment or to pathological insults (Prinz & Priller, 2014). These changes include gene expression, phagocytic capacity, altered density and/or ultrastructure (Lenz & Nelson, 2018).

Activated microglia have been observed in most neurodegenerative disorders, including Parkinson's disease (Moehle & West, 2015), Alzheimer's disease (AD) (Keren-Shaul et al., 2017), Multiple sclerosis (MS) and amylotrophic lateral sclerosis (ALS) (reviewed in (Crotti & Ransohoff, 2016). Although many morphological and molecular changes are known to take place during microglia activation (Hickman et al., 2013), understanding of the detailed molecular signature of microglial activation has been bolstered by single-cell resolution data on these cells (Hammond et al., 2019; Keren-Shaul et al., 2017; Mathys et al., 2017) including data from single cell RNA-seq (scRNA-seq). In contrast to bulk RNA-seq, scRNA-seq resolves gene expression patterns on a single cell basis, which is particularly important for cells that may populate a number of different states, such as activated microglia.

The studies reported in earlier chapters of this thesis were focused on analysis of primary cultured microglia and nominated several genes that are regulated by exposure to LPS

or PFFs. However, it is uncertain whether gene expression changes seen in cell culture are representative of similar effects *in vivo*. It is been shown in the literature that cultured microglia may have different molecular signatures compared to resident brain microglia cells (Butovsky et al., 2014). Therefore, in the experiments described in this chapter, I decided to use resident microglia acutely isolated from adult mouse brain to confirm or refute the hypothesis that there are gene expression changes nominated from the primary culture experiments.

Here, I performed single-cell sequencing of acutely isolated microglia from adult mice after a single intrastriatal injection of LPS to compare inflammatory microglial responses in LRRK2 animals. I also used the same dataset to analyze LRRK2 mRNA expression in different sub-populations of microglia.

7.2 Results

7.2.1 Acute isolation of brain microglia and experimental design

To minimize *ex vivo* activation and transcriptional activity during the isolation procedure, I generated single-cell suspensions at low temperatures. Following quick perfusion to remove circulating blood monocytes, brains were gently dissociated with Adult brain dissociation kit (Miltenyi Biotech) and subjected to Percoll gradient centrifugation to remove debris and myelin, which is important for getting higher purity and recovery of target cells. Microglia were then magnetically-sorted with CD11b-labelled microbeads as described in Material and Methods.

Isolated single cell suspensions were generated from the half-brain samples and undergo single cell RNA-sequencing utilizing a droplet-based RNA-seq approach (Zheng et al., 2017) with commercially available 10xChromium platform (see Material and Methods), (Figure 7-1).

In these experiments, we used 1 year old Cx3Cr1-GFP mice that express GFP in microglia and monocytes to allow visualization of microglial morphology. Mice were injected in the striatum with 5 µg LPS or PBS as a vehicle control.

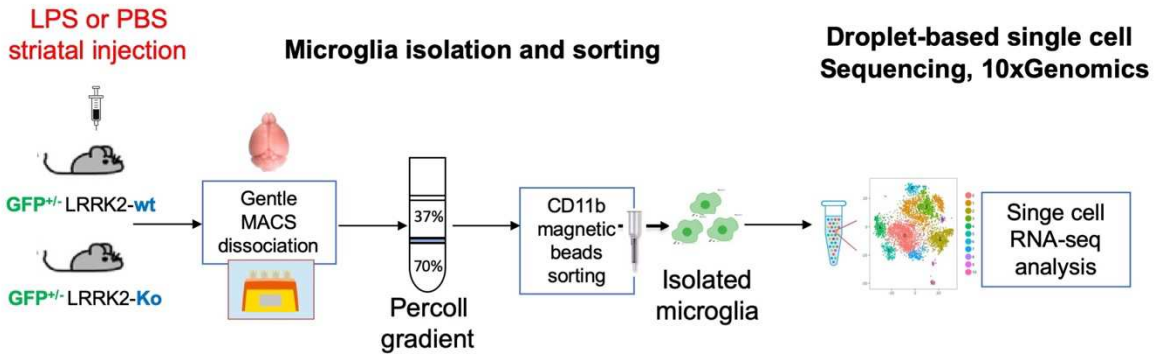

Figure 7-1. Schematic of acute isolation of brain microglia cells for scRNA-seq analysis. Microglia were isolated from the whole brains of LPS or PBS injected 1.y.o. mice using gentle dissociation, demyelination and CD11b magnetic sorting (MACS-technology). Isolated single cell solutions were subject to single cell sequencing using droplet-based 10xGenomics platform.

Three days after the injection, widespread activation of microglia was detected by fluorescent images from coronal sections of Cx3Cr1-GFP mice from cerebral cortex, striatum and the midbrain (Figure 7-2). In PBS-treated animals, microglia showed a fine branched morphology whereas after LPS-injection, ramified microglia with thicker processes were seen in all brain regions examined. We also noticed an increase in the number of Cx3Cr1-GFP positive cells, representing microglial proliferation in response to inflammatory stimulation, although we can't exclude some infiltration by peripheral monocytes. This is in agreement with literature that showing microglial proliferation resulting in a transient increase of microglial density, which returns to basal levels within 3 weeks after LPS-treatment (Furube et al., 2018). These results suggest that a single intrastriatal injection of LPS results in microglial activation and proliferation throughout the brain.

7.2.2 Single-cell RNA-sequencing of LRRK2 WT brain resident microglia and validation of LPS-induced gene expression.

We first performed a small scale single-cell RNA-sequencing experiment where WT animals expressing fluorescently labeled microglia (Cx3Cr1-GFP$^{+/-}$) were injected with either LPS or PBS. Subsequently, we conducted a second larger scale single-cell RNA-

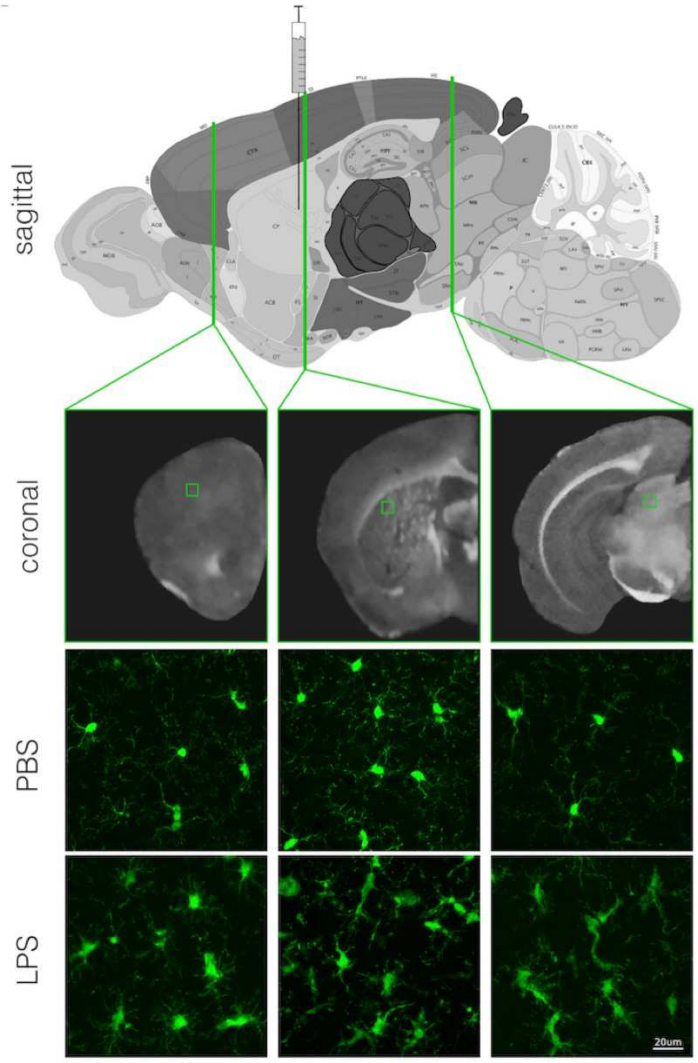

Figure 7-2. Schematic of the striatal injections and fluorescent images from coronal sections of LPS or PBS-injected Cx3Cr1-GFP mice. Scale bar indicates 20μm.

sequencing with brain microglia isolated from LRRK2-WT and KO animals (Cx3Cr1-GFP$^{+/-}$Lrrk2-WT and Cx3Cr1-GFP$^{+/-}$Lrrk2-KO) injected with the same inflammatory stimuli and vehicle control (LPS or PBS).

For the first experiment, sequenced CD11b-isolated cells from two treated LRRK2 WT animals were analyzed using Seurat (Stuart et al., 2019) in R (see Material and Methods). Using established cellular markers we informatically removed macrophages (based on cell marker Mrc1), endothelial cells (Cldn5-positive cells) and astrocytes (Aqp4-positive

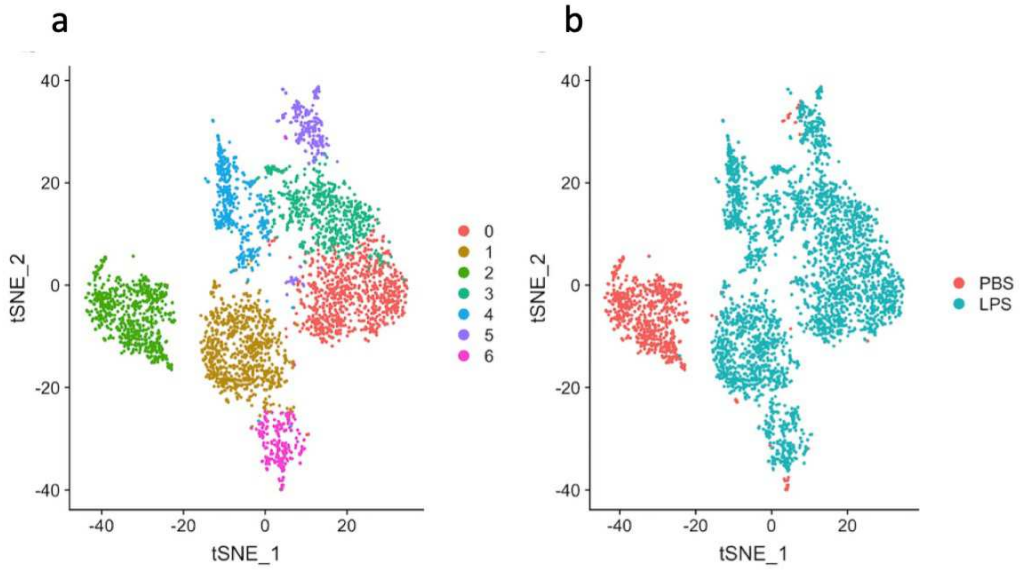

Figure 7-3. tSNE visualization of single cell RNA-seq analysis from LRRK2 WT mouse resident brain microglia. (a) Different colors represent different types of microglia clusters ordered by transcriptome similarities. **(b)** tSNE embedding showing clusters ordered by PBS or LPS-treated animals

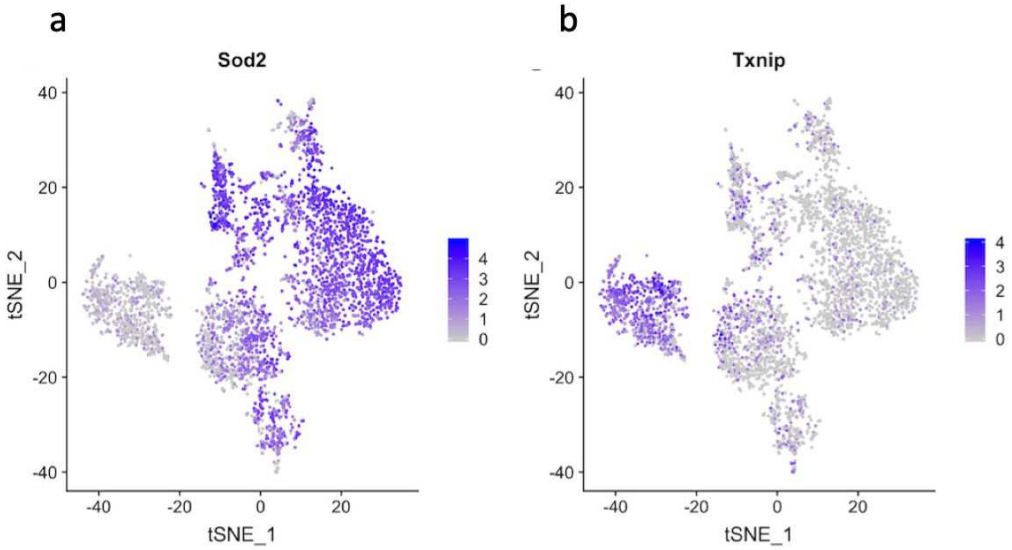

Figure 7-4. Visualization of scaled expression of 2 nominated differentially expressed genes, Sod2 and Txnip. (**a**)Sod2 is upregulated and (**b**) Txnip is downregulated in LPS-treated cells. Scales are log2 normalized scaled gene expression.

cells) from the total cellular data (9.6%, 1.2% and 1.2% of all cells respectively). After removal these non-microglial cells, the remaining 3,710 CD11b-positive cells were re-clustered and mapped to two-dimensional space using tSNE (t-distributed stochastic neighbor embedding). This analysis identified seven clusters of microglia (Figure 7-3a), of which six were predominantly from LPS-treated animals and one from PBS treated animals (Figure 7-3b).

Using this dataset, we were able to validate the expression changes of two nominated gene-candidates obtained from primary microglia using bulk-RNA-seq. Specifically, we determined that LPS stimulation of brain-resident microglia is associated with higher SOD2 expression and lower TXNIP expression (Figure 7-4). Moreover, different clusters of microglia were separated in Seurat analysis based on the levels of pro-inflammatory cytokine IL-1β, suggesting that microglia clustering represents levels of activation of resident microglia after inflammatory stimulation (Figure 7-5a). Using this approach, we were able to demonstrate that several additional genes nominated from the microglia cell culture experiments including Irg1, NFKBiz, Saa3 and Cd83 also correlated with activation state (Figure 7-5b). The data from this small-scale experiment, using acutely isolated brain microglia from LRRK2 WT mice injected with either LPS or PBS, suggest that it is feasible to in vivo validate gene expression changes that were obtained from the primary cell culture experiments.

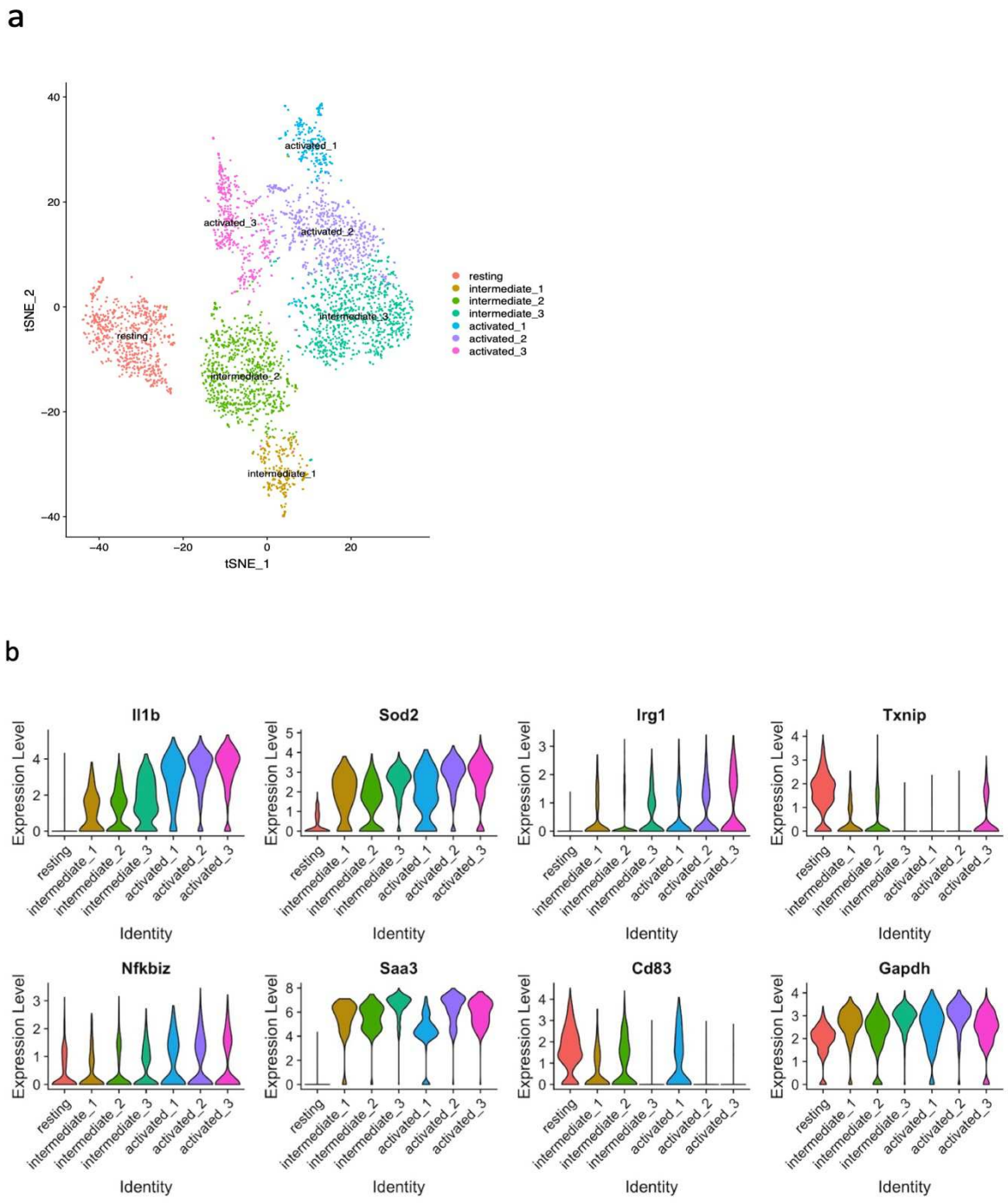

Figure 7-5. Validation of cell cultured microglia gene expression changes in vivo with scRNA-seq data from resident brain microglia. (a) tSNE clustering representing expression of pro-inflammatory cytokine IL1β corresponding to different levels of activated microglia. **(b)** Violin plots of gene expression for nominated differentially expressed genes Sod2, Irg1, Txnip, NFKBiz, Saa3 and Cd83 in clusters ordered by expression of IL1β. Gapdh is presented as a reference gene.

7.2.3 Single-cell RNA-sequencing of LRRK2 WT and KO brain resident microglia stimulated with LPS or PBS.

For the second experiment, two biological replicates per condition (LPS or PBS) were collected for a total of 37,675 sequenced microglia cells from 8 total animals (1 years old Cx3Cr1-GFP$^{+/-}$ Lrrk2$^{+/+}$ or Cx3Cr1-GFP$^{+/-}$ Lrrk2$^{-/-}$). As shown in Table 7-1, cells were sequenced to comparable sequencing depths (~50,000 reads/cell) and had median 1,888 genes detected per cell. A plot of cumulative unique molecular identifiers (UMI) per cell identifies the total number of valid barcoded cells detected above background signal (as shown in red line in Figure 7-6). A steep drop-off, indicating a good separation between the cell-associated barcodes and the barcodes associated with an empty droplets, was seen in this example, suggesting a high quality preparation of cellular libraries.

Sample code_name	Estimated Number of Cells	Mean Reads per Cell	Median Genes per Cell	Number of Reads	Reads Mapped Confidently to Genome	Fraction Reads in Cells	Total Genes Detected	Median UMI Counts per Cell
SCAF467_WT_LPS	5,265	52,451	2,426	276,156,207	86.70%	77.40%	17,608	9,546
SCAF468_WT_PBS	2,844	50,756	1,701	144,352,063	87.90%	64.30%	17,209	4,282
SCAF469_KO_LPS	6,102	53,560	2,467	326,826,863	86.80%	78.30%	18,233	10,102
SCAF470_KO_PBS	2,986	53,031	1,814	158,353,131	87.50%	69.30%	16,876	4,860
SCAF503_WT_LPS	5,790	51,518	1,886	298,293,388	89.70%	69.30%	18,462	6,630
SCAF502_WT_PBS	3,986	49,668	1,541	197,980,465	89.30%	71.30%	18,569	3,867
SCAF504_KO_LPS	5,581	52,781	1,924	294,576,061	90.20%	67.50%	18,508	6,971
SCAF505_KO_PBS	5,121	51,678	1,850	264,643,153	90.20%	68.40%	19,360	4,996

Table 7-1. Summary of QC metrics of LRRK2 WT and KO microglia samples submitted for single-cell RNA-sequencing.

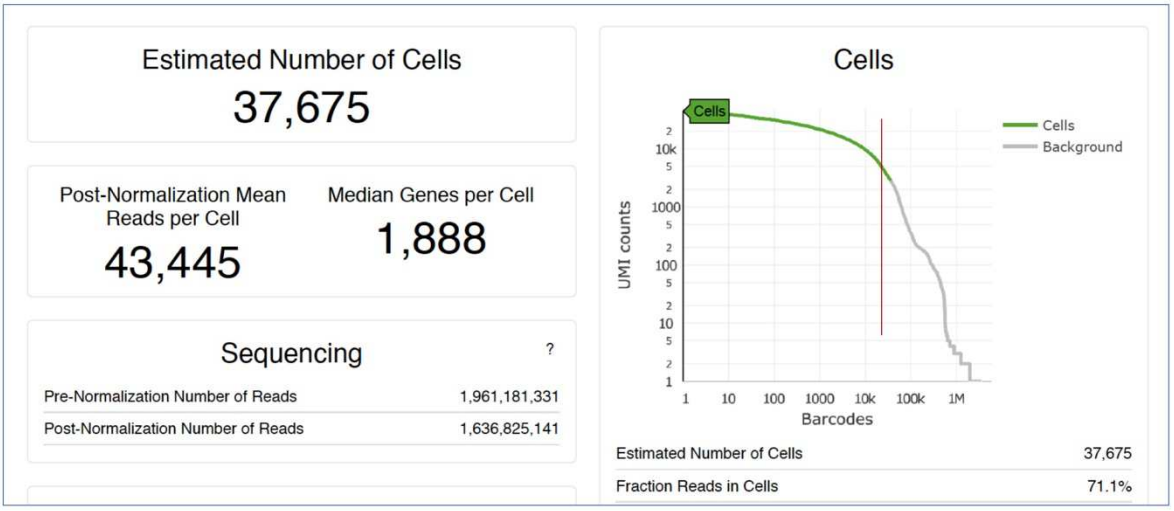

Figure 7-6. UMI per cell Plot ("Knee plot"). Shows the distribution of barcode counts and which barcodes were inferred to be associated with cells. The number of UMI counts (transcripts) mapped to each barcode versus number of barcoded cells below that value.

In this second experiment, tSNE embedding distinguished 18 different microglia clusters (Figure 7-7a). Integrated analysis of total amount of cells from all the animals and conditions, clearly separated between LPS and PBS-related cell clusters (Figure 7-7b). Gene expression analysis showed that the canonical microglial genes were highly expressed by most (but not all) cell clusters (Figure 7-8). In addition to the highly expressed canonical genes, we also identified some genes that were upregulated and probably unique to specific microglial clusters (Figure 7-9). Some genes were specific to macrophages, for example, Arg1, a common macrophage-specific marker arginase 1 was mostly present in cluster 2, likely due to the use of CD11b to isolate cells, which will include macrophages in addition to microglial cells.

Interestingly, a small amount of Arg1 was also present in microglial cluster 16, in agreement with recent literature (Hammond et al., 2019) showing that a small subset of microglia actually express Arg1 *in vivo*. Future analysis will be required to validate and better understand those types of clusters, also the growing datasets from different single-cell RNA-seq experiments might suggest that existing marker definitions will be updated.

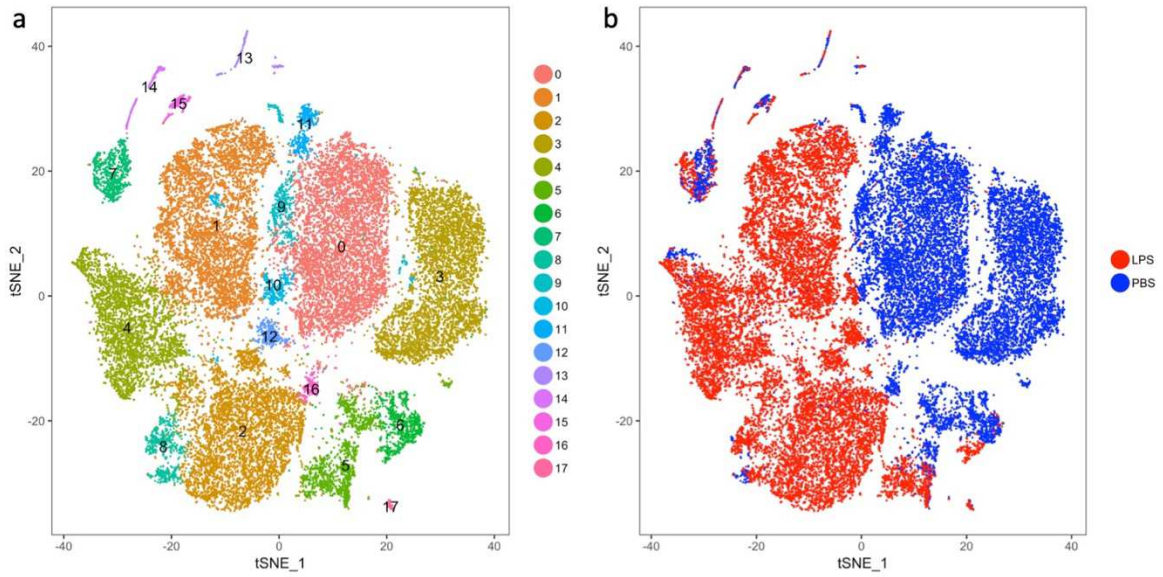

Figure 7-7. Integrated analysis of single-cell RNA-sequencing of resident microglia from Cx3Cr1-GFP-LRRK2 mice brain-injected with LPS or PBS. tSNE plot showing the overall gene expression relationship among the 37,675 single cells from all the animals and conditions. Different cell clusters are color-coded. **(a**) tSNE visualization distinguishes between 18 different cell-type clusters **(b**) tSNE projection of separate cell clusters in LPS or PBS-injected animals.

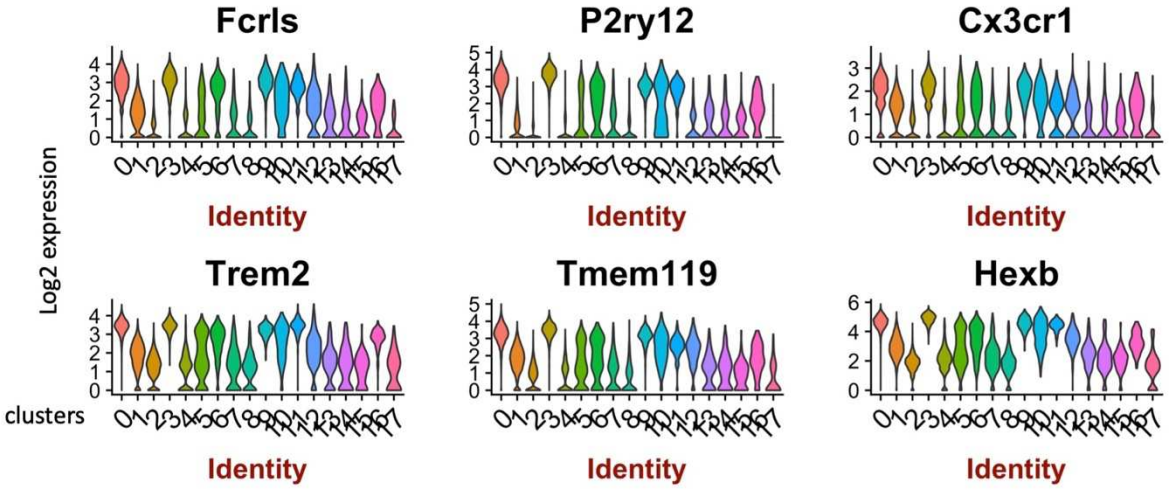

Figure 7-8. Violin plots showing the expression levels of canonical microglial genes in each of 18 detected clusters.

Microglia also expressed a number of inflammatory signals in this experiment in a cluster-dependent manner. We noted upregulation of the chemokine Ccl4 in clusters 9,10,12, as well as the inflammatory cytokine interleukin 1 beta in clusters 1,2,4,5,12,16. These results are in agreement with literature reporting that under neuroinflammatory conditions, microglia express and release chemokines including Ccl4 (Mammana et al., 2018) and high levels of the cardinal pro-inflammatory cytokine IL-1β are detected in microglial cells surrounding Aβ plaques in AD patient brains and cerebrospinal fluid (Heneka et al., 2015). In summary, our data show that inflammatory stimuli triggers brain microglia to shift toward more immunogenic profile including an increase in inflammatory-responsive microglia.

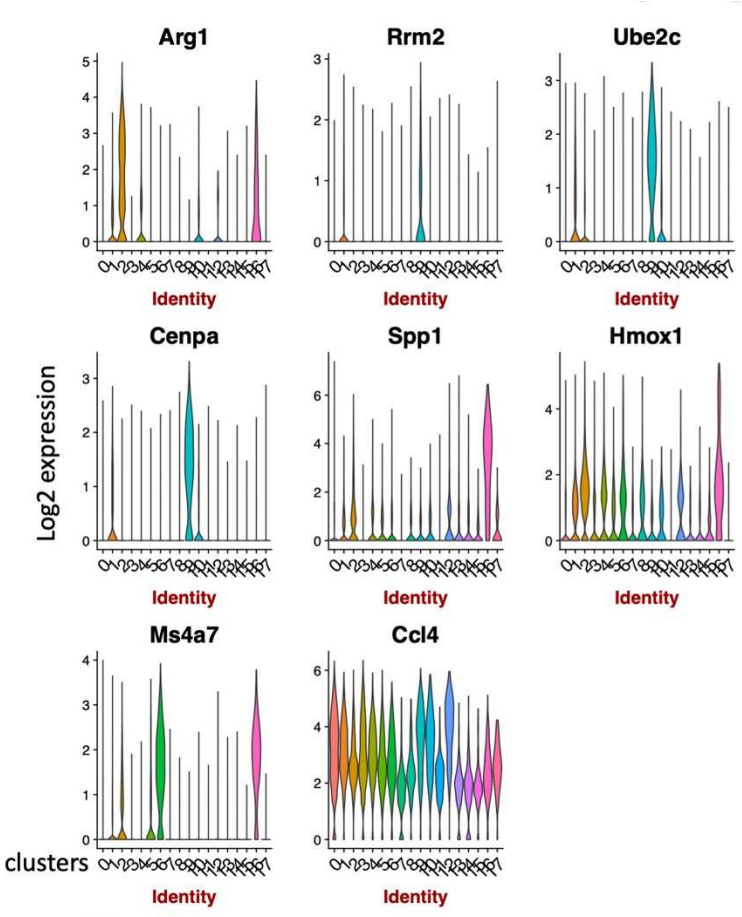

Figure 7-9. Violin plots of genes specifically upregulated in different cell clusters Some of the markers are cluster specific and some of them are generally expressed in microglia.

7.2.4 LRRK2 mRNA levels in resident brain microglia

In the literature, the topic of LRRK2 expression in the mouse brain's resident microglial is controversial. Some reports suggest that there is no LRRK2 expression in microglia even after LRRK2-upregulation resulting from intraperitoneal LPS injection (Kozina et al., 2018). In contrast, LRRK2 is expressed in primary rat microglia and can be upregulated in isolectin B4^{+} microglial/endothelial cells after intranigral LPS injections (Moehle et al., 2012).

We therefore examined our single-cell RNA-sequencing data for LRRK2 expression. We noted sparse expression in non-inflammatory microglia but it increased after LPS brain-stimulation (Figure 7-10).

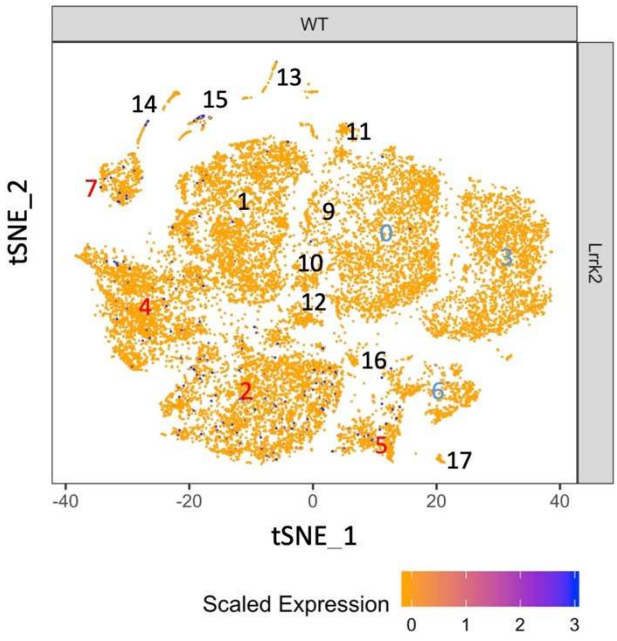

Figure 7-10. LRRK2 mRNA expression in resident brain microglia. LRRK2 expression (blue points) is very sparse in PBS-injected resident microglia cells (clusters 0,3 and 6, marked in light blue) and increased by LPS-microglial activation (clusters 2,4,5 and 7, marked in red). Each point is a single cell plotted in two tSNE dimentions.

In addition to data shown above and for our surprise, one of the small clusters, that was positive to endothelial cell marker Ly6c1 (cluster7) appeared to be positive for LRRK2 expression. To date, evidence for endothelial expression of LRRK2 has been limited to human umbilical vein endothelial cells (HUVECs) (Hongge, Kexin, Xiaojie, Nian, & Jinsha, 2015) and little is known about its expression in brain microvascular endothelial cells. The possibility of LRRK2 expression by brain endothelial cells was briefly discussed by Kozina et al.,(Kozina et al., 2018). If endothelial cells possess the ability to express LRRK2, they could, together with microglia, modulate neuroinflammatory response by expressing cytokine receptors. Future experiments will be needed to confirm our single-cell RNA-seq data.

7.2.5 Differential gene expression between LRRK2 genotypes and treatments

Differential gene expression analysis was performed as part of Seurat analysis comparing Lrrk2 WT and KO resident brain microglia within specific clusters. The PBS-treated (cluster 0) versus LPS-treated (cluster 4) did not reveal any differences, implying that LRRK2 had only a subtle effect on overall gene expression at the mRNA level (Figure 7-11). This result was in agreement with our bulk-RNA sequencing data, where LRRK2 deletion also had a small effect on gene expression.

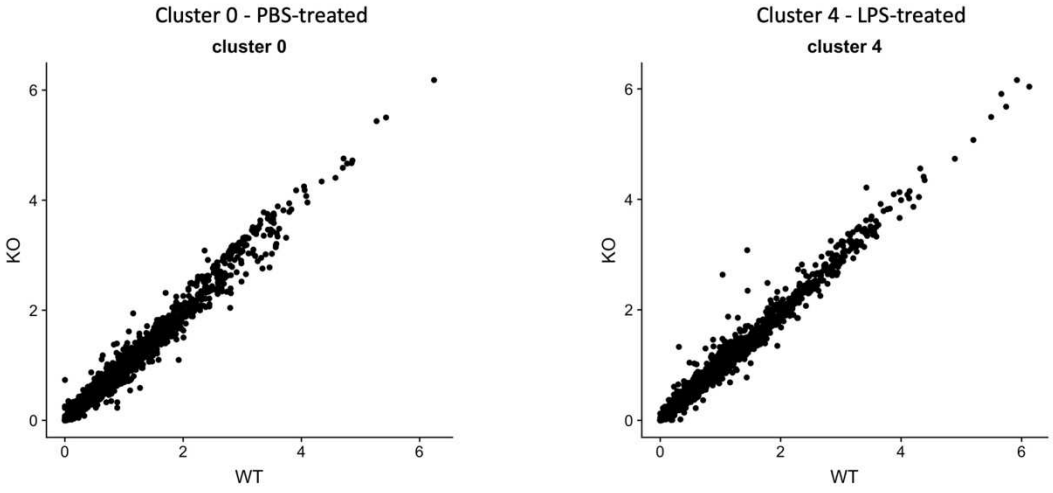

Figure 7-11. Differential gene expression between LRRK2 WT and LRRK2 KO resident brain microglia.

Using this dataset, we also tested nominated gene candidates from the original cell cultured microglia comparing between two Lrrk2 genotypes (WT and KO) and between the treatments (LPS and PBS). As shown by violin plots in Figure 7-12, both IL-1β and SOD2 have elevated mRNA expression after LPS-treatment, in opposite to TXNIP, which is downregulated upon inflammatory stimulus of the brain. Not much of the difference was detected between the genotypes.

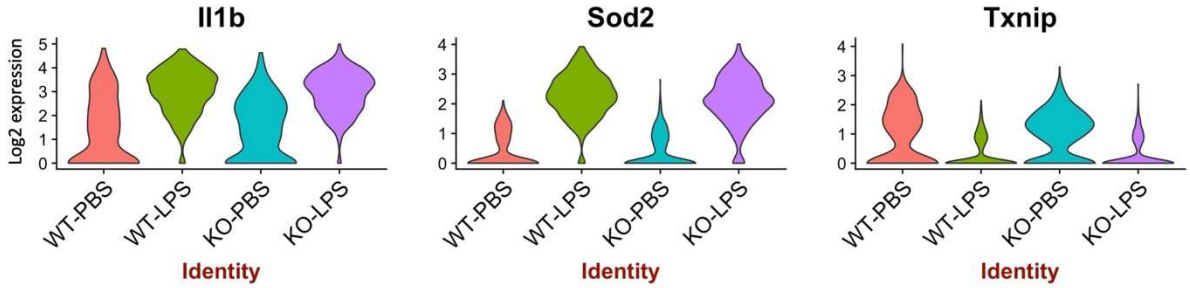

Figure 7-12. Violin plots of differential expression of nominated candidates, IL-1β, Sod2 and Txnip comparing genotypes and treatments.

7.3 Summary

Overall, the single cell RNA-sequencing data from both small-scale and expanded study, show that LPS-responsive brain microglia segregate from non-inflammatory microglia into separate clusters based on different transcriptome signature. We validated differentially expression changes nominated in primary culture experiment, including upregulation of IL-1β and SOD2 and downregulation of TXNIP in LPS stimulated resident microglia. However, the effects of LRRK2 were modest, probably due to the relatively low level of its expression. We haven't detected an attenuation of pro-inflammatory cytokine IL-1β in LPS-stimulated LRRK2 KO animals compare to stimulated LRRK2 WTs, as was reported in primary cultures (I. Russo et al., 2015). Given, that brain resident microglia were reported to have slightly different transcriptomic profile from that of primary culture (Butovsky et al., 2014), I can speculate that resident microglia can be less sensitive to the

Lrrk2 deletion by having compensatory mechanisms, which are not present in primary cultured cells. This finding is important as a precaution that not all the changes detectable in primary culture can be extrapolated to in vivo system.

Although LRRK2 shows low mRNA expression in this scRNA-seq dataset, the real picture can be masked by the low LRRK2 transcript abundance. Additional approach like deep sequencing (also referred as high-throughput sequencing) aiming for high number of unique reads of each region of a sequence (up to 250K mapped reads per cell versus 50K in the current experiment) might provide us with better information regarding the real picture of LRRK2 expression in resident brain microglia.

Chapter 8

LRRK2 protein expression in LPS-stimulated adult brain microglia at the single cell level

8.1 Introduction

Based on my single-cell RNA-sequencing data, Lrrk2 mRNA appears to be sparsely expressed in brain microglia and is elevated after inflammatory stimulation with LPS. Another way to characterize the level of LRRK2 expression at resident brain microglia would be to validate RNA-sequencing data at the protein level. Given the limited amount of isolated resident microglial cells per mouse brain, traditional western blotting is not likely to be optimal for detection of Lrrk2.

To overcome these limitations, I decided to use a new single-cell Western blotting (scWB) technology to investigate Lrrk2 expression at the protein level. Originally developed and optimized by Hughes and Kang (Hughes et al., 2014; Kang et al., 2016), scWB technology enables western-based detection of multiple proteins in thousands of single cells thus providing information on sample heterogeneity and allowing measurement of correlations between levels and/or activation states of different proteins in a single cell.

The Milo instrument (ProteinSimple) is the first commercially available scWB platform that runs a scWest chip, which is loaded with a single cell solution. Milo uses a Poisson distribution and controlled loading to distribute the sample, so many of the wells are empty and some contain single cell. The typical workflow is shown in Figure 8-1. Each chip contains pre-cast polyacrylamide gel with 6,400 microwells that able to capture ~1,000

single cells and run 1,000 Single-cell Westerns in parallel. The Milo instrument automatically lyses cells captured on the chip and performs an SDS-PAGE separation on each single cell lysate. UV light is used to activate a proprietary compound in the gel to crosslink the proteins in place, to minimize inherent protein losses due to the transfer step of traditional Western blots. After immobilization, the chip is probed with a primary antibody and fluorescently-labeled secondary antibody. The immunolabeled chip is scanned on a microarray scanner and images are analyzed with the software to identify each target protein per cell and quantitate its abundance. In general, Single-cell western assays have a dynamic range of 2-3 orders of magnitude (2-3-log dynamic range), which allowed detection of both low and high expressing cells in the same sample (Guerrero-Juarez et al., 2019; Wosczyna et al., 2019).

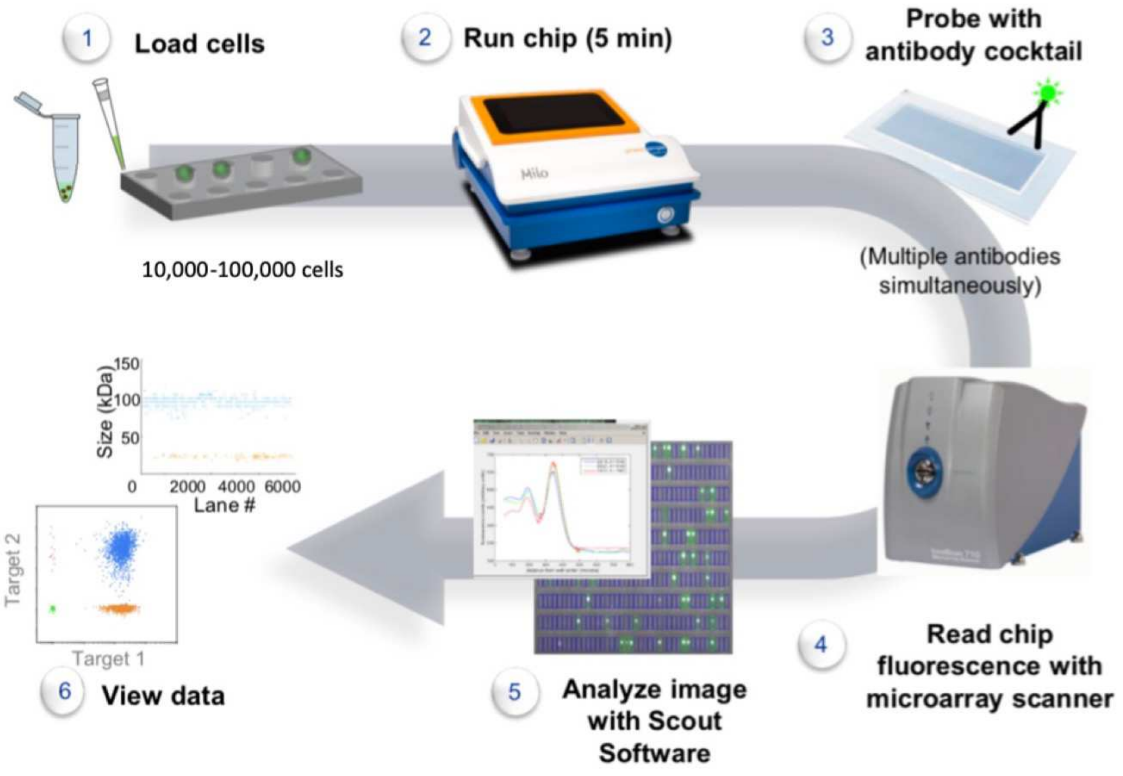

Figure 8-1. Single-cell resolution western blotting workflow.

8.2 Results

8.2.1 LRRK2 protein expression at single cell level in acutely isolated brain microglia

The pilot experiment reported here was done with support of the ProteinSimple team, using our purified cells and their demonstration equipment in our laboratory. All additional single cell Western Blot experiments were done at the NIH/NCI Core Facility under supervision of Dr. Noemi Kedei.

In the pilot experiment, we compared Lrrk2 expression in CD11b-purified resident microglia from untreated mouse brains of 1year old Lrrk2 WT and KO animals. Single cell suspensions of microglia from each genotype were loaded on small scWest chips for 15 minutes for cell settling to achieve single-cell occupancies of the wells. Approximately 100,000 cells were loaded on each chip with up to ~2,000 cells analyzed. Cell-loaded chips were then inserted into the Milo instrument and run with the following conditions; 0 sec lysis; electrophoresis separation for 150-170sec at 240V; and UV capture for 240sec. Primary antibodies were anti-LRRK2 (MJF2, Abcam) and anti-Vinculin antibody as a loading control (seeMaterial and Methods), following with fluorescently labeled secondary antibodies. Stained and dried scWest chips were scanned and images were analyzed with Scout Software.

Representative electropherograms and peaks for Lrrk2 and Vinculin are shown in Figure 8-2. In these experiments, migration distances on the chip are proportional to the molecular weight of the proteins and the area under the curve of each protein peak is proportional to the protein abundance. In this experiment, endogenous mouse brain microglial Lrrk2 (280kDA) runs at the top of the chip (as circled in red at the Figure 8-2, top) while Vinculin (116kDa) runs at a longer distance from the well center (Figure 8-2, bottom). There is no fluorescent signal for Lrrk2 in the KO sample compare to WT, although Vinculin was detected in both chips, demonstrating specificity of the signal. This result has validated brain resident microglia samples as being compatible with scWB in terms of specific LRRK2 protein detection.

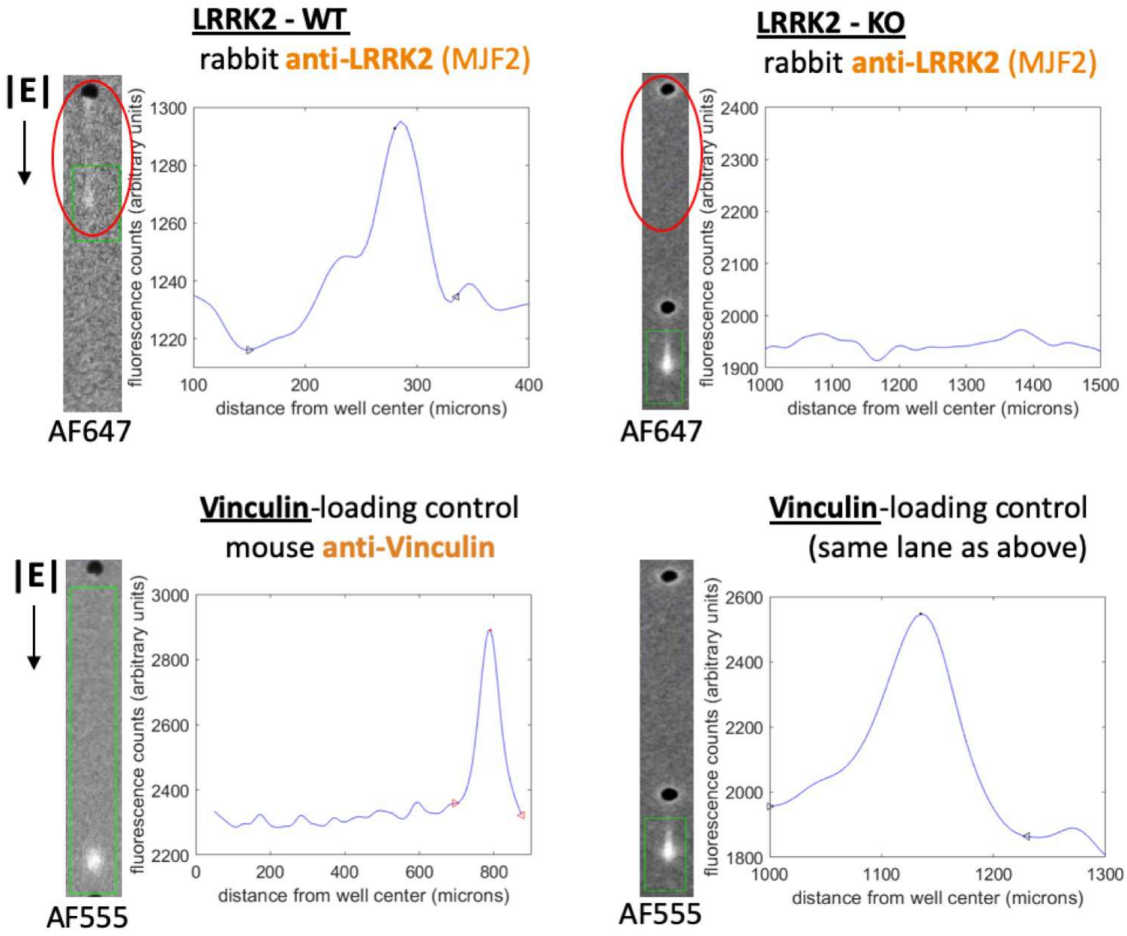

Figure 8-2. Single-Cell Western blot separation and intensity plots of mouse brain CD11b-isolated microglia probed with LRRK2 and Vinculin antibody.

8.2.2 Characterization of the LRRK2 antibodies for scWB

While optimizing scWB experimental conditions for microglial cells, I tested two commercially available Lrrk2 antibodies. In the optimal lysis condition of 10 sec (to optimize Lrrk2 protein extraction) and 130sec timing of electrophoresis, Abcam (c41-2) antibody had a stronger signal, but recognized multiple peaks, including a non-specific band in the Lrrk2 KO sample. (Figure 8-3), while CST (D18E12) antibody had a specific signal in recognition of Lrrk2 protein.

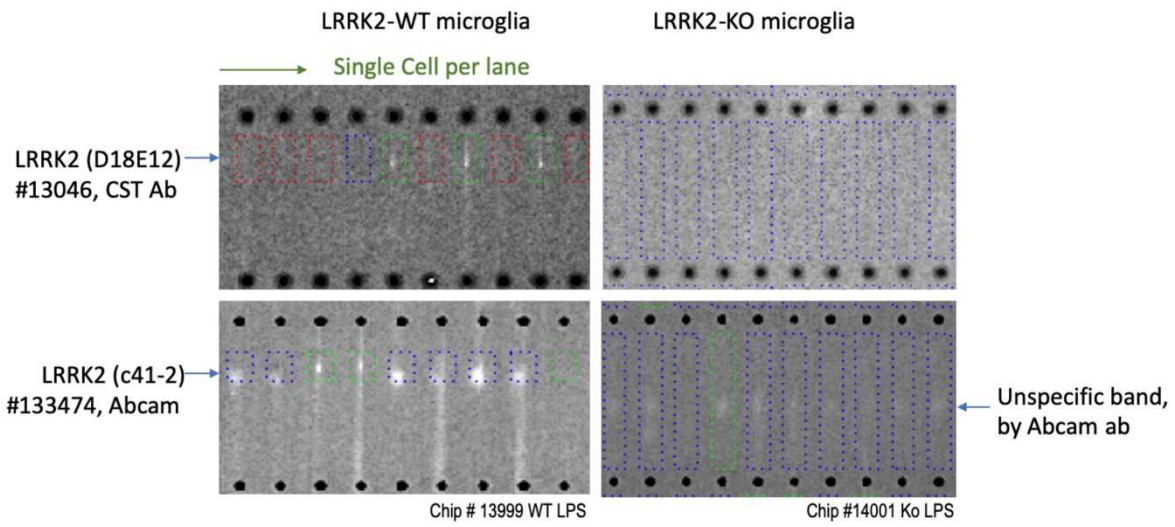

Figure 8-3. Characterization of the two main LRRK2 antibodies in the Single-Cell Western blot. CST antibody shows higher specificity in the current lysis conditions detecting Lrrk2 WT in brain resident individual microglia cells.

8.2.3 LRRK2 protein expression at single cell level in acutely isolated brain microglia stimulated with LPS

In the next experiment, I examined Lrrk2 protein expression in inflammatory stimulated versus control-treated resident brain microglia cells. For this purpose, Lrrk2 animals were injected into the striatum with LPS or vehicle control, PBS. Seventy two hours after injection, brain resident microglia cells were isolated with gentle MACS-dissociation, coupled with microglial CD11b-Ab magnetic beads.

Single cell solutions from mice were loaded on scWB chips as in prior experiments, starting with 300,000 cells. In this experiment, running conditions were 10 sec lysis, 130 sec electrophoresis and 240 sec for UV immobilization. The results are presented in Figure 8-4, where chips were probed with either LRRK2 (280kDa) antibody (from CST, D18E12) or PKC-delta (104kDa) as a loading control expressed in microglial cells. Although in the primary test experiment, we were using Vinculin as a loading control to validate LRRK2 migration distances on the chip), in this experiment Vinculin could not be

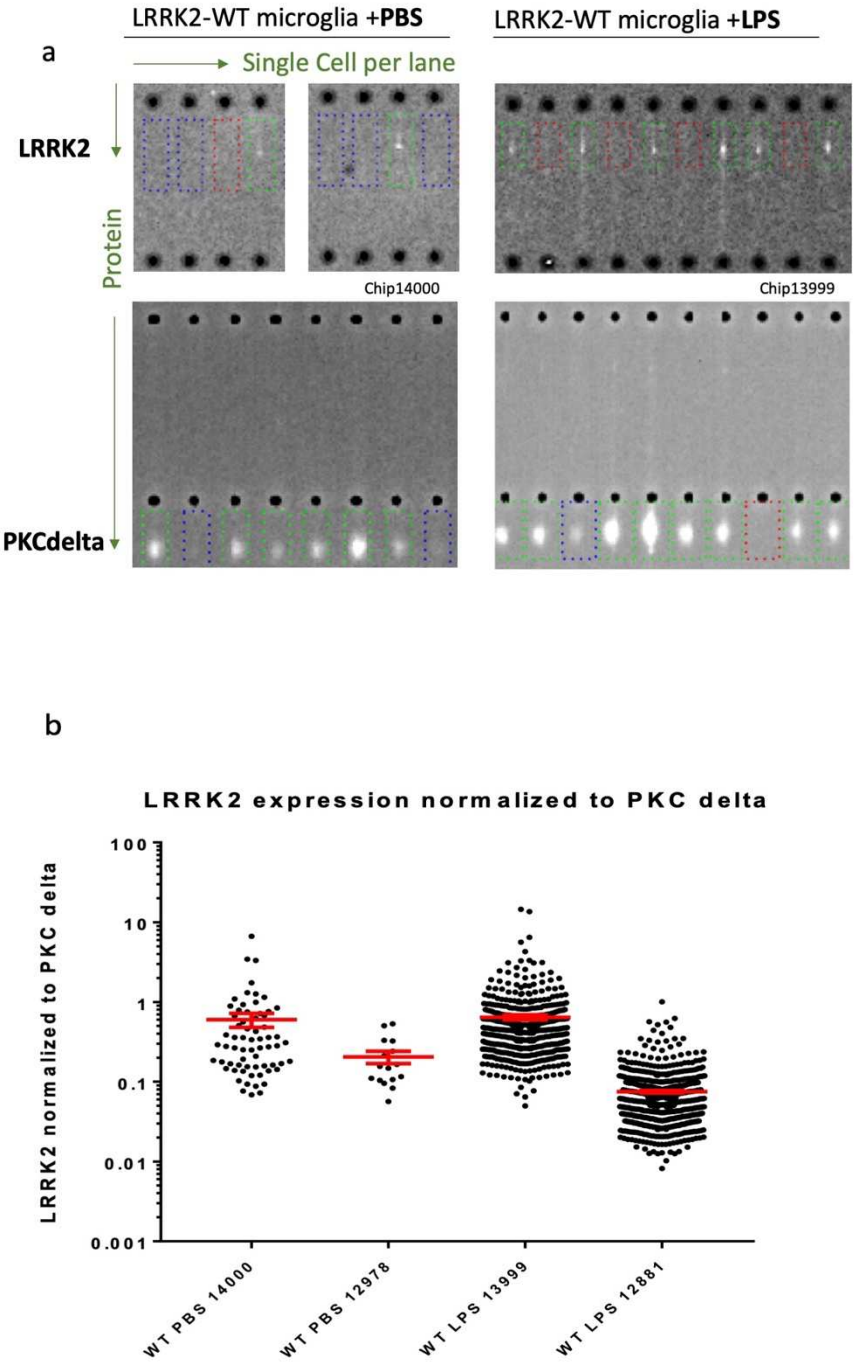

Figure 8-4. LRRK2 protein expression at the single-cell Western blot in acutely isolated brain microglia after LPS brain injections. (**a**) More brain microglia cells are expressing LRRK2 after LPS treatment, but the average expression levels per cell are not significantly different from PBS-injected brains. (**b**) Quantification of LRRK2 expression normalized to the loading control PKCdelta (scatter plot of the LRRK2 peak areas, mean +/-SEM). Each chip represents cells from one animal.

used as loading control across all samples, since LPS significantly increased Vinculin expression (data not shown). The imaged cells were analyzed using Scout v.2 Software to identify each target protein per cell and quantitate its abundance.

I found that more brain microglia cells express LRRK2 for LPS-treated animals compared to PBS-injected brains, where each point represents a single cell (Figure 8-4b). Specifically, about 30% of microglia are LRRK2 positive after LPS treatment compared to only about 3% LRRK2 expressing cells in the control-treated microglia (Figure 8-5).

a

	CHIP#	Size	Sample	Num of PKCd positive cells	% of LRRK2 positive cells
	13999	std	**WT LPS**	1656	31.46
	12881	small	**WT LPS**	2607	28.3
	14000	std	WT PBS	2455	3.8
	14816	std	WT PBS	N/A	4.56
	18978	small	WT PBS	1676	1.19
	14001	std	**KO LPS**	3583	0
	12880	small	**KO LPS**	2080	0
	13998	std	KO PBS	2075	0
	14823	std	KO PBS	N/A	0
	12877	small	KO PBS	1511	0
Avg number of loaded cells				**2205**	
Avg % of LRRK2 positive cells (PBS treatment)					**3.18**
% of LRRK2 positive cells (LPS treatment)					**29.8**

b

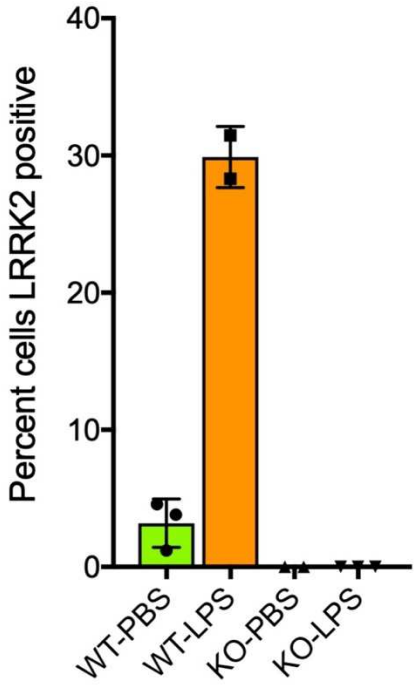

Figure 8-5. Quantification of LRRK2 protein expression in individual brain microglia after LPS or PBS brain injections. (a) Percent of LRRK2 positive cells detected in each chip based on Scout software image analysis. Each chip represents cells from one animal. **(b)** Average percentage of LRRK2 positive resident brain microglia cells after PBS or LPS striatal injections, n=3 animals WT-PBS, KO-PBS; n=2 WT-LPS, KO-LPS.

The results of scWB show that although more brain microglia cells express Lrrk2 after LPS exposure, the average expression level per cell was not significantly different from PBS-treated brains (Figure 8-6). These results therefore show that inflammagen exposure increases the proportion of microglia that express Lrrk2 rather than increased amounts per cell.

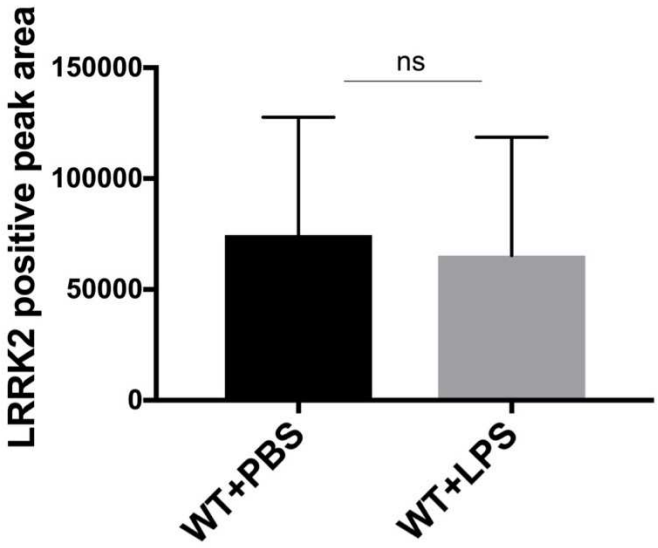

Figure 8-6. Average expression level of LRRK2 protein per cell between PBS and LPS-injected resident brain microglia.
No significant difference in LRRK2 expression level per cell has been detected after LPS-treatment using single cell western blot method.
Unpaired t-test, data combined from 2 chips (2 animals) per treatment with total about 800 and 200 LRRK2-positive cells for LPS chips and PBS chips respectively.

8.3 Summary

Overall, the data show that more brain microglia cells are expressing LRRK2 after LPS treatment, but the average expression levels per cell do not seem to be significantly different from PBS-injected brains.

Higher amount of LRRK2-positive LPS-treated cells could result from proliferating microglia as a response to the strong inflammatory stimulus. Additionally, non-microglial LRRK2-positive cells could add to the total number of LRRK2 expression – those could result from a small amount of brain recruited (infiltrating) macrophages or be a non-specific part of CD11b-pull purification. Also, it can be an elevated level of CD11b marker expression which can allow better CD11b exposure on the cell surface for the antibody recognition during the purification step of microglia. To distinguish between those possibilities, I would need to probe the single-cell West chip with the recently characterized brain-specific microglial marker, Tmem119, which is expressed on microglia but not on recruited macrophages (M. L. Bennett et al., 2016). Unfortunately, at the moment Tmem119 antibody is not available for the western blot application, so future experiments will be needed to complete this task.

Chapter 9

General Discussion

In this work I investigated the contribution of microglial cells to the pathogenic mechanisms behind LRRK2-associated Parkinson's disease (PD). Microglia are immune cells in the brain, playing critical roles during the innate inflammatory response (Perry & Holmes, 2014).

Although PD mainly occurs as a sporadic syndrome, about 5% of cases are inherited (Klein & Westenberger, 2012). Among the genes mutated in familial PD, those encoding LRRK2 and α-synuclein play major roles in the pathogenic mechanisms leading to neurodegeneration (Hernandez et al., 2016).

Several studies suggest a connection between LRRK2 and the neuropathology caused by α-synuclein. For example, LRRK2 mediates pro-inflammatory responses in activated microglia (N. L. Dzamko, 2017; Isabella Russo et al., 2014) and α-synuclein released by dying neurons, can exacerbate microglia activation (Maekawa et al., 2016). However, the detailed mechanisms behind these observations are currently unresolved. Previous studies have emphasized a connection between LRRK2 activity and the biology of microglia (Isabella Russo et al., 2014; Schapansky et al., 2015). Dissecting the role of LRRK2 in brain immune cells, both under resting and inflammatory conditions, is crucial to understand whether deregulated LRRK2 activity in these cells has an indirect and harmful impact on neuronal functions.

In the first part of this work I investigated LRRK2 transcriptome profile under resting and inflammatory conditions in primary microglia cells. In the second part I moved to a more physiological system, e.g. resident microglia acutely isolated from the mouse brain, and

investigated the morphological, functional and transcriptional phenotypes under inflammatory stimuli *in vivo* and *in vitro*.

The first aim of this work was to gain insights into the effects of LRRK2 deficiency on inflammatory signaling. We performed an RNA-sequencing (RNA-seq) analysis of LRRK2 wild-type (WT) and knockout (KO) primary microglia either under basal conditions or treated with the two inflammatory stimuli, PD-related α-synuclein PFFs or with more general inflammagen lipopolysaccharide (LPS). Based on differential gene expression analysis, we found that: (i) Lrrk2 genetic deletion has only a subtle influence on basal gene expression in untreated samples and that (ii) although LPS and α-synuclein PFFs have partially overlapping effects on gene expression profiles, primary microglial responses are also distinct. One distinct effect in response to stimulation with α-synuclein PFFs was associated with oxidative stress.

The possible explanation of this result can be related to the difference in the cell receptors responsible for the signaling of each inflammatory stimuli. Notably, the induction of superoxide dismutase 2 (SOD2) by PFFs was decreased in Lrrk2 KO microglia, supporting the notion that LRRK2 positively regulate microglial response (Russo et al., 2015).

Usually, inflammatory response processes depend on the precise nature of the initial stimulus, which is recognized by the cell surface pattern receptors (L. Chen et al., 2018). Extensive literature showed that LPS activates microglia through the engagement of Toll-like receptor 4 (TLR4) (Lien et al., 2000; Yao et al., 2013). In contrast, the receptors responding to the α-synuclein aggregated forms are still controversial and could be multiple.

It was suggested that α-synuclein induces microglial-associated inflammation through different processes including receptor-mediated endocytosis (H. J. Lee, Suk, Bae, & Lee, 2008), ligand-receptor interaction including TLR1/2 or scavenger receptors (Beraud & Maguire-Zeiss, 2012; Daniele et al., 2015). TLR2 receptor was reported to have an increased staining in post-mortem PD-brains and its levels correlated with the accumulation of pathological α-synuclein (N. Dzamko et al., 2017).

TLR-ligand activity of α-synuclein may be conformation-sensitive, as suggested by a study showing that only oligomeric species can interact and activate microglial TLR2 (C. Kim et al., 2013). Additionally, TLR4 has been also proposed to mediate responses to α-synuclein pathological forms (Fellner et al., 2013), suggesting an overlapping signaling with LPS.
Overall, it is possible that, in comparison to LPS, α-synuclein PFFs activate microglia either through different receptors or the complexity of the ligand-receptor interaction activate additional factors, which in turn, mediate differential response, as suggested by our RNA-seq transcriptomic analysis.

According to our results, we observed only small transcriptional differences between LRRK2 WT and KO genotypes in unstimulated cells. A possible explanation could be that, in the absence of inflammatory stimuli, LRRK2 is inactive or, that LRRK2 KO microglia activate alternative pathways that compensate the absence of LRRK2 activity. In contrast, under stimulated conditions, LRRK2 KO microglia cells displayed attenuated induction of mitochondrial SOD2 in response to α-synuclein PFFs, which suggest a reduced or delayed response compare to WT microglia. In agreement with this results, it has been previously showed that after LPS-stimulation, microglia expressed lower levels of nitric oxide synthase in the case of LRRK2 knock-down or inhibition of LRRK2 kinase activity (B. Kim et al., 2012; Moehle et al., 2012). In our study we also found a robust increased of S935 LRRK2 phosphorylation upon α-synuclein PFFs stimulation, which may implicate the involvement of LRRK2 activity in response to PD-related inflammatory insult. Taken together, these results indicate that LRRK2 confers a greater susceptibility to some inflammatory stimuli.

Importantly, upon LPS stimulation, expression of IL-1β was lower in LRRK2 KO microglia compared to WT, confirming previous observations (I. Russo et al., 2015).

Gene ontology analysis of the pathways associated with microglial responses revealed that although the responses to each inflammagen overlapped, each set had also unique elements. Specifically, LPS exposure resulted in alterations of “regulation of nitrogen compound metabolic process” category that contained the Thioredoxin Interacting Protein (TXNIP), which is known to regulate metabolism, ER stress and has been shown to have

impact on autophagy. Conversely, α-synuclein PFFs alter the “regulation of reactive oxygen species metabolic process” category, which includes SOD2, an enzyme playing a crucial role in clearing mitochondrial reactive oxygen species (ROS) and protecting cells against oxidative stress and damage.

We technically validated both TXNIP and SOD2 by qRT-PCR, confirming that TXNIP transcript was downregulated by LPS exposure compare to untreated and α-synuclein PFFs stimulated cells and that SOD2 was upregulated by both stimuli with a much stronger effect upon α-synuclein PFFs.
Additionally, we validated α-synuclein PFFs-mediated SOD2 induction at the protein level. We showed that SOD2 is increased after both α-synuclein PFFs and LPS priming, but that levels are enhanced upon α-synuclein PFFs, confirming that α-synuclein PFFs mediate a microglial response with a higher oxidative stress component compared to LPS. The effect of genotypes was more subtle, with SOD2 only displaying a modest decrease in LRRK2 KO.

In the attempt of translating these findings into a functional effect due to SOD2 deregulation, I compared ROS production in LRRK2 WT and KO microglial cells upon LPS and synuclein PFFs priming. I tried a few approaches, including MitoSOX labeling for mitochondrial ROS measurements (Wojtala et al., 2014), which, however, did not result in a specific ROS mitochondrial signal in microglia. An attempt was also made by transfecting genetically encoded reduction-oxidation sensitive GFP (roGFP), however the transfection efficiency in primary microglia was too low to obtain reliable measurements. Additionally, since mitochondrial SOD2 activity is partially regulated via acetylation at its lysine residues, the acetylated status of SOD2 by SIRT3 (M. L. Chen et al., 2017) was evaluated by western blot. Unfortunately, the results were inconclusive as the antibody anti-AcSOD2 recognized non-specific targets (data not shown).

Mitochondrial SOD2 transforms toxic superoxide anion into hydrogen peroxide, which both, at low doses, are essential in many intracellular signaling processes, however, at high doses, especially superoxide anion, result in oxidative stress and cellular damage (Fukai & Ushio-Fukai, 2011). It has been reported that α-synuclein toxic species may disturb mitochondrial respiration and/or uncouple oxidative phosphorylation leading to

accumulation of ROS, as reviewed in (Nakamura, 2013). Overall, a higher increase of SOD2 transcript and protein expression in response to α-synuclein PFFs compare to LPS stimulation, suggest that microglia cells exhibit an alteration of ROS-related pathways and may recruit antioxidant enzymes including SOD2 to protect the cell against oxidative stress and damage.

TXNIP is an endogenous inhibitor of ROS elimination by binding and inhibiting thioredoxin protein, therefore TXNIP is associated with activation of oxidative stress (Alhawiti, Al Mahri, Aziz, Malik, & Mohammad, 2017). Thus, we can speculate that downregulation of TXNIP in our experiments, in response to LPS stimulation of the primary microglia, will increase an antioxidant power of thioredoxin protein, leading to the overall antioxidant response.

However, some evidences point out that TXNIP might act as a scaffolding protein in signaling complex independent of cellular redox regulation (Yoshihara et al., 2014).

A recent publication identified TXNIP as a key factor mediating the LRRK2-G2019S pathological phenotypes in the 3D environment of midbrain organoids (H. Kim et al., 2019). Additionally, TXNIP was found to significantly accelerate the accumulation of α-synuclein through inhibition of lysosomal membrane protein ATP13A2. Moreover, increased TXNIP in substantia nigra pars compacta (SNpc) after stereotactical injections, induced a 30% loss of DA neurons compared with control mice (Su et al., 2017). This data might implicate TXNIP as a disease-modulating protein in PD and future investigation of its role in microglia will be critically important.

Unfortunately, I was unable to validate downregulation of TXNIP at the protein level because of the lack of reliable antibodies.

To further explore possible differences between microglia LPS and α-synuclein PFFs treated microglia, we performed ELISA assays to evaluate the cytokine profile of WT microglia. We observed a differential cytokine profiles between stimulation with LPS and α-synuclein PFFs. We discovered that seven out of sixteen tested cytokines showed enhanced secretion by stimulated microglial cells, while IL-6 and TNF-α were specifically induced by LPS and not by α-synuclein fibrils, demonstrating that the two inflammagenes produce different cytokine profiles. Additionally, the amount of IL-1β, secreted in response

to α-synuclein fibrils stimulation in WT cells was much lower compared to LPS, while MCP-1 levels were elevated and similar to LPS. In agreement with our findings, one study showed that nitrated α-synuclein increased the production of MCP-1 (Allen Reish & Standaert, 2015). Instead, the modest release of TNF-α and IL-1β that we observed in response to α-synuclein PFFs contradicts the data reported in the literature, as reviewed by (S. A. Ferreira & Romero-Ramos, 2018), although the differences may be explained by different experimental settings (e.g. α-synuclein conformation) and timing of inflammatory stimulation. Accordingly, oligomeric α-synuclein induced a proinflammatory microglial phenotype leading to increased production of TNF-α and IL-1β (Daniele et al., 2015). Thus, different α-synuclein aggregation state may activate different receptors leading to differential immune responses.

Overall, our data support the existence of somewhat differential receptor recognition and downstream pathways between LPS and α-synuclein.

The role of inflammatory cytokines in the pathogenesis of PD has been broadly discussed in the literature (Hanisch, 2002; Y. S. Kim & Joh, 2006). It has been shown that inflammation caused by LPS increased the vulnerability of midbrain DA neurons to PD-like degeneration *in vivo*, and identified the specific changes in cytokine brain tissue levels associated with the increased risk of degeneration (Sadek, Almohari, & Renno, 2014). In another study, LPS induced secretion of cytokines and predisposed rat DA neurons to be more vulnerable to a subsequent low dose of 6-hydroxydopamine. Alterations in cytokines release, especially in interleukin-1beta (IL-1β), were identified as potential mediators of this effect, which was also associated with activation of microglia (Koprich, Reske-Nielsen, Mithal, & Isacson, 2008). Relevant for human disease, high levels of pro-inflammatory cytokines were detected in patients with severe LRRK2-associated PD-phenotypes, suggesting that cytokines may be included in biomarker panels (Brockmann et al., 2017).

A delicate equilibrium of microglial-derived factors, including cytokines, might determine the neurotrophic or neurotoxic effect of activated microglia (Koprich et al., 2008). Since pro-inflammatory cytokines may accelerate disease progression, modulation of microglial functional states may be a useful tool to intervene in the progression of PD.

The results from the first part of my work nominated a panel of genes that are regulated by exposure to LPS or α-synuclein PFFs in primary microglial cultures. However, it is uncertain whether gene expression changes seen in cell culture are also representative of similar effects *in vivo*. It was reported in the literature, that some molecular signatures (for example, TGF-β1 signaling) could be missing in primary versus acute *ex vivo* adult microglia (Butovsky et al., 2014). Additionally, the main concern of using cultured cells is that the process of isolation and culturing might induce baseline activation that could mask gene expression changes that would be seen *in vivo*.

Based on these premises, the second aim of this work was to characterize resident microglia isolated from the adult brains of LRRK2 WT, KO and mutant G2019S and R1441C mice stimulated with LPS.

Brain resident microglia were isolated and characterized functionally (using *ex-vivo* phagocytic assay) and morphologically (in striatal brain slices). Additionally, single cell RNA-sequencing was conducted on LRRK2 WT versus KO brains injected with LPS in the striatum and genes nominated from the primary culture experiment were evaluated. Additionally, LRRK2 protein level was evaluated using single cell western blot technology.

I found that acutely isolated brain microglia contain pure population of the cells expressing the classical microglial protein marker Iba1 and preserve its essential phagocytic function. I then compared phagocytic properties of resident microglia cells from LRRK2 WT, KO and two PD-related pathogenic mutations, G2019S and R1441C, which are characterized by overactive kinase activity and decreased GTPase activity (R1441C).

Although I did not observe differences in phagocytic ability in unstimulated microglia, phagocytic activity was elevated in LRRK2 WT and was the highest in LRRK2 KO cells upon treatment with α-synuclein PFFs. This might implicate LRRK2 as a negative regulator of phagocytosis in the context of α-synuclein stimulated inflammation. Of interest, none of the mutants showed consistent differences in phagocytic ability upon α-synuclein PFFs stimulation. This result is very interesting as it suggests that mutant LRRK2 may have defective phagocytosis, which results in accumulation of toxic extracellular material (e.g. α-synuclein released by dying neurons, neuronal debris) that

further fuel the a neuroinflammatory vicious cycle (Figure 9-1). These data however contradict with the recent findings by Kim et al (K. S. Kim et al., 2018), who reported elevated phagocytic response in macrophages from LRRK2–G2019S PD patients and downregulation of phagocytic activity in LRRK2 KO cells. One possible explanation of this discrepancy may be related to the different experimental settings, including different type of microglial stimulation and phagocytic material. Additionally, the increase in phagocytic activity might actually be the consequence of delayed degradation of ingulfed material. Multiple studies in the neurodegenerative disease field has focused on protein degradation, turnover and related protein aggregation. Autophagy-lysosomal pathway is one of the major proteolytic systems involved in protein degradation and is vital for the maintenance of protein homeostasis in cells, as reviewed by (Lynch-Day, Mao, Wang, Zhao, & Klionsky, 2012; Roosen & Cookson, 2016).

Since the lysosomal pathway is known to be impaired in LRRK2-KO animals (Pellegrini et al., 2018; Y. Tong et al., 2012), the elevated phagocytic material present in stimulated LRRK2-KO microglia might actually represent a delayed lysosomal degradation in our experimental system. Future studies will be needed to evaluate the lysosomal degradation rate in LRRK2 KO and PD-mutant microglia in comparison to WT cells. A better understanding of the involvement of lysosomal pathway and the implication of PD pathological mutations in the context of microglial phagocytosis might be helpful to understand the molecular basis of neurodegeneration in PD.

Next, we used intrastriatal brain injections with LPS-inflammatory agent or with PBS as a control, to evaluate morphological changes in the brain sections of GFP endogenously labeled microglia of LRRK2 WT, KO, G2019S and R1441C. The results demonstrated significant changes in microglial shape (increase in circularity and soma area) in LPS-injected animals compare to PBS-treated and modest differences across LRRK2 genotypes. On the other hand, the branch complexity was reduced in LPS injected animals with stronger effect in LRRK2-KO and R1441C genotypes and less response in G2019S animals.

We can speculate that the kinase overactive G2019S LRRK2 mutant may exhibit an elevated basal level of microglia activation, thus masking an overall inflammatory

response in these cells (Figure 9-1). The similar response of LRRK2 KO and R1414C (mutant with the reduced GTPase activity) can have a few interpretations. First, as discussed in the literature, microglia possess very pleiotropic functions (Heindl et al., 2018) and morphological response might be too general to reflect detailed functional changes between LRRK2-KO and R1441C mutant. Second, since the microglial regional heterogeneity was widely reported (Lehmann et al., 2016; Morrison & Filosa, 2013), it is possible that, in addition to the evaluated striatal region (which was directly subjected to LPS stereotactic injection), there are other neighboring regions that might reflect morphological differences between the mutants. Future use of automated algorithms for morphological analysis that allow to evaluate a broad panel of features and very large cell numbers, might help to distinguish the possible detailed differences between the mutants (Heindl et al., 2018; York, LeDue, Bernier, & MacVicar, 2018).

Changes in microglia morphology represent reasonable marker for studying the general activation state of microglia in reaction to a pathogen, tissue injury or direct inflammatory stimulation with LPS. However, microglia have pleiotropic functions, which become apparent through complex transcription profiles demonstrated in recent publications (Crotti & Ransohoff, 2016; Hickman et al., 2013; Keren-Shaul et al., 2017). Thus, analysis of morphology based on immunohistological sections provides valuable topographical information about microglial activation. Nevertheless, for investigating microglial function additional methods are necessary, e.g., flow cytometry and transcriptomic studies.

Given the highly heterogenous cellular composition of the brain, we decided to utilize a new method of acutely isolated resident microglia to explore transcriptomic changes in LRRK2 WT and KO microglia striatally injected with a strong inflammatory stimuli LPS.

We used scRNA-Seq to examine the gene expression profile at the single cell level and to evaluate whether some of the candidate genes found from cell culture are also differentially evaluated in vivo. The power of scRNA-Seq is that some of these genes, including SOD2, are expressed in both microglia and many other cell types and might not be seen to be regulated by inflammatory stimuli in bulk tissue. We were able to confirm a substantial upregulation of SOD2 and downregulation of TXNIP transcripts in this model. As said, it is unlikely that this could have been detected from bulk RNA-Seq in brain samples as many cells other than microglia express these genes. Future studies will

extend this model to include mutant genotypes so that we can assess the contribution of LRRK2 to microglial gene expression under inflammatory conditions *in vivo*.

Additionally, we found, that although LRRK2 WT had very subtle effect on overall gene expression, which is in agreement with our bulk RNA-seq data, tSNE embedding identified different clusters of microglia cells based on transcriptomic similarities.

Intriguingly, we found a small transcriptomic cluster of cells positive to endothelial marker Ly6c1, that was also positive for LRRK2 expression. The possible expression of LRRK2 in endothelial cells was discussed by Kozina et al (Kozina et al., 2018), suggesting that endothelial cells together with microglia, can modulate neuroinflammatory response by expressing cytokine receptors.

Based on our scRNA-seq data we were able to evaluate the level of LRRK2 expression, which was detected as very sparse in PBS-injected resident microglia and increased by LPS-microglial activation. To examine whether an increase in LRRK2 level is due to higher protein expression per cell or to increased cell proliferation, I used single cell western blot technology. I found that inflammatory stimulation increased the proportion of microglia cells expressing LRRK2 rather than its level per cell. This, to date, is the first attempt to analyze LRRK2 protein expression at the single cell level in the brain isolated microglia.

Taken together, the findings in this thesis underscore an important role of microglia in the inflammatory response behind LRRK2-associated Parkinson's disease. Moreover, the presented method of isolation and analysis of the resident brain microglia shows that this system could serve a valuable tool for the future research.

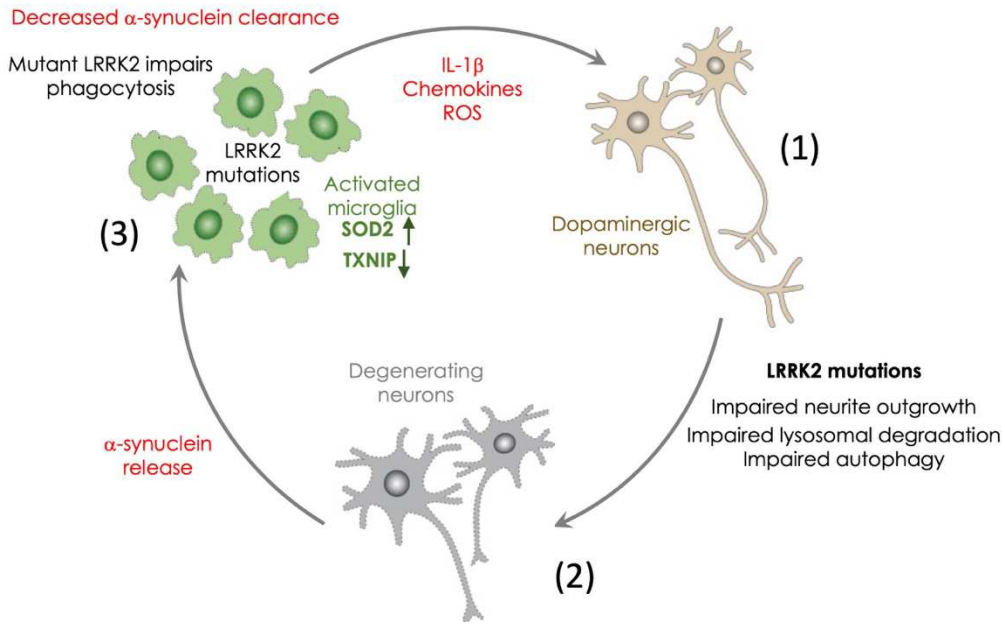

Figure 9-1. Model of PD pathogenesis involving activated microglia. LRRK2 mutations in DA neurons can cause impairment of lysosomal degradation (1), leading to neuronal death and release of toxic α-synuclein, which can activate microglia (2). Upon activation, microglia release pro-inflammatory cytokines and ROS, causing additional damage to LRRK2 mutated DA neurons (3). Mutant LRRK2 microglia might have impaired phagocytosis of toxic extracellular materials, decreasing α-synuclein clearance and causing additional damage to neurons. To keep the homeostatic balance, microglia produce anti-inflammatory response, increasing antioxidant SOD2 expression and downregulating TXNIP.

Outlook

Microglia cells are fundamental for the development and function of a healthy brain and also play a role in immune host defense of the CNS. The fine tuning of microglia helps balancing the immune response, coordinating the interaction between neurons and other glia cells (astrocytes and oligodendrocytes). As every complex system, which brain definitely is, it has interconnections and compensatory mechanisms.

Neuroinflammation and protein accumulation are hallmarks of both normal aging and age-related neurodegenerative disease and chronic neuroinflammation in the brain contributes to neurodegeneration. PD-related mutations in LRRK2 (G2019S, R1441C) may exaggerate the neuroinflammatory response leading to predisposition to PD or

modifying disease progression. Although we detected low level of LRRK2 expression in brain resident microglia, there are several points that would be important to consider.

First, low level of LRRK2 in mouse brain microglia can still have a strong impact on astrocytes and other glial cells, that will, in turn, influence neurons.

Second, since majority of the present mouse models do not manifest a clear PD phenotype, it is debatable whether these models recapitulate the real picture of complex human brain. Recent studies of scRNA-seq from postmortem human brains reveal that human and mouse microglia respond differently to disease, moreover, human microglia has distinct gene signature from that seen earlier in mouse models (Masuda et al., 2019; Mathys et al., 2019). So, in human brain, LRRK2 level in microglial cells might be different from one we found in mice.

Third, in addition to investigation of whole brain microglia, the isolation of LRRK2 WT and PD-related LRRK2 mutants microglial cells from specific brain regions might help to dissect the role of microglial LRRK2 by identifying discrete microglia phenotypes.

Overall, combining genomic data with molecular biology, complementing with advanced research technology will contribute to our future understanding of Parkinson's disease and will bring us to the step of finding a cure.

References

Agamanolis, D.P (2011), Neuropathology. Chapter 9. Available at http://neuropathology-web.org/chapter9/chapter9dPD.html

Aharon-Peretz, J., Rosenbaum, H., & Gershoni-Baruch, R. (2004). Mutations in the glucocerebrosidase gene and Parkinson's disease in Ashkenazi Jews. *N Engl J Med, 351*(19), 1972-1977. doi:10.1056/NEJMoa033277

Alhawiti, N. M., Al Mahri, S., Aziz, M. A., Malik, S. S., & Mohammad, S. (2017). TXNIP in Metabolic Regulation: Physiological Role and Therapeutic Outlook. *Curr Drug Targets, 18*(9), 1095-1103. doi:10.2174/1389450118666170130145514

Ali, K., & Morris, H. R. (2015). Parkinson's disease: chameleons and mimics. *Pract Neurol, 15*(1), 14-25. doi:10.1136/practneurol-2014-000849

Allen Reish, H. E., & Standaert, D. G. (2015). Role of alpha-synuclein in inducing innate and adaptive immunity in Parkinson disease. *J Parkinsons Dis, 5*(1), 1-19. doi:10.3233/JPD-140491

Alvarez-Erviti, L., Rodriguez-Oroz, M. C., Cooper, J. M., Caballero, C., Ferrer, I., Obeso, J. A., & Schapira, A. H. (2010). Chaperone-mediated autophagy markers in Parkinson disease brains. *Arch Neurol, 67*(12), 1464-1472. doi:10.1001/archneurol.2010.198

Araki, M., Ito, G., & Tomita, T. (2018). Physiological and pathological functions of LRRK2: implications from substrate proteins. *Neuronal Signaling*, NS20180005. doi:10.1042/ns20180005

Askew, K., Li, K., Olmos-Alonso, A., Garcia-Moreno, F., Liang, Y., Richardson, P., . . . Gomez-Nicola, D. (2017). Coupled Proliferation and Apoptosis Maintain the Rapid Turnover of Microglia in the Adult Brain. *Cell Rep, 18*(2), 391-405. doi:10.1016/j.celrep.2016.12.041

Bae, E. J., Kim, D. K., Kim, C., Mante, M., Adame, A., Rockenstein, E., . . . Lee, S. J. (2018). LRRK2 kinase regulates alpha-synuclein propagation via RAB35 phosphorylation. *Nat Commun, 9*(1), 3465. doi:10.1038/s41467-018-05958-z

Beilina, A., Rudenko, I. N., Kaganovich, A., Civiero, L., Chau, H., Kalia, S. K., . . . Cookson, M. R. (2014). Unbiased screen for interactors of leucine-rich repeat kinase 2 supports a common pathway for sporadic and familial Parkinson disease. *Proc Natl Acad Sci U S A, 111*(7), 2626-2631. doi:10.1073/pnas.1318306111

Benamer, H. T., & de Silva, R. (2010). LRRK2 G2019S in the North African population: a review. *Eur Neurol, 63*(6), 321-325. doi:10.1159/000279653

Bennett, J. P., Jr., Keeney, P. M., & Brohawn, D. G. (2019). RNA Sequencing Reveals Small and Variable Contributions of Infectious Agents to Transcriptomes of Postmortem Nervous Tissues From Amyotrophic Lateral Sclerosis, Alzheimer's Disease and Parkinson's Disease Subjects, and Increased Expression of Genes From Disease-Activated Microglia. *Front Neurosci, 13*, 235. doi:10.3389/fnins.2019.00235

Bennett, M. L., Bennett, F. C., Liddelow, S. A., Ajami, B., Zamanian, J. L., Fernhoff, N. B., . . . Barres, B. A. (2016). New tools for studying microglia in the mouse and human CNS. *Proc Natl Acad Sci U S A, 113*(12), E1738-1746. doi:10.1073/pnas.1525528113

Beraud, D., & Maguire-Zeiss, K. A. (2012). Misfolded alpha-synuclein and Toll-like receptors: therapeutic targets for Parkinson's disease. *Parkinsonism Relat Disord, 18 Suppl 1*, S17-20. doi:10.1016/S1353-8020(11)70008-6

Berger, Z., Smith, K. A., & Lavoie, M. J. (2010). Membrane localization of LRRK2 is associated with increased formation of the highly active LRRK2 dimer and changes in its phosphorylation. *Biochemistry, 49*(26), 5511-5523. doi:10.1021/bi100157u

Bertler, A., & Rosengren, E. (1959). Occurrence and distribution of catechol amines in brain. *Acta Physiol Scand, 47*, 350-361. Retrieved from https://www.ncbi.nlm.nih.gov/pubmed/13799995

Bialecka, M., Klodowska-Duda, G., Kurzawski, M., Slawek, J., Gorzkowska, A., Opala, G., . . . Drozdzik, M. (2008). Interleukin-10 (IL10) and tumor necrosis factor alpha (TNF) gene polymorphisms in Parkinson's disease patients. *Parkinsonism Relat Disord, 14*(8), 636-640. doi:10.1016/j.parkreldis.2008.02.001

Billingsley, K. J., Bandres-Ciga, S., Saez-Atienzar, S., & Singleton, A. B. (2018). Genetic risk factors in Parkinson's disease. *Cell Tissue Res, 373*(1), 9-20. doi:10.1007/s00441-018-2817-y

Biosa, A., Trancikova, A., Civiero, L., Glauser, L., Bubacco, L., Greggio, E., & Moore, D. J. (2013). GTPase activity regulates kinase activity and cellular phenotypes of Parkinson's disease-associated LRRK2. *Hum Mol Genet, 22*(6), 1140-1156. doi:10.1093/hmg/dds522

Bliederhaeuser, C., Grozdanov, V., Speidel, A., Zondler, L., Ruf, W. P., Bayer, H., . . . Danzer, K. M. (2016). Age-dependent defects of alpha-synuclein oligomer uptake in microglia and monocytes. *Acta Neuropathol, 131*(3), 379-391. doi:10.1007/s00401-015-1504-2

Blinzinger, K., & Kreutzberg, G. (1968). Displacement of synaptic terminals from regenerating motoneurons by microglial cells. *Z Zellforsch Mikrosk Anat, 85*(2), 145-157. Retrieved from https://www.ncbi.nlm.nih.gov/pubmed/5706753

Bonifati, V. (2007). LRRK2 low-penetrance mutations (Gly2019Ser) and risk alleles (Gly2385Arg)-linking familial and sporadic Parkinson's disease. *Neurochem Res, 32*(10), 1700-1708. doi:10.1007/s11064-007-9324-y

Braak, H., & Braak, E. (1991). Neuropathological stageing of Alzheimer-related changes. *Acta Neuropathol, 82*(4), 239-259. doi:10.1007/bf00308809

Brockmann, K., Schulte, C., Schneiderhan-Marra, N., Apel, A., Pont-Sunyer, C., Vilas, D., . . . Maetzler, W. (2017). Inflammatory profile discriminates clinical subtypes in LRRK2-associated Parkinson's disease. *Eur J Neurol, 24*(2), 427-e426. doi:10.1111/ene.13223

Brown, G. C., & Neher, J. J. (2014). Microglial phagocytosis of live neurons. *Nature Reviews Neuroscience, 15*, 209. doi:10.1038/nrn3710

Brundin, P., Dave, K. D., & Kordower, J. H. (2017). Therapeutic approaches to target alpha-synuclein pathology. *Exp Neurol, 298*(Pt B), 225-235. doi:10.1016/j.expneurol.2017.10.003

Burre, J., Sharma, M., & Sudhof, T. C. (2015). Definition of a molecular pathway mediating alpha-synuclein neurotoxicity. *J Neurosci, 35*(13), 5221-5232. doi:10.1523/JNEUROSCI.4650-14.2015

Butler, A., Hoffman, P., Smibert, P., Papalexi, E., & Satija, R. (2018). Integrating single-cell transcriptomic data across different conditions, technologies, and species. *Nature Biotechnology, 36*, 411. doi:10.1038/nbt.4096

https://www.nature.com/articles/nbt.4096#supplementary-information

Butovsky, O., Jedrychowski, M. P., Moore, C. S., Cialic, R., Lanser, A. J., Gabriely, G., . . . Weiner, H. L. (2014). Identification of a unique TGF-beta-dependent molecular and functional signature in microglia. *Nat Neurosci, 17*(1), 131-143. doi:10.1038/nn.3599

Buttgereit, A., Lelios, I., Yu, X., Vrohlings, M., Krakoski, N. R., Gautier, E. L., . . . Greter, M. (2016). Sall1 is a transcriptional regulator defining microglia identity and function. *Nat Immunol, 17*(12), 1397-1406. doi:10.1038/ni.3585

Carlsson, A., Lindqvist, M., Magnusson, T., & Waldeck, B. (1958). On the presence of 3-hydroxytyramine in brain. *Science, 127*(3296), 471. doi:10.1126/science.127.3296.471

Casano, A. M., & Peri, F. (2015). Microglia: multitasking specialists of the brain. *Dev Cell, 32*(4), 469-477. doi:10.1016/j.devcel.2015.01.018

Cebrian, C., Loike, J. D., & Sulzer, D. (2015). Neuroinflammation in Parkinson's disease animal models: a cell stress response or a step in neurodegeneration? *Curr Top Behav Neurosci, 22*, 237-270. doi:10.1007/7854_2014_356

Charcot, J. M. (1886). *Lecons sur, les maladies du système nerveux* (Vol. 1): Lecrosnier et Babé.

Chen, L., Deng, H., Cui, H., Fang, J., Zuo, Z., Deng, J., . . . Zhao, L. (2018). Inflammatory responses and inflammation-associated diseases in organs. *Oncotarget, 9*(6), 7204-7218. doi:10.18632/oncotarget.23208

Chen, M. L., Zhu, X. H., Ran, L., Lang, H. D., Yi, L., & Mi, M. T. (2017). Trimethylamine-N-Oxide Induces Vascular Inflammation by Activating the NLRP3 Inflammasome Through the SIRT3-SOD2-mtROS Signaling Pathway. *J Am Heart Assoc, 6*(9). doi:10.1161/JAHA.117.006347

Cogo, S., Greggio, E., & Lewis, P. A. (2017). Leucine Rich Repeat Kinase 2: beyond Parkinson's and beyond kinase inhibitors. *Expert Opinion on Therapeutic Targets, 21*(8), 751-753. doi:10.1080/14728222.2017.1342968

Cookson, M. R. (2010). The role of leucine-rich repeat kinase 2 (LRRK2) in Parkinson's disease. *Nat Rev Neurosci, 11*(12), 791-797. doi:10.1038/nrn2935

Cookson, M. R. (2015). LRRK2 Pathways Leading to Neurodegeneration. *Curr Neurol Neurosci Rep, 15*(7), 42. doi:10.1007/s11910-015-0564-y

Cookson, M. R. (2017). Mechanisms of Mutant LRRK2 Neurodegeneration. *Adv Neurobiol, 14*, 227-239. doi:10.1007/978-3-319-49969-7_12

Crotti, A., & Ransohoff, R. M. (2016). Microglial Physiology and Pathophysiology: Insights from Genome-wide Transcriptional Profiling. *Immunity, 44*(3), 505-515. doi:10.1016/j.immuni.2016.02.013

Daher, J. P. (2017). Interaction of LRRK2 and alpha-Synuclein in Parkinson's Disease. *Adv Neurobiol, 14*, 209-226. doi:10.1007/978-3-319-49969-7_11

Daniele, S. G., Beraud, D., Davenport, C., Cheng, K., Yin, H., & Maguire-Zeiss, K. A. (2015). Activation of MyD88-dependent TLR1/2 signaling by misfolded alpha-synuclein, a protein linked to neurodegenerative disorders. *Sci Signal, 8*(376), ra45. doi:10.1126/scisignal.2005965

Daniëls, V., Vancraenenbroeck, R., Law, B., Greggio, E., Lobbestael, E., Gao, F., . . . Taymans, J.-M. (2010). Insight into the mode of action of the LRRK2 Y1699C pathogenic mutant. *Journal of neurochemistry, 116*, 304-315. doi:10.1111/j.1471-4159.2010.07105.x

De Carlos, J. A., & Borrell, J. (2007). A historical reflection of the contributions of Cajal and Golgi to the foundations of neuroscience. *Brain Res Rev, 55*(1), 8-16. doi:10.1016/j.brainresrev.2007.03.010

Deczkowska, A., Keren-Shaul, H., Weiner, A., Colonna, M., Schwartz, M., & Amit, I. (2018). Disease-Associated Microglia: A Universal Immune Sensor of Neurodegeneration. *Cell, 173*(5), 1073-1081. doi:10.1016/j.cell.2018.05.003

Dehay, B., Bove, J., Rodriguez-Muela, N., Perier, C., Recasens, A., Boya, P., & Vila, M. (2010). Pathogenic lysosomal depletion in Parkinson's disease. *J Neurosci, 30*(37), 12535-12544. doi:10.1523/JNEUROSCI.1920-10.2010

Depboylu, C., Stricker, S., Ghobril, J. P., Oertel, W. H., Priller, J., & Hoglinger, G. U. (2012). Brain-resident microglia predominate over infiltrating myeloid cells in activation, phagocytosis and interaction with T-lymphocytes in the MPTP mouse model of Parkinson disease. *Exp Neurol, 238*(2), 183-191. doi:10.1016/j.expneurol.2012.08.020

Dzamko, N., Deak, M., Hentati, F., Reith, A. D., Prescott, A. R., Alessi, D. R., & Nichols, R. J. (2010). Inhibition of LRRK2 kinase activity leads to dephosphorylation of Ser(910)/Ser(935), disruption of 14-3-3 binding and altered cytoplasmic localization. *Biochem J, 430*(3), 405-413. doi:10.1042/BJ20100784

Dzamko, N., Gysbers, A., Perera, G., Bahar, A., Shankar, A., Gao, J., . . . Halliday, G. M. (2017). Toll-like receptor 2 is increased in neurons in Parkinson's disease brain and may contribute to alpha-synuclein pathology. *Acta Neuropathol, 133*(2), 303-319. doi:10.1007/s00401-016-1648-8

Dzamko, N. L. (2017). LRRK2 and the Immune System. *Adv Neurobiol, 14*, 123-143. doi:10.1007/978-3-319-49969-7_7

Ehringer, H., & Hornykiewicz, O. (1960). [Distribution of noradrenaline and dopamine (3-hydroxytyramine) in the human brain and their behavior in diseases of the extrapyramidal system]. *Klin Wochenschr, 38*, 1236-1239. doi:10.1007/bf01485901

Fava, V. M., Manry, J., Cobat, A., Orlova, M., Van Thuc, N., Ba, N. N., . . . Canadian Lrrk2 in Inflammation, T. (2016). A Missense LRRK2 Variant Is a Risk Factor for Excessive Inflammatory Responses in Leprosy. *PLoS Negl Trop Dis, 10*(2), e0004412. doi:10.1371/journal.pntd.0004412

Fearnley, J. M., & Lees, A. J. (1991). Ageing and Parkinson's disease: substantia nigra regional selectivity. *Brain, 114 (Pt 5)*, 2283-2301. doi:10.1093/brain/114.5.2283

Fellner, L., Irschick, R., Schanda, K., Reindl, M., Klimaschewski, L., Poewe, W., . . . Stefanova, N. (2013). Toll-like receptor 4 is required for alpha-synuclein dependent activation of microglia and astroglia. *Glia, 61*(3), 349-360. doi:10.1002/glia.22437

Fernandez-Arjona, M. D. M., Grondona, J. M., Granados-Duran, P., Fernandez-Llebrez, P., & Lopez-Avalos, M. D. (2017). Microglia Morphological Categorization in a Rat Model of Neuroinflammation by Hierarchical Cluster and Principal Components Analysis. *Front Cell Neurosci, 11*, 235. doi:10.3389/fncel.2017.00235

Ferreira, S. A., & Romero-Ramos, M. (2018). Microglia Response During Parkinson's Disease: Alpha-Synuclein Intervention. *Front Cell Neurosci, 12*, 247. doi:10.3389/fncel.2018.00247

Ferreira, T. A., Blackman, A. V., Oyrer, J., Jayabal, S., Chung, A. J., Watt, A. J., . . . van Meyel, D. J. (2014). Neuronal morphometry directly from bitmap images. *Nat Methods, 11*(10), 982-984. doi:10.1038/nmeth.3125

Fukai, T., & Ushio-Fukai, M. (2011). Superoxide dismutases: role in redox signaling, vascular function, and diseases. *Antioxid Redox Signal, 15*(6), 1583-1606. doi:10.1089/ars.2011.3999

Funayama, M., Hasegawa, K., Kowa, H., Saito, M., Tsuji, S., & Obata, F. (2002). A new locus for Parkinson's disease (PARK8) maps to chromosome 12p11.2-q13.1. *Ann Neurol, 51*(3), 296-301. Retrieved from https://www.ncbi.nlm.nih.gov/pubmed/11891824

Furube, E., Kawai, S., Inagaki, H., Takagi, S., & Miyata, S. (2018). Brain Region-dependent Heterogeneity and Dose-dependent Difference in Transient Microglia Population Increase during Lipopolysaccharide-induced Inflammation. *Scientific Reports, 8*(1), 2203. doi:10.1038/s41598-018-20643-3

Gao, H. M., & Hong, J. S. (2008). Why neurodegenerative diseases are progressive: uncontrolled inflammation drives disease progression. *Trends Immunol, 29*(8), 357-365. doi:10.1016/j.it.2008.05.002

Garcia-Reitboeck, P., Phillips, A., Piers, T. M., Villegas-Llerena, C., Butler, M., Mallach, A., . . . Pocock, J. M. (2018). Human Induced Pluripotent Stem Cell-Derived Microglia-Like Cells Harboring TREM2 Missense Mutations Show Specific Deficits in Phagocytosis. *Cell Rep, 24*(9), 2300-2311. doi:10.1016/j.celrep.2018.07.094

Garden, G. A., & Moller, T. (2006). Microglia biology in health and disease. *J Neuroimmune Pharmacol, 1*(2), 127-137. doi:10.1007/s11481-006-9015-5

Gardet, A., Benita, Y., Li, C., Sands, B. E., Ballester, I., Stevens, C., . . . Podolsky, D. K. (2010). LRRK2 is involved in the IFN-gamma response and host response to pathogens. *J Immunol, 185*(9), 5577-5585. doi:10.4049/jimmunol.1000548

George, J. L., Mok, S., Moses, D., Wilkins, S., Bush, A. I., Cherny, R. A., & Finkelstein, D. I. (2009). Targeting the progression of Parkinson's disease. *Curr Neuropharmacol, 7*(1), 9-36. doi:10.2174/157015909787602814

Gerhard, A., Pavese, N., Hotton, G., Turkheimer, F., Es, M., Hammers, A., . . . Brooks, D. J. (2006). In vivo imaging of microglial activation with [11C](R)-PK11195 PET in idiopathic Parkinson's disease. *Neurobiol Dis, 21*(2), 404-412. doi:10.1016/j.nbd.2005.08.002

Gillardon, F., Schmid, R., & Draheim, H. (2012). Parkinson's disease-linked leucine-rich repeat kinase 2(R1441G) mutation increases proinflammatory cytokine release from activated primary microglial cells and resultant neurotoxicity. *Neuroscience, 208*, 41-48. doi:10.1016/j.neuroscience.2012.02.001

Ginhoux, F., Greter, M., Leboeuf, M., Nandi, S., See, P., Gokhan, S., . . . Merad, M. (2010). Fate mapping analysis reveals that adult microglia derive from primitive macrophages. *Science, 330*(6005), 841-845. doi:10.1126/science.1194637

Goedert, M. (2001). Alpha-synuclein and neurodegenerative diseases. *Nature Reviews Neuroscience, 2*(7), 492-501. doi:10.1038/35081564

Goedert, M., Spillantini, M. G., Del Tredici, K., & Braak, H. (2013). 100 years of Lewy pathology. *Nat Rev Neurol, 9*(1), 13-24. doi:10.1038/nrneurol.2012.242

Goetz, C. G. (2011). The history of Parkinson's disease: early clinical descriptions and neurological therapies. *Cold Spring Harb Perspect Med, 1*(1), a008862. doi:10.1101/cshperspect.a008862

Greenfield, J. G., & Bosanquet, F. D. (1953). The brain-stem lesions in Parkinsonism. *J Neurol Neurosurg Psychiatry, 16*(4), 213-226. doi:10.1136/jnnp.16.4.213

Greggio, E., & Cookson, M. R. (2009). Leucine-rich repeat kinase 2 mutations and Parkinson's disease: three questions. *ASN Neuro, 1*(1). doi:10.1042/AN20090007

Greggio, E., Jain, S., Kingsbury, A., Bandopadhyay, R., Lewis, P., Kaganovich, A., . . . Cookson, M. R. (2006). Kinase activity is required for the toxic effects of mutant LRRK2/dardarin. *Neurobiol Dis, 23*(2), 329-341. doi:10.1016/j.nbd.2006.04.001

Greggio, E., Zambrano, I., Kaganovich, A., Beilina, A., Taymans, J. M., Daniels, V., . . . Cookson, M. R. (2008). The Parkinson disease-associated leucine-rich repeat kinase 2 (LRRK2) is a dimer that undergoes intramolecular autophosphorylation. *J Biol Chem, 283*(24), 16906-16914. doi:10.1074/jbc.M708718200

Guerrero-Juarez, C. F., Dedhia, P. H., Jin, S., Ruiz-Vega, R., Ma, D., Liu, Y., . . . Plikus, M. V. (2019). Single-cell analysis reveals fibroblast heterogeneity and myeloid-derived adipocyte progenitors in murine skin wounds. *Nature Communications, 10*(1), 650. doi:10.1038/s41467-018-08247-x

Hakimi, M., Selvanantham, T., Swinton, E., Padmore, R. F., Tong, Y., Kabbach, G., . . . Schlossmacher, M. G. (2011). Parkinson's disease-linked LRRK2 is expressed in circulating and tissue immune cells and upregulated following recognition of microbial structures. *J Neural Transm (Vienna), 118*(5), 795-808. doi:10.1007/s00702-011-0653-2

Hammond, T. R., Dufort, C., Dissing-Olesen, L., Giera, S., Young, A., Wysoker, A., . . . Stevens, B. (2019). Single-Cell RNA Sequencing of Microglia throughout the Mouse Lifespan and in the Injured Brain Reveals Complex Cell-State Changes. *Immunity, 50*(1), 253-271 e256. doi:10.1016/j.immuni.2018.11.004

Hamza, T. H., Zabetian, C. P., Tenesa, A., Laederach, A., Montimurro, J., Yearout, D., . . . Payami, H. (2010). Common genetic variation in the HLA region is associated with late-onset sporadic Parkinson's disease. *Nat Genet, 42*(9), 781-785. doi:10.1038/ng.642

Hanisch, U. K. (2002). Microglia as a source and target of cytokines. *Glia, 40*(2), 140-155. doi:10.1002/glia.10161

Haugarvoll, K., & Wszolek, Z. K. (2009). Clinical features of LRRK2 parkinsonism. *Parkinsonism Relat Disord, 15 Suppl 3*, S205-208. doi:10.1016/S1353-8020(09)70815-6

Heindl, S., Gesierich, B., Benakis, C., Llovera, G., Duering, M., & Liesz, A. (2018). Automated Morphological Analysis of Microglia After Stroke. *Front Cell Neurosci, 12*, 106. doi:10.3389/fncel.2018.00106

Henderson, M. X., Peng, C., Trojanowski, J. Q., & Lee, V. M. Y. (2018). LRRK2 activity does not dramatically alter alpha-synuclein pathology in primary neurons. *Acta Neuropathol Commun, 6*(1), 45. doi:10.1186/s40478-018-0550-0

Heneka, M. T., Carson, M. J., El Khoury, J., Landreth, G. E., Brosseron, F., Feinstein, D. L., . . . Kummer, M. P. (2015). Neuroinflammation in Alzheimer's disease. *Lancet Neurol, 14*(4), 388-405. doi:10.1016/S1474-4422(15)70016-5

Hernandez, D. G., Reed, X., & Singleton, A. B. (2016). Genetics in Parkinson disease: Mendelian versus non-Mendelian inheritance. *J Neurochem, 139 Suppl 1*, 59-74. doi:10.1111/jnc.13593

Herzig, M. C., Bidinosti, M., Schweizer, T., Hafner, T., Stemmelen, C., Weiss, A., . . . Shimshek, D. R. (2012). High LRRK2 levels fail to induce or exacerbate neuronal alpha-synucleinopathy in mouse brain. *PLoS One, 7*(5), e36581. doi:10.1371/journal.pone.0036581

Herzig, M. C., Kolly, C., Persohn, E., Theil, D., Schweizer, T., Hafner, T., . . . Shimshek, D. R. (2011). LRRK2 protein levels are determined by kinase function and are crucial for kidney and lung homeostasis in mice. *Hum Mol Genet, 20*(21), 4209-4223. doi:10.1093/hmg/ddr348

Hickman, S. E., Kingery, N. D., Ohsumi, T. K., Borowsky, M. L., Wang, L. C., Means, T. K., & El Khoury, J. (2013). The microglial sensome revealed by direct RNA sequencing. *Nat Neurosci, 16*(12), 1896-1905. doi:10.1038/nn.3554

Hinkle, K. M., Yue, M., Behrouz, B., Dachsel, J. C., Lincoln, S. J., Bowles, E. E., . . . Melrose, H. L. (2012). LRRK2 knockout mice have an intact dopaminergic system but display alterations in exploratory and motor co-ordination behaviors. *Mol Neurodegener, 7*, 25. doi:10.1186/1750-1326-7-25

Hoehn, M. M., & Yahr, M. D. (1967). Parkinsonism: onset, progression and mortality. *Neurology, 17*(5), 427-442. doi:10.1212/wnl.17.5.427

Hoffmann, A., Ettle, B., Bruno, A., Kulinich, A., Hoffmann, A. C., von Wittgenstein, J., . . . Schlachetzki, J. C. M. (2016). Alpha-synuclein activates BV2 microglia dependent on its aggregation state. *Biochem Biophys Res Commun, 479*(4), 881-886. doi:10.1016/j.bbrc.2016.09.109

Hongge, L., Kexin, G., Xiaojie, M., Nian, X., & Jinsha, H. (2015). The role of LRRK2 in the regulation of monocyte adhesion to endothelial cells. *J Mol Neurosci, 55*(1), 233-239. doi:10.1007/s12031-014-0312-9

Huang, Y., Deng, L., Zhong, Y., & Yi, M. (2018). The Association between E326K of GBA and the Risk of Parkinson's Disease. *Parkinsons Dis, 2018*, 1048084. doi:10.1155/2018/1048084

Hughes, A. J., Spelke, D. P., Xu, Z., Kang, C. C., Schaffer, D. V., & Herr, A. E. (2014). Single-cell western blotting. *Nat Methods, 11*(7), 749-755. doi:10.1038/nmeth.2992

Hur, E. M., Jang, E. H., Jeong, G. R., & Lee, B. D. (2019). LRRK2 and membrane trafficking: nexus of Parkinson's disease. *BMB Rep, 52*(9), 533-539. Retrieved from https://www.ncbi.nlm.nih.gov/pubmed/31383252

Imamura, K., Hishikawa, N., Sawada, M., Nagatsu, T., Yoshida, M., & Hashizume, Y. (2003). Distribution of major histocompatibility complex class II-positive microglia and cytokine profile of Parkinson's disease brains. *Acta Neuropathol, 106*(6), 518-526. doi:10.1007/s00401-003-0766-2

Inzelberg, R., Hassin-Baer, S., & Jankovic, J. (2014). Genetic movement disorders in patients of Jewish ancestry. *JAMA Neurol, 71*(12), 1567-1572. doi:10.1001/jamaneurol.2014.1364

Ito, D., Tanaka, K., Suzuki, S., Dembo, T., & Fukuuchi, Y. (2001). Enhanced expression of Iba1, ionized calcium-binding adapter molecule 1, after transient focal cerebral ischemia in rat brain. *Stroke, 32*(5), 1208-1215. doi:10.1161/01.str.32.5.1208

Jaleel, M., Nichols, R. J., Deak, M., Campbell, D. G., Gillardon, F., Knebel, A., & Alessi, D. R. (2007). LRRK2 phosphorylates moesin at threonine-558: characterization of how

Parkinson's disease mutants affect kinase activity. *Biochem J, 405*(2), 307-317. doi:10.1042/BJ20070209

Janda, E., Boi, L., & Carta, A. R. (2018). Microglial Phagocytosis and Its Regulation: A Therapeutic Target in Parkinson's Disease? *Front Mol Neurosci, 11*, 144. doi:10.3389/fnmol.2018.00144

Jellinger, K. A. (2012). Neuropathology of sporadic Parkinson's disease: evaluation and changes of concepts. *Mov Disord, 27*(1), 8-30. doi:10.1002/mds.23795

Jung, S., Aliberti, J., Graemmel, P., Sunshine, M. J., Kreutzberg, G. W., Sher, A., & Littman, D. R. (2000). Analysis of fractalkine receptor CX(3)CR1 function by targeted deletion and green fluorescent protein reporter gene insertion. *Mol Cell Biol, 20*(11), 4106-4114. doi:10.1128/mcb.20.11.4106-4114.2000

Kaiser, T., & Feng, G. (2019). Tmem119-EGFP and Tmem119-CreERT2 Transgenic Mice for Labeling and Manipulating Microglia. *eNeuro, 6*(4). doi:10.1523/ENEURO.0448-18.2019

Kalogeropulou, A. F., Zhao, J., Bolliger, M. F., Memou, A., Narasimha, S., Molitor, T. P., . . . Nichols, R. J. (2018). P62/SQSTM1 is a novel leucine-rich repeat kinase 2 (LRRK2) substrate that enhances neuronal toxicity. *Biochem J, 475*(7), 1271-1293. doi:10.1042/BCJ20170699

Kang, C. C., Yamauchi, K. A., Vlassakis, J., Sinkala, E., Duncombe, T. A., & Herr, A. E. (2016). Single cell-resolution western blotting. *Nat Protoc, 11*(8), 1508-1530. doi:10.1038/nprot.2016.089

Karimi-Moghadam, A., Charsouei, S., Bell, B., & Jabalameli, M. R. (2018). Parkinson Disease from Mendelian Forms to Genetic Susceptibility: New Molecular Insights into the Neurodegeneration Process. *Cell Mol Neurobiol, 38*(6), 1153-1178. doi:10.1007/s10571-018-0587-4

Keren-Shaul, H., Spinrad, A., Weiner, A., Matcovitch-Natan, O., Dvir-Szternfeld, R., Ulland, T. K., . . . Amit, I. (2017). A Unique Microglia Type Associated with Restricting Development of Alzheimer's Disease. *Cell, 169*(7), 1276-1290 e1217. doi:10.1016/j.cell.2017.05.018

Kettenmann, H., Hanisch, U. K., Noda, M., & Verkhratsky, A. (2011). Physiology of microglia. *Physiol Rev, 91*(2), 461-553. doi:10.1152/physrev.00011.2010

Kettenmann, H., Kirchhoff, F., & Verkhratsky, A. (2013). Microglia: new roles for the synaptic stripper. *Neuron, 77*(1), 10-18. doi:10.1016/j.neuron.2012.12.023

Kettenmann, H., & Verkhratsky, A. (2008). Neuroglia: the 150 years after. *Trends in neurosciences, 31*(12), 653-659.

Kim, B., Yang, M. S., Choi, D., Kim, J. H., Kim, H. S., Seol, W., . . . Joe, E. H. (2012). Impaired inflammatory responses in murine Lrrk2-knockdown brain microglia. *PLoS One, 7*(4), e34693. doi:10.1371/journal.pone.0034693

Kim, C., Ho, D. H., Suk, J. E., You, S., Michael, S., Kang, J., . . . Lee, S. J. (2013). Neuron-released oligomeric alpha-synuclein is an endogenous agonist of TLR2 for paracrine activation of microglia. *Nat Commun, 4*, 1562. doi:10.1038/ncomms2534

Kim, H., Park, H. J., Choi, H., Chang, Y., Park, H., Shin, J., . . . Kim, J. (2019). Modeling G2019S-LRRK2 Sporadic Parkinson's Disease in 3D Midbrain Organoids. *Stem Cell Reports, 12*(3), 518-531. doi:10.1016/j.stemcr.2019.01.020

Kim, K. S., Marcogliese, P. C., Yang, J., Callaghan, S. M., Resende, V., Abdel-Messih, E., . . . Park, D. S. (2018). Regulation of myeloid cell phagocytosis by LRRK2 via WAVE2 complex

stabilization is altered in Parkinson's disease. *Proc Natl Acad Sci U S A, 115*(22), E5164-E5173. doi:10.1073/pnas.1718946115

Kim, Y. S., & Joh, T. H. (2006). Microglia, major player in the brain inflammation: their roles in the pathogenesis of Parkinson's disease. *Exp Mol Med, 38*(4), 333-347. doi:10.1038/emm.2006.40

Klein, C., & Westenberger, A. (2012). Genetics of Parkinson's disease. *Cold Spring Harb Perspect Med, 2*(1), a008888. doi:10.1101/cshperspect.a008888

Koprich, J. B., Reske-Nielsen, C., Mithal, P., & Isacson, O. (2008). Neuroinflammation mediated by IL-1beta increases susceptibility of dopamine neurons to degeneration in an animal model of Parkinson's disease. *J Neuroinflammation, 5*, 8. doi:10.1186/1742-2094-5-8

Korecka, J. A., Thomas, R., Christensen, D. P., Hinrich, A. J., Ferrari, E. J., Levy, S. A., . . . Isacson, O. (2019). Mitochondrial clearance and maturation of autophagosomes are compromised in LRRK2 G2019S familial Parkinson's disease patient fibroblasts. *Hum Mol Genet*. doi:10.1093/hmg/ddz126

Kotzbauer, P. T., Trojanowsk, J. Q., & Lee, V. M. (2001). Lewy body pathology in Alzheimer's disease. *J Mol Neurosci, 17*(2), 225-232. Retrieved from https://www.ncbi.nlm.nih.gov/pubmed/11816795

Kozina, E., Sadasivan, S., Jiao, Y., Dou, Y., Ma, Z., Tan, H., . . . Smeyne, R. J. (2018). Mutant LRRK2 mediates peripheral and central immune responses leading to neurodegeneration in vivo. *Brain, 141*(6), 1753-1769. doi:10.1093/brain/awy077

Kuhn, A., Kumar, A., Beilina, A., Dillman, A., Cookson, M. R., & Singleton, A. B. (2012). Cell population-specific expression analysis of human cerebellum. *BMC Genomics, 13*, 610. doi:10.1186/1471-2164-13-610

Kumar, K. R., Djarmati-Westenberger, A., & Grunewald, A. (2011). Genetics of Parkinson's disease. *Semin Neurol, 31*(5), 433-440. doi:10.1055/s-0031-1299782

Kumaran, R., & Cookson, M. R. (2015). Pathways to Parkinsonism Redux: convergent pathobiological mechanisms in genetics of Parkinson's disease. *Hum Mol Genet, 24*(R1), R32-44. doi:10.1093/hmg/ddv236

Lavalley, N. J., Slone, S. R., Ding, H., West, A. B., & Yacoubian, T. A. (2016). 14-3-3 Proteins regulate mutant LRRK2 kinase activity and neurite shortening. *Hum Mol Genet, 25*(1), 109-122. doi:10.1093/hmg/ddv453

Lee, H., James, W. S., & Cowley, S. A. (2017). LRRK2 in peripheral and central nervous system innate immunity: its link to Parkinson's disease. *Biochem Soc Trans, 45*(1), 131-139. doi:10.1042/BST20160262

Lee, H. J., Suk, J. E., Bae, E. J., & Lee, S. J. (2008). Clearance and deposition of extracellular alpha-synuclein aggregates in microglia. *Biochem Biophys Res Commun, 372*(3), 423-428. doi:10.1016/j.bbrc.2008.05.045

Lee, J. W., & Cannon, J. R. (2015). LRRK2 mutations and neurotoxicant susceptibility. *Exp Biol Med (Maywood), 240*(6), 752-759. doi:10.1177/1535370215579162

Lees, A. J., Hardy, J., & Revesz, T. (2009). Parkinson's disease. *Lancet, 373*(9680), 2055-2066. doi:10.1016/S0140-6736(09)60492-X

Lehmann, M. L., Cooper, H. A., Maric, D., & Herkenham, M. (2016). Social defeat induces depressive-like states and microglial activation without involvement of peripheral macrophages. *J Neuroinflammation, 13*(1), 224. doi:10.1186/s12974-016-0672-x

Lenz, K. M., & Nelson, L. H. (2018). Microglia and Beyond: Innate Immune Cells As Regulators of Brain Development and Behavioral Function. *Front Immunol, 9*, 698. doi:10.3389/fimmu.2018.00698

Lewis, P. A. (2018). Mutations in LRRK2 amplify cell-to-cell protein aggregate propagation: a hypothesis. *Acta Neuropathol, 135*(6), 973-976. doi:10.1007/s00401-018-1838-7

Lewis, P. A., Greggio, E., Beilina, A., Jain, S., Baker, A., & Cookson, M. R. (2007). The R1441C mutation of LRRK2 disrupts GTP hydrolysis. *Biochem Biophys Res Commun, 357*(3), 668-671. doi:10.1016/j.bbrc.2007.04.006

Li, J. Q., Tan, L., & Yu, J. T. (2014). The role of the LRRK2 gene in Parkinsonism. *Mol Neurodegener, 9*, 47. doi:10.1186/1750-1326-9-47

Li, Q., & Barres, B. A. (2018). Microglia and macrophages in brain homeostasis and disease. *Nat Rev Immunol, 18*(4), 225-242. doi:10.1038/nri.2017.125

Liao, J., Wu, C. X., Burlak, C., Zhang, S., Sahm, H., Wang, M., . . . Hoang, Q. Q. (2014). Parkinson disease-associated mutation R1441H in LRRK2 prolongs the "active state" of its GTPase domain. *Proc Natl Acad Sci U S A, 111*(11), 4055-4060. doi:10.1073/pnas.1323285111

Lien, E., Means, T. K., Heine, H., Yoshimura, A., Kusumoto, S., Fukase, K., . . . Golenbock, D. T. (2000). Toll-like receptor 4 imparts ligand-specific recognition of bacterial lipopolysaccharide. *J Clin Invest, 105*(4), 497-504. doi:10.1172/JCI8541

Lin, X., Parisiadou, L., Gu, X. L., Wang, L., Shim, H., Sun, L., . . . Cai, H. (2009). Leucine-rich repeat kinase 2 regulates the progression of neuropathology induced by Parkinson's-disease-related mutant alpha-synuclein. *Neuron, 64*(6), 807-827. doi:10.1016/j.neuron.2009.11.006

Liu, Z., Mobley, J. A., DeLucas, L. J., Kahn, R. A., & West, A. B. (2016). LRRK2 autophosphorylation enhances its GTPase activity. *FASEB J, 30*(1), 336-347. doi:10.1096/fj.15-277095

Lobbestael, E., Baekelandt, V., & Taymans, J. M. (2012). Phosphorylation of LRRK2: from kinase to substrate. *Biochem Soc Trans, 40*(5), 1102-1110. doi:10.1042/BST20120128

Love, M. I., Huber, W., & Anders, S. (2014). Moderated estimation of fold change and dispersion for RNA-seq data with DESeq2. *Genome Biol, 15*(12), 550. doi:10.1186/s13059-014-0550-8

Ludolph, A. C., Kassubek, J., Landwehrmeyer, B. G., Mandelkow, E., Mandelkow, E. M., Burn, D. J., . . . Reisensburg Working Group for Tauopathies With, P. (2009). Tauopathies with parkinsonism: clinical spectrum, neuropathologic basis, biological markers, and treatment options. *Eur J Neurol, 16*(3), 297-309. doi:10.1111/j.1468-1331.2008.02513.x

Lull, M. E., & Block, M. L. (2010). Microglial activation and chronic neurodegeneration. *Neurotherapeutics, 7*(4), 354-365. doi:10.1016/j.nurt.2010.05.014

Luzio, J. P., Pryor, P. R., & Bright, N. A. (2007). Lysosomes: fusion and function. *Nat Rev Mol Cell Biol, 8*(8), 622-632. doi:10.1038/nrm2217

Lynch-Day, M. A., Mao, K., Wang, K., Zhao, M., & Klionsky, D. J. (2012). The role of autophagy in Parkinson's disease. *Cold Spring Harb Perspect Med, 2*(4), a009357. doi:10.1101/cshperspect.a009357

Ma, B., Xu, L., Pan, X., Sun, L., Ding, J., Xie, C., . . . Cai, H. (2016). LRRK2 modulates microglial activity through regulation of chemokine (C-X3-C) receptor 1 -mediated signalling pathways. *Hum Mol Genet, 25*(16), 3515-3523. doi:10.1093/hmg/ddw194

Macallan, D. C., Wallace, D. L., Zhang, Y., Ghattas, H., Asquith, B., de Lara, C., . . . Beverley, P. C. (2005). B-cell kinetics in humans: rapid turnover of peripheral blood memory cells. *Blood, 105*(9), 3633-3640. doi:10.1182/blood-2004-09-3740

MacLeod, D., Dowman, J., Hammond, R., Leete, T., Inoue, K., & Abeliovich, A. (2006). The familial Parkinsonism gene LRRK2 regulates neurite process morphology. *Neuron, 52*(4), 587-593. doi:10.1016/j.neuron.2006.10.008

Maekawa, T., Sasaoka, T., Azuma, S., Ichikawa, T., Melrose, H. L., Farrer, M. J., & Obata, F. (2016). Leucine-rich repeat kinase 2 (LRRK2) regulates alpha-synuclein clearance in microglia. *BMC Neurosci, 17*(1), 77. doi:10.1186/s12868-016-0315-2

Mammana, S., Fagone, P., Cavalli, E., Basile, M. S., Petralia, M. C., Nicoletti, F., . . . Mazzon, E. (2018). The Role of Macrophages in Neuroinflammatory and Neurodegenerative Pathways of Alzheimer's Disease, Amyotrophic Lateral Sclerosis, and Multiple Sclerosis: Pathogenetic Cellular Effectors and Potential Therapeutic Targets. *Int J Mol Sci, 19*(3). doi:10.3390/ijms19030831

Manzoni, C., Mamais, A., Roosen, D. A., Dihanich, S., Soutar, M. P., Plun-Favreau, H., . . . Lewis, P. A. (2016). mTOR independent regulation of macroautophagy by Leucine Rich Repeat Kinase 2 via Beclin-1. *Sci Rep, 6*, 35106. doi:10.1038/srep35106

Marques, O., & Outeiro, T. F. (2012). Alpha-synuclein: from secretion to dysfunction and death. *Cell Death Dis, 3*, e350. doi:10.1038/cddis.2012.94

Martin, I., Kim, J. W., Lee, B. D., Kang, H. C., Xu, J. C., Jia, H., . . . Dawson, V. L. (2014). Ribosomal protein s15 phosphorylation mediates LRRK2 neurodegeneration in Parkinson's disease. *Cell, 157*(2), 472-485. doi:10.1016/j.cell.2014.01.064

Masuda, T., Sankowski, R., Staszewski, O., Böttcher, C., Amann, L., Sagar, . . . Prinz, M. (2019). Spatial and temporal heterogeneity of mouse and human microglia at single-cell resolution. *Nature, 566*(7744), 388-392. doi:10.1038/s41586-019-0924-x

Mata, I. F., Davis, M. Y., Lopez, A. N., Dorschner, M. O., Martinez, E., Yearout, D., . . . Zabetian, C. P. (2016). The discovery of LRRK2 p.R1441S, a novel mutation for Parkinson's disease, adds to the complexity of a mutational hotspot. *Am J Med Genet B Neuropsychiatr Genet, 171*(7), 925-930. doi:10.1002/ajmg.b.32452

Mathys, H., Adaikkan, C., Gao, F., Young, J. Z., Manet, E., Hemberg, M., . . . Tsai, L. H. (2017). Temporal Tracking of Microglia Activation in Neurodegeneration at Single-Cell Resolution. *Cell Rep, 21*(2), 366-380. doi:10.1016/j.celrep.2017.09.039

Mathys, H., Davila-Velderrain, J., Peng, Z., Gao, F., Mohammadi, S., Young, J. Z., . . . Tsai, L. H. (2019). Single-cell transcriptomic analysis of Alzheimer's disease. *Nature, 570*(7761), 332-337. doi:10.1038/s41586-019-1195-2

Matta, S., Van Kolen, K., da Cunha, R., van den Bogaart, G., Mandemakers, W., Miskiewicz, K., . . . Verstreken, P. (2012). LRRK2 controls an EndoA phosphorylation cycle in synaptic endocytosis. *Neuron, 75*(6), 1008-1021. doi:10.1016/j.neuron.2012.08.022

McGeer, P. L., Itagaki, S., Boyes, B. E., & McGeer, E. G. (1988). Reactive microglia are positive for HLA-DR in the substantia nigra of Parkinson's and Alzheimer's disease brains. *Neurology, 38*(8), 1285-1291. doi:10.1212/wnl.38.8.1285

Menassa, D. A., & Gomez-Nicola, D. (2018). Microglial Dynamics During Human Brain Development. *Front Immunol, 9*, 1014. doi:10.3389/fimmu.2018.01014

Mittelbronn, M., Dietz, K., Schluesener, H. J., & Meyermann, R. (2001). Local distribution of microglia in the normal adult human central nervous system differs by up to one order of magnitude. *Acta Neuropathol, 101*(3), 249-255. doi:10.1007/s004010000284

Mizee, M. R., Miedema, S. S., van der Poel, M., Adelia, Schuurman, K. G., van Strien, M. E., . . . Huitinga, I. (2017). Isolation of primary microglia from the human post-mortem brain: effects of ante- and post-mortem variables. *Acta Neuropathol Commun, 5*(1), 16. doi:10.1186/s40478-017-0418-8

Moehle, M. S., Webber, P. J., Tse, T., Sukar, N., Standaert, D. G., DeSilva, T. M., . . . West, A. B. (2012). LRRK2 inhibition attenuates microglial inflammatory responses. *J Neurosci, 32*(5), 1602-1611. doi:10.1523/JNEUROSCI.5601-11.2012

Moehle, M. S., & West, A. B. (2015). M1 and M2 immune activation in Parkinson's Disease: Foe and ally? *Neuroscience, 302*, 59-73. doi:10.1016/j.neuroscience.2014.11.018

Mogi, M., Harada, M., Riederer, P., Narabayashi, H., Fujita, K., & Nagatsu, T. (1994). Tumor necrosis factor-alpha (TNF-alpha) increases both in the brain and in the cerebrospinal fluid from parkinsonian patients. *Neurosci Lett, 165*(1-2), 208-210. doi:10.1016/0304-3940(94)90746-3

Morrison, H. W., & Filosa, J. A. (2013). A quantitative spatiotemporal analysis of microglia morphology during ischemic stroke and reperfusion. *J Neuroinflammation, 10*, 4. doi:10.1186/1742-2094-10-4

Muffat, J., Li, Y., Yuan, B., Mitalipova, M., Omer, A., Corcoran, S., . . . Jaenisch, R. (2016). Efficient derivation of microglia-like cells from human pluripotent stem cells. *Nat Med, 22*(11), 1358-1367. doi:10.1038/nm.4189

Nakamura, K. (2013). alpha-Synuclein and mitochondria: partners in crime? *Neurotherapeutics, 10*(3), 391-399. doi:10.1007/s13311-013-0182-9

Nalls, M. A., Blauwendraat, C., Vallerga, C. L., Heilbron, K., Bandres-Ciga, S., Chang, D., . . . Singleton, A. B. (2019). Expanding Parkinson’s disease genetics: novel risk loci, genomic context, causal insights and heritable risk. *bioRxiv*, 388165. doi:10.1101/388165

Nalls, M. A., Pankratz, N., Lill, C. M., Do, C. B., Hernandez, D. G., Saad, M., . . . Singleton, A. B. (2014). Large-scale meta-analysis of genome-wide association data identifies six new risk loci for Parkinson's disease. *Nat Genet, 46*(9), 989-993. doi:10.1038/ng.3043

Ness, D., Ren, Z., Gardai, S., Sharpnack, D., Johnson, V. J., Brennan, R. J., . . . Olaharski, A. J. (2013). Leucine-rich repeat kinase 2 (LRRK2)-deficient rats exhibit renal tubule injury and perturbations in metabolic and immunological homeostasis. *PLoS One, 8*(6), e66164. doi:10.1371/journal.pone.0066164

Neudorfer, O., Giladi, N., Elstein, D., Abrahamov, A., Turezkite, T., Aghai, E., . . . Zimran, A. (1996). Occurrence of Parkinson's syndrome in type I Gaucher disease. *QJM, 89*(9), 691-694. doi:10.1093/qjmed/89.9.691

Neumann, H., Kotter, M. R., & Franklin, R. J. (2009). Debris clearance by microglia: an essential link between degeneration and regeneration. *Brain, 132*(Pt 2), 288-295. doi:10.1093/brain/awn109

Nguyen, A. P., & Moore, D. J. (2017). Understanding the GTPase Activity of LRRK2: Regulation, Function, and Neurotoxicity. *Adv Neurobiol, 14*, 71-88. doi:10.1007/978-3-319-49969-7_4

Nichols, R. (2017). LRRK2 phosphorylation. In (Vol. 14, pp. 51-70).

Nichols, R. J., Dzamko, N., Morrice, N. A., Campbell, D. G., Deak, M., Ordureau, A., . . . Alessi, D. R. (2010). 14-3-3 binding to LRRK2 is disrupted by multiple Parkinson's disease-associated mutations and regulates cytoplasmic localization. *Biochem J, 430*(3), 393-404. doi:10.1042/BJ20100483

Nimmerjahn, A., Kirchhoff, F., & Helmchen, F. (2005). Resting microglial cells are highly dynamic surveillants of brain parenchyma in vivo. *Science, 308*(5726), 1314-1318. doi:10.1126/science.1110647

Norden, D. M., Trojanowski, P. J., Villanueva, E., Navarro, E., & Godbout, J. P. (2016). Sequential activation of microglia and astrocyte cytokine expression precedes increased Iba-1 or GFAP immunoreactivity following systemic immune challenge. *Glia, 64*(2), 300-316. doi:10.1002/glia.22930

Obeso, J. A., Marin, C., Rodriguez-Oroz, C., Blesa, J., Benitez-Temino, B., Mena-Segovia, J., . . . Olanow, C. W. (2008). The basal ganglia in Parkinson's disease: current concepts and unexplained observations. *Ann Neurol, 64 Suppl 2*, S30-46. doi:10.1002/ana.21481

Ohsawa, K., & Kohsaka, S. (2011). Dynamic motility of microglia: purinergic modulation of microglial movement in the normal and pathological brain. *Glia, 59*(12), 1793-1799. doi:10.1002/glia.21238

Olah, M., Patrick, E., Villani, A. C., Xu, J., White, C. C., Ryan, K. J., . . . Bradshaw, E. M. (2018). A transcriptomic atlas of aged human microglia. *Nat Commun, 9*(1), 539. doi:10.1038/s41467-018-02926-5

Paisan-Ruiz, C., Jain, S., Evans, E. W., Gilks, W. P., Simon, J., van der Brug, M., . . . Singleton, A. B. (2004). Cloning of the gene containing mutations that cause PARK8-linked Parkinson's disease. *Neuron, 44*(4), 595-600. doi:10.1016/j.neuron.2004.10.023

Paisan-Ruiz, C., Lewis, P. A., & Singleton, A. B. (2013). LRRK2: cause, risk, and mechanism. *J Parkinsons Dis, 3*(2), 85-103. doi:10.3233/JPD-130192

Pandya, H., Shen, M. J., Ichikawa, D. M., Sedlock, A. B., Choi, Y., Johnson, K. R., . . . Park, J. K. (2017). Differentiation of human and murine induced pluripotent stem cells to microglia-like cells. *Nat Neurosci, 20*(5), 753-759. doi:10.1038/nn.4534

Parisiadou, L., Xie, C., Cho, H. J., Lin, X., Gu, X. L., Long, C. X., . . . Cai, H. (2009). Phosphorylation of ezrin/radixin/moesin proteins by LRRK2 promotes the rearrangement of actin cytoskeleton in neuronal morphogenesis. *J Neurosci, 29*(44), 13971-13980. doi:10.1523/JNEUROSCI.3799-09.2009

Parkhurst, C. N., Yang, G., Ninan, I., Savas, J. N., Yates, J. R., 3rd, Lafaille, J. J., . . . Gan, W. B. (2013). Microglia promote learning-dependent synapse formation through brain-derived neurotrophic factor. *Cell, 155*(7), 1596-1609. doi:10.1016/j.cell.2013.11.030

Parkinson, J. (2002). An essay on the shaking palsy. 1817. *J Neuropsychiatry Clin Neurosci, 14*(2), 223-236; discussion 222. doi:10.1176/jnp.14.2.223

Patro, R., Duggal, G., Love, M. I., Irizarry, R. A., & Kingsford, C. (2017). Salmon provides fast and bias-aware quantification of transcript expression. *Nature Methods, 14*, 417. doi:10.1038/nmeth.4197

https://www.nature.com/articles/nmeth.4197#supplementary-information

Pellegrini, L., Hauser, D. N., Li, Y., Mamais, A., Beilina, A., Kumaran, R., . . . Harvey, K. (2018). Proteomic analysis reveals co-ordinated alterations in protein synthesis and degradation

pathways in LRRK2 knockout mice. *Human Molecular Genetics, 27*(18), 3257-3271. doi:10.1093/hmg/ddy232
Perry, V. H., & Holmes, C. (2014). Microglial priming in neurodegenerative disease. *Nat Rev Neurol, 10*(4), 217-224. doi:10.1038/nrneurol.2014.38
Polymeropoulos, M. H., Higgins, J. J., Golbe, L. I., Johnson, W. G., Ide, S. E., Di Iorio, G., . . . Duvoisin, R. C. (1996). Mapping of a gene for Parkinson's disease to chromosome 4q21-q23. *Science, 274*(5290), 1197-1199. doi:10.1126/science.274.5290.1197
Postuma, R. B., Berg, D., Stern, M., Poewe, W., Olanow, C. W., Oertel, W., . . . Deuschl, G. (2015). MDS clinical diagnostic criteria for Parkinson's disease. *Mov Disord, 30*(12), 1591-1601. doi:10.1002/mds.26424
Pradhan, S., & Andreasson, K. (2013). Commentary: Progressive inflammation as a contributing factor to early development of Parkinson's disease. *Exp Neurol, 241*, 148-155. doi:10.1016/j.expneurol.2012.12.008
Price, A., Manzoni, C., Cookson, M. R., & Lewis, P. A. (2018). The LRRK2 signalling system. *Cell Tissue Res, 373*(1), 39-50. doi:10.1007/s00441-017-2759-9
Prinz, M., & Priller, J. (2014). Microglia and brain macrophages in the molecular age: from origin to neuropsychiatric disease. *Nat Rev Neurosci, 15*(5), 300-312. doi:10.1038/nrn3722
Puccini, J. M., Marker, D. F., Fitzgerald, T., Barbieri, J., Kim, C. S., Miller-Rhodes, P., . . . Gelbard, H. A. (2015). Leucine-rich repeat kinase 2 modulates neuroinflammation and neurotoxicity in models of human immunodeficiency virus 1-associated neurocognitive disorders. *J Neurosci, 35*(13), 5271-5283. doi:10.1523/JNEUROSCI.0650-14.2015
Ramonet, D., Daher, J. P., Lin, B. M., Stafa, K., Kim, J., Banerjee, R., . . . Moore, D. J. (2011). Dopaminergic neuronal loss, reduced neurite complexity and autophagic abnormalities in transgenic mice expressing G2019S mutant LRRK2. *PLoS One, 6*(4), e18568. doi:10.1371/journal.pone.0018568
Reimand, J., Arak, T., Adler, P., Kolberg, L., Reisberg, S., Peterson, H., & Vilo, J. (2016). g:Profiler-a web server for functional interpretation of gene lists (2016 update). *Nucleic Acids Res, 44*(W1), W83-89. doi:10.1093/nar/gkw199
Reu, P., Khosravi, A., Bernard, S., Mold, J. E., Salehpour, M., Alkass, K., . . . Frisen, J. (2017). The Lifespan and Turnover of Microglia in the Human Brain. *Cell Rep, 20*(4), 779-784. doi:10.1016/j.celrep.2017.07.004
Rezaie, P., & Male, D. (2002). Mesoglia & microglia--a historical review of the concept of mononuclear phagocytes within the central nervous system. *J Hist Neurosci, 11*(4), 325-374. doi:10.1076/jhin.11.4.325.8531
Rideout, H. J., & Stefanis, L. (2014). The neurobiology of LRRK2 and its role in the pathogenesis of Parkinson's disease. *Neurochem Res, 39*(3), 576-592. doi:10.1007/s11064-013-1073-5
Roosen, D. A., & Cookson, M. R. (2016). LRRK2 at the interface of autophagosomes, endosomes and lysosomes. *Mol Neurodegener, 11*(1), 73. doi:10.1186/s13024-016-0140-1
Rosario, A. M., Cruz, P. E., Ceballos-Diaz, C., Strickland, M. R., Siemienski, Z., Pardo, M., . . . Chakrabarty, P. (2016). Microglia-specific targeting by novel capsid-modified AAV6 vectors. *Mol Ther Methods Clin Dev, 3*, 16026. doi:10.1038/mtm.2016.26
Ross, O. A., Soto-Ortolaza, A. I., Heckman, M. G., Aasly, J. O., Abahuni, N., Annesi, G., . . . Genetic Epidemiology Of Parkinson's Disease, C. (2011). Association of LRRK2 exonic

variants with susceptibility to Parkinson's disease: a case-control study. *Lancet Neurol, 10*(10), 898-908. doi:10.1016/S1474-4422(11)70175-2

Rubio, J. P., Topp, S., Warren, L., St Jean, P. L., Wegmann, D., Kessner, D., . . . Mooser, V. E. (2012). Deep sequencing of the LRRK2 gene in 14,002 individuals reveals evidence of purifying selection and independent origin of the p.Arg1628Pro mutation in Europe. *Hum Mutat, 33*(7), 1087-1098. doi:10.1002/humu.22075

Rudenko, I. N., & Cookson, M. R. (2014). Heterogeneity of leucine-rich repeat kinase 2 mutations: genetics, mechanisms and therapeutic implications. *Neurotherapeutics, 11*(4), 738-750. doi:10.1007/s13311-014-0284-z

Russo, I., Berti, G., Plotegher, N., Bernardo, G., Filograna, R., Bubacco, L., & Greggio, E. (2015). Leucine-rich repeat kinase 2 positively regulates inflammation and down-regulates NF-kappaB p50 signaling in cultured microglia cells. *J Neuroinflammation, 12*, 230. doi:10.1186/s12974-015-0449-7

Russo, I., Bubacco, L., & Greggio, E. (2014). LRRK2 and neuroinflammation: partners in crime in Parkinson's disease? *Journal of Neuroinflammation, 11*(1), 52. doi:10.1186/1742-2094-11-52

Russo, I., Di Benedetto, G., Kaganovich, A., Ding, J., Mercatelli, D., Morari, M., . . . Greggio, E. (2018). Leucine-rich repeat kinase 2 controls protein kinase A activation state through phosphodiesterase 4. *J Neuroinflammation, 15*(1), 297. doi:10.1186/s12974-018-1337-8

Sadek, H., Almohari, S., & Renno, W. (2014). The Inflammatory Cytokines in the Pathogenesis of Parkinson's Disease. *Journal of Alzheimer's Disease & Parkinsonism, 04*. doi:10.4172/2161-0460.1000148

Schapansky, J., Nardozzi, J. D., Felizia, F., & LaVoie, M. J. (2014). Membrane recruitment of endogenous LRRK2 precedes its potent regulation of autophagy. *Hum Mol Genet, 23*(16), 4201-4214. doi:10.1093/hmg/ddu138

Schapansky, J., Nardozzi, J. D., & LaVoie, M. J. (2015). The complex relationships between microglia, alpha-synuclein, and LRRK2 in Parkinson's disease. *Neuroscience, 302*, 74-88. doi:10.1016/j.neuroscience.2014.09.049

Schapira, A. H., & Jenner, P. (2011). Etiology and pathogenesis of Parkinson's disease. *Mov Disord, 26*(6), 1049-1055. doi:10.1002/mds.23732

Schoenen, J. (1982). The dendritic organization of the human spinal cord: the dorsal horn. *Neuroscience, 7*(9), 2057-2087. doi:10.1016/0306-4522(82)90120-8

Seol, W., Nam, D., & Son, I. (2019). Rab GTPases as Physiological Substrates of LRRK2 Kinase. *Exp Neurobiol, 28*(2), 134-145. doi:10.5607/en.2019.28.2.134

Shahmoradian, S. H., Lewis, A. J., Genoud, C., Hench, J., Moors, T. E., Navarro, P. P., . . . Lauer, M. E. (2019). Lewy pathology in Parkinson's disease consists of crowded organelles and lipid membranes. *Nature Neuroscience, 22*(7), 1099-1109. doi:10.1038/s41593-019-0423-2

Sheng, Z., Zhang, S., Bustos, D., Kleinheinz, T., Le Pichon, C. E., Dominguez, S. L., . . . Zhu, H. (2012). Ser1292 autophosphorylation is an indicator of LRRK2 kinase activity and contributes to the cellular effects of PD mutations. *Sci Transl Med, 4*(164), 164ra161. doi:10.1126/scitranslmed.3004485

Sholl, D. A. (1953). Dendritic organization in the neurons of the visual and motor cortices of the cat. *J Anat, 87*(4), 387-406. Retrieved from https://www.ncbi.nlm.nih.gov/pubmed/13117757

Sidransky, E., Nalls, M. A., Aasly, J. O., Aharon-Peretz, J., Annesi, G., Barbosa, E. R., . . . Ziegler, S. G. (2009). Multicenter analysis of glucocerebrosidase mutations in Parkinson's disease. *N Engl J Med, 361*(17), 1651-1661. doi:10.1056/NEJMoa0901281

Simon-Sanchez, J., Schulte, C., Bras, J. M., Sharma, M., Gibbs, J. R., Berg, D., . . . Gasser, T. (2009). Genome-wide association study reveals genetic risk underlying Parkinson's disease. *Nat Genet, 41*(12), 1308-1312. doi:10.1038/ng.487

Simons, M., & Trotter, J. (2007). Wrapping it up: the cell biology of myelination. *Curr Opin Neurobiol, 17*(5), 533-540. doi:10.1016/j.conb.2007.08.003

Singleton, A., & Hardy, J. (2011). A generalizable hypothesis for the genetic architecture of disease: pleomorphic risk loci. *Hum Mol Genet, 20*(R2), R158-162. doi:10.1093/hmg/ddr358

Singleton, A., & Hardy, J. (2016). The Evolution of Genetics: Alzheimer's and Parkinson's Diseases. *Neuron, 90*(6), 1154-1163. doi:10.1016/j.neuron.2016.05.040

Smits, L. M., Reinhardt, L., Reinhardt, P., Glatza, M., Monzel, A. S., Stanslowsky, N., . . . Schwamborn, J. C. (2019). Modeling Parkinson's disease in midbrain-like organoids. *npj Parkinson's Disease, 5*(1), 5. doi:10.1038/s41531-019-0078-4

Soneson, C., Love, M. I., & Robinson, M. D. (2015). Differential analyses for RNA-seq: transcript-level estimates improve gene-level inferences. *F1000Res, 4*, 1521. doi:10.12688/f1000research.7563.2

Sousa, C., Biber, K., & Michelucci, A. (2017). Cellular and Molecular Characterization of Microglia: A Unique Immune Cell Population. *Front Immunol, 8*, 198. doi:10.3389/fimmu.2017.00198

Spillantini, M. G., Schmidt, M. L., Lee, V. M. Y., Trojanowski, J. Q., Jakes, R., & Goedert, M. (1997). α-Synuclein in Lewy bodies. *Nature, 388*(6645), 839-840. doi:10.1038/42166

Stefanis, L. (2012). alpha-Synuclein in Parkinson's disease. *Cold Spring Harb Perspect Med, 2*(2), a009399. doi:10.1101/cshperspect.a009399

Steger, M., Tonelli, F., Ito, G., Davies, P., Trost, M., Vetter, M., . . . Mann, M. (2016). Phosphoproteomics reveals that Parkinson's disease kinase LRRK2 regulates a subset of Rab GTPases. *Elife, 5*. doi:10.7554/eLife.12813

Stence, N., Waite, M., & Dailey, M. E. (2001). Dynamics of microglial activation: a confocal time-lapse analysis in hippocampal slices. *Glia, 33*(3), 256-266. Retrieved from https://www.ncbi.nlm.nih.gov/pubmed/11241743

Stevens, B., Allen, N. J., Vazquez, L. E., Howell, G. R., Christopherson, K. S., Nouri, N., . . . Barres, B. A. (2007). The classical complement cascade mediates CNS synapse elimination. *Cell, 131*(6), 1164-1178. doi:10.1016/j.cell.2007.10.036

Stokholm, M. G., Iranzo, A., Ostergaard, K., Serradell, M., Otto, M., Svendsen, K. B., . . . Pavese, N. (2017). Assessment of neuroinflammation in patients with idiopathic rapid-eye-movement sleep behaviour disorder: a case-control study. *Lancet Neurol, 16*(10), 789-796. doi:10.1016/S1474-4422(17)30173-4

Stuart, T., Butler, A., Hoffman, P., Hafemeister, C., Papalexi, E., Mauck, W. M., 3rd, . . . Satija, R. (2019). Comprehensive Integration of Single-Cell Data. *Cell, 177*(7), 1888-1902.e1821. doi:10.1016/j.cell.2019.05.031

Su, C. J., Feng, Y., Liu, T. T., Liu, X., Bao, J. J., Shi, A. M., . . . Yu, Y. L. (2017). Thioredoxin-interacting protein induced alpha-synuclein accumulation via inhibition of autophagic flux: Implications for Parkinson's disease. *CNS Neurosci Ther, 23*(9), 717-723. doi:10.1111/cns.12721

Tamashiro, T. T., Dalgard, C. L., & Byrnes, K. R. (2012). Primary microglia isolation from mixed glial cell cultures of neonatal rat brain tissue. *J Vis Exp*(66), e3814. doi:10.3791/3814

Tansey, M. G., & Goldberg, M. S. (2010). Neuroinflammation in Parkinson's disease: its role in neuronal death and implications for therapeutic intervention. *Neurobiol Dis, 37*(3), 510-518. doi:10.1016/j.nbd.2009.11.004

Tarakad, A., & Jankovic, J. (2017). Diagnosis and Management of Parkinson's Disease. *Semin Neurol, 37*(2), 118-126. doi:10.1055/s-0037-1601888

Tong, Y., Giaime, E., Yamaguchi, H., Ichimura, T., Liu, Y., Si, H., . . . Shen, J. (2012). Loss of leucine-rich repeat kinase 2 causes age-dependent bi-phasic alterations of the autophagy pathway. *Mol Neurodegener, 7*, 2. doi:10.1186/1750-1326-7-2

Tong, Y., Pisani, A., Martella, G., Karouani, M., Yamaguchi, H., Pothos, E. N., & Shen, J. (2009). R1441C mutation in LRRK2 impairs dopaminergic neurotransmission in mice. *Proc Natl Acad Sci U S A, 106*(34), 14622-14627. doi:10.1073/pnas.0906334106

Tong, Y., Yamaguchi, H., Giaime, E., Boyle, S., Kopan, R., Kelleher, R. J., & Shen, J. (2010). Loss of leucine-rich repeat kinase 2 causes impairment of protein degradation pathways, accumulation of α-synuclein, and apoptotic cell death in aged mice. *Proceedings of the National Academy of Sciences, 107*(21), 9879-9884. doi:10.1073/pnas.1004676107

Tremblay, M.-E., Cookson, M. R., & Civiero, L. (2019). Glial phagocytic clearance in Parkinson's disease. *Molecular Neurodegeneration, 14*(1), 16. doi:10.1186/s13024-019-0314-8

Tremblay, M. E., Stevens, B., Sierra, A., Wake, H., Bessis, A., & Nimmerjahn, A. (2011). The role of microglia in the healthy brain. *J Neurosci, 31*(45), 16064-16069. doi:10.1523/JNEUROSCI.4158-11.2011

Tsunemi, T., & Krainc, D. (2014). Zn(2)(+) dyshomeostasis caused by loss of ATP13A2/PARK9 leads to lysosomal dysfunction and alpha-synuclein accumulation. *Hum Mol Genet, 23*(11), 2791-2801. doi:10.1093/hmg/ddt572

Umeno, J., Asano, K., Matsushita, T., Matsumoto, T., Kiyohara, Y., Iida, M., . . . Kubo, M. (2011). Meta-analysis of published studies identified eight additional common susceptibility loci for Crohn's disease and ulcerative colitis. *Inflamm Bowel Dis, 17*(12), 2407-2415. doi:10.1002/ibd.21651

Valente, V., Teixeira, S. A., Neder, L., Okamoto, O. K., Oba-Shinjo, S. M., Marie, S. K., . . . Carlotti, C. G., Jr. (2009). Selection of suitable housekeeping genes for expression analysis in glioblastoma using quantitative RT-PCR. *BMC Mol Biol, 10*, 17. doi:10.1186/1471-2199-10-17

Volpicelli-Daley, L. A., Abdelmotilib, H., Liu, Z., Stoyka, L., Daher, J. P., Milnerwood, A. J., . . . West, A. B. (2016). G2019S-LRRK2 Expression Augments alpha-Synuclein Sequestration into Inclusions in Neurons. *J Neurosci, 36*(28), 7415-7427. doi:10.1523/JNEUROSCI.3642-15.2016

Wallings, R., Manzoni, C., & Bandopadhyay, R. (2015). Cellular processes associated with LRRK2 function and dysfunction. *FEBS J, 282*(15), 2806-2826. doi:10.1111/febs.13305

Wandu, W. S., Tan, C., Ogbeifun, O., Vistica, B. P., Shi, G., Hinshaw, S. J., . . . Gery, I. (2015). Leucine-Rich Repeat Kinase 2 (Lrrk2) Deficiency Diminishes the Development of Experimental Autoimmune Uveitis (EAU) and the Adaptive Immune Response. *PLoS One, 10*(6), e0128906. doi:10.1371/journal.pone.0128906

Wauters, F., Cornelissen, T., Imberechts, D., Martin, S., Koentjoro, B., Sue, C., . . . Vandenberghe, W. (2019). LRRK2 mutations impair depolarization-induced mitophagy through inhibition of mitochondrial accumulation of RAB10. *Autophagy*, 1-20. doi:10.1080/15548627.2019.1603548

Weng, Y. H., Chen, C. Y., Lin, K. J., Chen, Y. L., Yeh, T. H., Hsiao, I. T., . . . Wang, H. L. (2016). (R1441C) LRRK2 induces the degeneration of SN dopaminergic neurons and alters the expression of genes regulating neuronal survival in a transgenic mouse model. *Exp Neurol, 275 Pt 1*, 104-115. doi:10.1016/j.expneurol.2015.09.001

West, A. B., Cowell, R. M., Daher, J. P., Moehle, M. S., Hinkle, K. M., Melrose, H. L., . . . Volpicelli-Daley, L. A. (2014). Differential LRRK2 expression in the cortex, striatum, and substantia nigra in transgenic and nontransgenic rodents. *J Comp Neurol, 522*(11), 2465-2480. doi:10.1002/cne.23583

West, A. B., Moore, D. J., Biskup, S., Bugayenko, A., Smith, W. W., Ross, C. A., . . . Dawson, T. M. (2005). Parkinson's disease-associated mutations in leucine-rich repeat kinase 2 augment kinase activity. *Proc Natl Acad Sci U S A, 102*(46), 16842-16847. doi:10.1073/pnas.0507360102

Wojtala, A., Bonora, M., Malinska, D., Pinton, P., Duszynski, J., & Wieckowski, M. R. (2014). Methods to monitor ROS production by fluorescence microscopy and fluorometry. *Methods Enzymol, 542*, 243-262. doi:10.1016/B978-0-12-416618-9.00013-3

Wolf, S. A., Boddeke, H. W., & Kettenmann, H. (2017). Microglia in Physiology and Disease. *Annu Rev Physiol, 79*, 619-643. doi:10.1146/annurev-physiol-022516-034406

Wosczyna, M. N., Konishi, C. T., Perez Carbajal, E. E., Wang, T. T., Walsh, R. A., Gan, Q., . . . Rando, T. A. (2019). Mesenchymal Stromal Cells Are Required for Regeneration and Homeostatic Maintenance of Skeletal Muscle. *Cell Rep, 27*(7), 2029-2035 e2025. doi:10.1016/j.celrep.2019.04.074

Xiong, Y., Dawson, T. M., & Dawson, V. L. (2017). Models of LRRK2-Associated Parkinson's Disease. *Adv Neurobiol, 14*, 163-191. doi:10.1007/978-3-319-49969-7_9

Xiromerisiou, G., Houlden, H., Sailer, A., Silveira-Moriyama, L., Hardy, J., & Lees, A. J. (2012). Identical twins with Leucine rich repeat kinase type 2 mutations discordant for Parkinson's disease. *Mov Disord, 27*(10), 1323. doi:10.1002/mds.24924

Yao, L., Kan, E. M., Lu, J., Hao, A., Dheen, S. T., Kaur, C., & Ling, E.-A. (2013). Toll-like receptor 4 mediates microglial activation and production of inflammatory mediators in neonatal rat brain following hypoxia: role of TLR4 in hypoxic microglia. *Journal of Neuroinflammation, 10*(1), 785. doi:10.1186/1742-2094-10-23

York, E. M., LeDue, J. M., Bernier, L. P., & MacVicar, B. A. (2018). 3DMorph Automatic Analysis of Microglial Morphology in Three Dimensions from Ex Vivo and In Vivo Imaging. *eNeuro, 5*(6). doi:10.1523/ENEURO.0266-18.2018

Yoshihara, E., Masaki, S., Matsuo, Y., Chen, Z., Tian, H., & Yodoi, J. (2014). Thioredoxin/Txnip: redoxisome, as a redox switch for the pathogenesis of diseases. *Front Immunol, 4*, 514. doi:10.3389/fimmu.2013.00514

Yue, M., Hinkle, K. M., Davies, P., Trushina, E., Fiesel, F. C., Christenson, T. A., . . . Melrose, H. L. (2015). Progressive dopaminergic alterations and mitochondrial abnormalities in LRRK2 G2019S knock-in mice. *Neurobiol Dis, 78*, 172-195. doi:10.1016/j.nbd.2015.02.031

Zhang, W., Wang, T., Pei, Z., Miller, D. S., Wu, X., Block, M. L., . . . Zhang, J. (2005). Aggregated alpha-synuclein activates microglia: a process leading to disease progression in Parkinson's disease. *FASEB J, 19*(6), 533-542. doi:10.1096/fj.04-2751com

Zhao, Y., & Dzamko, N. (2019). Recent Developments in LRRK2-Targeted Therapy for Parkinson's Disease. *Drugs, 79*(10), 1037-1051. doi:10.1007/s40265-019-01139-4

Zheng, G. X., Terry, J. M., Belgrader, P., Ryvkin, P., Bent, Z. W., Wilson, R., . . . Bielas, J. H. (2017). Massively parallel digital transcriptional profiling of single cells. *Nat Commun, 8*, 14049. doi:10.1038/ncomms14049

Zimprich, A., Biskup, S., Leitner, P., Lichtner, P., Farrer, M., Lincoln, S., . . . Gasser, T. (2004). Mutations in LRRK2 cause autosomal-dominant parkinsonism with pleomorphic pathology. *Neuron, 44*(4), 601-607. doi:10.1016/j.neuron.2004.11.005